

DEVELOPMENT AND CHARACTERIZATION OF  
THERMOELECTRIC GENERATORS FOR  
THERMAL ENERGY RECOVERY FROM  
RECIPROCATING INTERNAL COMBUSTION  
ENGINES

**Martí Comamala Laguna**

Per citar o enllaçar aquest document:  
Para citar o enlazar este documento:  
Use this url to cite or link to this publication:  
<http://hdl.handle.net/10803/668142>



<http://creativecommons.org/licenses/by/4.0/deed.ca>

Aquesta obra està subjecta a una llicència Creative Commons Reconeixement

Esta obra está bajo una licencia Creative Commons Reconocimiento

This work is licensed under a Creative Commons Attribution licence



**DOCTORAL THESIS**

---

**“DEVELOPMENT AND CHARACTERIZATION OF  
THERMOELECTRIC GENERATORS FOR THERMAL  
ENERGY RECOVERY FROM RECIPROCATING  
INTERNAL COMBUSTION ENGINES”.**

---

*MARTÍ COMAMALA LAGUNA*

2019

Technology Doctoral Program

Directed by:  
Dr. José Ramón González Castro  
Dr. Lino Montoro Moreno



# Compendium of publications

This Ph.D. Thesis has produced a collection of published articles which are included in the document. The results section of this thesis is formed by the three original papers that have published in peer-reviewed journals. The impact factors of the journals are from the first and the second quartiles, according to the Journal Citation Reports (JCR) for the year 2018, for the subject categories *Energy and Fuels*.

The complete reference of the papers and the impact factor of the journals are:

- M Comamala, I Ruiz, A Massaguer, E Massaguer, T Pujol. **Effects of design parameters on fuel economy and output power in an automotive thermoelectric generator.** *Energies*, 11, 3274, 2018. ISSN 1996-1073 (Impact factor 2.676; Journal 48 of 97; 2nd quartile; Energy and Fuels)
- M Comamala, T Pujol, I Ruiz, E Massaguer, A Massaguer. **Power and Fuel Economy of a Radial Automotive Thermoelectric Generator: Experimental and Numerical Studies.** *Energies*, 11, 2720, 2018. ISSN 1996-1073 (Impact factor 2.676; Journal 48 of 97; 2nd quartile; Energy and Fuels)
- M. Comamala, A Massaguer, E Massaguer, T. Pujol. **Validation of a fuel economy prediction method based on thermoelectric energy recovery for mid-size vehicles.** *Applied Energy*. *Energies* 2018, 11(10), 2720 ISSN 0306-2619 (Impact factor 7,182; Journal 6 of 92; 1st quartile; Energy and Fuels)



Universitat de Girona  
**Departament d'Enginyeria Mecànica  
i de la Construcció Industrial**

El Dr. Josep Ramon Gonzalez Castro amb DNI 40311653J i el Dr. Lino Montoro Moreno amb DNI 23009352Z com a directores de la tesi doctoral del Sr Martí Comamala Laguna,

Exposen:

Que consideren idònia la presentació de la tesi doctoral titulada "Desenvolupament i caracterització de generadors termoelectrics per a recuperació d'energia tèrmica residual de motors de combustió interna alternatius" realitzada pel Sr. Martí Comamala Laguna dins del Programa de Doctorat en Tecnologia en format de compendi de publicacions.

Que la contribució específica del doctorand a les publicacions en què es basa la tesi és la següent:

Article: M Comamala, T Pujol, I Ruiz, E Massaguer, A Massaguer. Power and fuel economy of a radial automotive thermoelectric generator: experimental and numerical studies. *Energies*, **11**, 2720, 2018. ISSN 1996-1073 (Factor d'impacte: 2,676; Journal 48 de 97; 2n quartil a la categoria Energy and Fuels)

Contribució del doctorand: Realització de l'estudi experimental incloent la posada a punt del banc motor. Contribució en el desenvolupament i validació del model de simulació. Anàlisi de les dades i redacció de la major part de l'article.

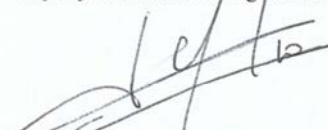
Article: M Comamala, I Ruiz, A Massaguer, E Massaguer, T Pujol. Effects of design parameters on fuel economy and output power in an automotive thermoelectric generator. *Energies*, **11**, 3274, 2018. ISSN 1996-1073 (Factor d'impacte: 2,676; Journal 48 de 97; 2n quartil a la categoria Energy and Fuels)

Contribució del doctorand: Realització de l'estudi experimental incloent la posada a punt del banc motor, del banc de flux i del dispositiu d'assaig de mòduls termoelectrics. Desenvolupament i validació del model de simulació. Anàlisi de les dades i redacció de la major part de l'article.

Article: M Comamala, A Massaguer, E Massaguer, T Pujol. Validation of a fuel economy prediction method based on thermoelectric energy recovery for mid-size vehicles. Enviat a *Applied Energy*. ISSN 0306-2619 (Factor d'impacte: 7,182; Journal 6 de 92; 1r quartil a la categoria Energy and Fuels)

Contribució del doctorand: Col·laboració en el disseny i fabricació del nou ATEG. Col·laboració en el dissenys del test experimental. Anàlisi de les dades. Redacció de la major part de l'article.

I, perquè així consti i tingui els efectes oportuns, signem aquest document,



Josep Ramon Gonzalez Castro



Lino Montoro Moreno

Girona, 17 de desembre de 2018

Escola Politècnica Superior - Edifici P-II  
17071 Girona  
Tel. 972 41 83 84  
Fax 972 41 80 98  
dir.depemci@udg.edu

# Nomenclature

$A$	area of the aluminum channel in contact with water ( $m^2$ )
$A_b$	block surface area ( $mm^2$ )
$A_{TEM}$	TEM surface area ( $mm^2$ )
$D$	diameter of the cylindrical holes (m)
$F_e$	fuel economy (%)
$F_{e,ATEG}$	fuel economy resulting from the power generated by the ATEG (%)
$F_{e,BP}$	fuel consumption due to overcome the back pressure (%)
$F_{e,m}$	fuel consumption due to increase in weight (%)
$g$	acceleration of gravity ( $m \cdot s^{-2}$ )
$h$	heat transfer coefficient ( $W \cdot K^{-1} \cdot m^{-2}$ )
$I_{TEM}$	electrical current (A)
$k_b$	block thermal conductivity ( $W \cdot K^{-1} \cdot m^{-1}$ )
$k_e$	TEM effective thermal conductivity ( $W \cdot K^{-1} \cdot m^{-1}$ )
$L$	height of the cooling channel (mm)
$L_b$	block height (mm)
$L_{TEM}$	TEM height (mm)
$m_{ATEG}$	ATEG mass (kg)
$\dot{m}_g$	exhaust gas mass flow rate ( $g \cdot s^{-1}$ )
$N$	number of samples in the data series
$P_{ATEG}$	ATEG electrical output power (W)
$P_e$	engine-shaft power (W)
$P_{n,ATEG}$	net ATEG electrical output power (W)
$P_{TEM}$	TEM electrical output power (W)
$P_{wp}$	power consumed by the water pump (W)
$Q_c$	heat flow on the cold side of the TEM (W)
$Q_h$	heat flow on the hot side of the TEM (W)
$r$	ratio of Figure of merit
$R_c$	thermal contact resistance (cold side) ( $m^2 \cdot K \cdot W^{-1}$ )

## Nomenclature

$R_h$	thermal contact resistance (hot side) ( $\text{m}^2 \cdot \text{K} \cdot \text{W}^{-1}$ )
$R_{ie}$	TEM effective internal electrical resistance ( $\Omega$ )
$R_L$	external electrical load resistance ( $\Omega$ )
$\bar{T}$	$(T_h + T_c)/2$ (K)
$T_c$	TEM cold side temperature ( $^{\circ}\text{C}$ )
$T_g$	exhaust gas temperature ( $^{\circ}\text{C}$ )
$T_h$	TEM hot side temperature ( $^{\circ}\text{C}$ )
$T_w$	coolant temperature ( $^{\circ}\text{C}$ )
$v$	vehicle velocity ( $\text{m} \cdot \text{s}^{-1}$ )
$V_{oc}$	open-circuit voltage (V)
$\dot{V}_w$	volumetric flow of the ATEG coolant ( $\text{L} \cdot \text{h}^{-1}$ )
$ZT_e$	effective Figure of merit
$z_{\alpha/2}$	confidence range
$\alpha_e$	TEM effective Seebeck coefficient ( $\text{V} \cdot \text{K}^{-1}$ )
$\Delta p_{bp}$	back pressure increase due to the ATEG (Pa)
$\varepsilon_e$	uncertainty of the equipment
$\varepsilon_s$	uncertainty of the mean values
$\varepsilon_t$	total uncertainty of data
$\eta$	ATEG efficiency
$\eta_G$	efficiency of the alternator
$\eta_{PCU}$	efficiency of the power converter unit
$\lambda$	air–fuel equivalence ratio
$\xi$	vehicle rolling resistance
$\rho_e$	effective electrical resistivity ( $\Omega \cdot \text{m}$ )
$\sigma$	standard deviation

## Subscript

i	inlet
max	maximum conditions
o	outlet

## Nomenclature

### *Abbreviations*

AFR	air–fuel ratio
AFR <sub>s</sub>	stoichiometric air–fuel ratio
ATEG	Automotive thermoelectric generator
CAE	computer-aided engineering
CI	compression ignition
CSHE	cold-side heat exchanger
EGR	exhaust gas recirculation
HDV	heavy-duty vehicle
HexS	hexagonal cross-section
HP	heat pipes
HSHE	hot-side heat exchanger
ICE	internal combustion engine
OctS	octagonal cross-section
PCU	power converter unit
SI	spark ignition
TEG	thermoelectric generator
TEM	thermoelectric module
2PP	two parallel plates
4SSP	four square section plates



## List of Figures

(Only concern to chapters 1, 5 and 6)

Figure 1.1 : Parts of an TEM and the energy flow in Seebeck mode.....	32
Figure 1.2 :ATEG engine installed (a). Parts of the ATEG (b) .....	35
Figure 1.3 : GTSUITE model for an complete SUV vehicle.....	37
Figure 1.4 : radial ATEG XUD7/K engine installed... ..	38
Figure 1.5 : New prototype of ATEG tested at IDIADA.....	40

## List of Tables

(Only concern to chapters 1, 5 and 6)

There are no tables on chapters 1, 5 and 6



*To my mother † and my father*





# Acknowledgements

This work would not have been possible without the support of some people that surround me, so in my personal life as with the professional. I would like to greatly thank the dedication and involvement of colleagues in the Fluid Mechanics - Thermal Engines Area , Drs. Toni Pujol, Albert Massaguer, Eduard Massaguer and Ivan Ruiz. To my thesis supervisors Drs. JRamon Gonzàlez and Lino Montoro who have been guided and animated in hard times, I thank them for their wise words and, above all, for the good atmosphere they have lived.

To my family for the patience shown and the moods they have given me at all times, especially to my wife Cristina for providing the necessary love in the difficult stages of this milestone.



# Contents

Compendium of publications .....	3
Nomenclature .....	5
List of Figures .....	9
List of Tables .....	10
Acknowledgements.....	13
Contents.....	15
Abstract.....	17
Resum .....	21
Resumen .....	25
Chapter 1 Introduction.....	29
1.1 Introduction .....	30
1.2 Objectives.....	41
1.3 Thesis organization .....	43
1.4 References .....	44
Chapter 2 Effects of Design Parameters on Fuel Economy and Output Power in an Automotive Thermoelectric Generator .....	47
Chapter 3 Power and Fuel Economy of a Radial Automotive Thermoelectric Generator: Experimental and Numerical Studies .....	77
Chapter 4 Validation of a fuel economy prediction method based on thermoelectric energy recovery for mid-size vehicles .....	101
Chapter 5 Results and discussion .....	115
Chapter 6 Conclusions .....	123



# Abstract

Since the beginnings of the automotive driven with internal combustion engines all the cycles used in the alternative motors share a thermal characteristic, a large amount of heat released by the fuel is lost in the form of hot gases that exits from the exhaust system. This characteristic would not be very relevant in stationary engines or even in marine propulsion, where by the characteristics of the site, the installation and above all the mode of operation at almost constant load of the engine it is possible to recover very efficiently part of this energy and transform it into a hot fluid in a liquid or vapor state that can be used for other purposes.

The heat recovering from exhaust gas is a milestone pursued by many manufacturers and researchers in the automotive field; this research has intensified in recent years due to the consequences of climate change, and above all, the Administration pressure on automotive manufacturers regarding the reduction of pollutant emissions, especially CO<sub>2</sub>.

A recovery heat system installed in a vehicle must meet certain technical requirements, should weigh less, it must be compatible with the rest of the vehicle's systems, it should require little maintenance and, finally, the product not should be very expensive.

The system proposed in this thesis uses the advantages that thermoelectricity can provide, a thermoelectric generator can meet the requirements mentioned above. The scope of application of thermoelectric materials is very large, from temperature sensors, through portable coolers, to solar power generators. In general, these applications can be classified according to the direction of the energy conversion. While the Peltier effect is used in solid-state refrigeration, the Seebeck effect is responsible for converting the temperature differences into electrical voltage in energy recovery systems.

The Seebeck effect is what our want to produce in a vehicle when you want to recover heat energy, because thanks to the thermoelectric materials the

electricity produced can be injected into the vehicle's electric system by reducing the load of the alternator and therefore the overall consumption of the thermal engine.

This doctoral thesis addresses aspects that until now had been little explored by the researchers: (i) the effects on the behavior of the motor when a new system is introduced in the exhaust line, (ii) the use of software sufficiently powerful to simulate the integration of the thermoelectric generator into a complete vehicle and (iii) the experimental quantification of the consumption savings when thermoelectric generators are incorporated.

The first part of the thesis is divided into three main research lines, the first one is predominantly experimental and focuses on studying a thermoelectric generator model (ATEG) that had already been used in previous research projects. In this part the ATEG is installed in a PSA XUD7 diesel engine and experimental data are obtained in 7 stationary operating points where the engine load, the exhaust gas flow rate and the exhaust gas temperature vary, allowing us to evaluate the thermal and electrical behavior of the generating system. In a complementary way, in this line it is necessary to build a thermoelectric module test apparatus since the data provided by the manufacturers do not coincide with those observed in the experiments.

In the second line of research mainly goal is the work of simulation and adjustments of thermal parameters. The software used is the GT-Suite, multi-physical software used by most engine and vehicle manufacturers around the world. It is the only one that can offer us a specific module of simulation of thermoelectric generators and that can then be incorporated into the model of a whole vehicle, including peripheral systems such as alternator, air conditioning, lubrication system, transmission system and cooling system.

The results of the simulation of the 7 stationary operating points show a very good correlation with the experimental data, showing a variation of less than 5% in the data of exhaust gas output temperature, ATEG cooling water temperature

and electric production. The validation of the model is assured.

The advantage of using software of these characteristics where the ATEG model construction is modular, scalable and parametric allows you to investigate different configurations of the generator with respect to those of the physical model. Different flow rates of cooling water, different contact area in the cold-side exchanger and different hot gas passage diameters in the hot-side exchanger are studied. On the one hand each of these parameters is optimized to obtain the maximum electrical power of the ATEG and on the other to achieve the minimum back pressure to the exhaust gases. The results are combined using empirical expressions obtained by other researchers and that configuration is obtained that would result in a minimum consumption.

The research demonstrates what was already suspected and was confirmed by the research of other members of our research group GREFEMA, the design of thermoelectric generators cannot focused exclusively on obtaining the maximum electrical power and that the thermoelectric modules used in the design should be chosen not depending on the maximum temperature they support, but on the combination between their conversion efficiency and the bearable temperature.

The second part of the doctoral thesis has two lines of research, firstly a new thermoelectric generator that offers lower back pressure, uses more efficient thermoelectric modules but with lower maximum admissible temperatures and is tested experimentally on a BMW X1 fuel petrol. Global design aims to reduce the thermal inertia of the whole. The tests are carried out under various stationary operating conditions and also following the new WLTC emission homologation cycle obtaining the thermal and electrical operating parameters of the new ATEG but above all the consumption of the vehicle with and without the device. Finally concluding this doctoral thesis, with the experimental results obtained and with the knowledge acquired in the previous studies of the author proposes a methodology to evaluate the performance of the ATEG and be able to predict the expected fuel savings.





# Resum

Des dels inicis de l'automoció propulsada amb motors de combustió interna tots els cicles emprats en els motors alternatius comparteixen una característica tèrmica, una gran quantitat de calor alliberada pel combustible es perd en forma de gasos calents que surten pel sistema d'escapament. Aquesta característica no seria tan rellevant en motors estacionaris o els emprats en propulsió marítima, on per les característiques de l'emplaçament, de la instal·lació i sobretot del modus de funcionament a càrrega quasi constant del motor és possible recuperar de forma molt eficient part d'aquesta energia i transformar-la en un fluid calent en estat líquid o vapor que pot ser utilitzat per altres usos tèrmics.

L'aprofitament energètic de la calor residual dels gasos d'escapament és una fita perseguida per molts fabricants i investigadors en el camp de l'automoció. Aquesta recerca s'ha intensificat en els últims anys motivada per les conseqüències del canvi climàtic, i sobretot, per la pressió de les administracions sobre els fabricants d'automoció pel que fa a la disminució de les emissions contaminants, especialment del CO<sub>2</sub>.

Un sistema d'aprofitament de calor residual instal·lat en un vehicle ha de complir certs requisits tècnics, ha de pesar poc, ha de ser compatible amb la resta de sistemes del vehicle, ha de necessitar poc manteniment i finalment ha d'encarir molt poc el producte.

El sistema proposat en aquesta tesi utilitza els avantatges que pot proporcionar la termoelectricitat, considerant que un generador termoelèctric pot satisfer els requisits esmentats anteriorment. L'àmbit d'aplicació dels materials termoelèctrics és molt gran, des de sensors de temperatura, passant per refrigeradors portàtils, fins a generadors d'energia solar. En general, aquestes aplicacions es poden classificar segons la direcció de la conversió energètica. Mentre l'efecte Peltier s'utilitza per refrigeració en estat sòlid, l'efecte Seebeck és responsable de convertir les diferències de temperatura en tensió elèctrica en sistemes de recuperació d'energia.

L'efecte Seebeck és el que interessa en un vehicle quan es vol recuperar energia calorífica, doncs gràcies als materials termoelèctrics l'electricitat produïda es pot injectar al sistema elèctric del vehicle reduint la càrrega de l'alternador i per tant el consum global del motor tèrmic.

Aquesta tesi doctoral aborda aspectes que fins ara havien estat molt poc explorats pels investigadors : (i) els efectes sobre el comportament del motor quan s'introdueix un sistema nou a la línia d'escapament, (ii) la utilització de software suficientment potent per simular la integració del generador termoelèctric en un vehicle complet, i (iii) la quantificació experimental de l'estalvi de consum quan s'incorporen generadors termoelèctrics.

La primera part de la tesi es divideix en tres línies d'investigació principals, la primera és predominantment experimental i es centra en estudiar un model de generador termoelèctric (TEG) que ja havia estat utilitzat en treballs d'investigació previs. En aquesta part el TEG s'instal·la en un motor dièsel PSA XUD7 i s'obtenen dades experimentals en 7 punts de funcionament estacionaris on es varia la càrrega del motor, el cabal i la temperatura de gasos d'escapament, que ens permeten avaluar el comportament tèrmic i elèctric del sistema generador. De forma complementària, durant la investigació en aquesta línia es va veure necessària la construcció d'un aparell de test de mòduls termoelèctrics donat que les dades proporcionades pels fabricants no coincidien amb les observades en els experiments.

En la segona línia d'investigació predomina el treball de simulació i ajustos de paràmetres tèrmics. El software utilitzat es el GT-Suite, un programari multi-físic que fan servir una bona part de fabricants de motors i vehicles a tot el món. És l'únic que ens pot oferir un mòdul específic de simulació de generadors termoelèctrics i que després es pot incorporar al model d'un vehicle sencer, incloent els sistemes perifèrics com ara alternador, aire condicionat, sistema de lubricació, sistema de transmissió i sistema de refrigeració.

Els resultats de la simulació dels 7 punts de funcionament estacionaris mostren una molt bona correlació amb les dades experimentals, mostrant una variació inferior al 5% en les dades de temperatura de sortida de gasos d'escapament, temperatura d'aigua de refrigeració del TEG i producció elèctrica. Gràcies a

l'elevada correlació entre les dades experimentals i les simulades es considera que els comportaments tèrmic i elèctric de les diferents variacions efectuades sobre el model serien reproduïts en un TEG real sempre i quan l'arquitectura proposada sigui similar a la utilitzada.

L'avantatge d'utilitzar un software d'aquestes característiques on es pot dissenyar un TEG modulable, escalable i parametritzable permet investigar diferents configuracions del generador respecte les del model físic. S'han dut a estudi diferents variants, cabals d'aigua de refrigeració, diferent àrea de contacte en el bescanviador de cara freda i diferents diàmetres de pas de gasos calents en el bescanviador de cara calenta. Per una banda cadascun d'aquests paràmetres s'optimitza per a obtenir la màxima potència elèctrica del TEG i per l'altra aconseguir la mínima contrapressió als gasos d'escapament. Els resultats es combinen utilitzant expressions empíriques obtingudes per altres investigadors i s'obté aquella configuració que en resultaria un mínim consum.

La investigació demostra el que ja es sospitava i s'estava confirmant gràcies a les investigacions d'altres membres del nostre grup de recerca GREFEMA, el disseny de generadors termoelèctrics no pot centrar-se exclusivament en l'obtenció de la màxima potencia elèctrica i que els mòduls termoelèctrics emprats en el disseny es poden escollir no tant en funció de la màxima temperatura que suporten sinó de la combinació entre la seva eficiència de conversió i la temperatura suportable.

La tercera línia d'investigació d'aquesta primera part pretén obtenir uns millors resultats gràcies a un disseny de TEG radial que es construeix i es prova experimentalment sobre el mateix motor PSA XUD7. Els resultats experimentals ens mostren comportaments molt similars als que s'havien observat en l'estudi anterior, el nivell de contrapressió generada a la línia d'escapament degut a la incorporació d'un TEG resulta determinant per a obtenir una reducció de consum real. Es proposa un paràmetre adimensional que serveixi per a determinar la validesa d'un generador termoelèctric si es vol instal·lar en un vehicle.

La segona part de la tesi doctoral té dues línies d'investigació, en primer lloc es construeix i es prova experimentalment sobre un BMW X1 de gasolina un nou

tipus de generador termoelèctric que ofereix menor contrapressió, utilitza mòduls termoelèctrics més eficients amb menors temperatures màximes admissibles i amb un disseny global que pretén disminuir la inèrcia tèrmica del conjunt. Les proves es realitzen sota varies condicions de funcionament estacionàries i també seguint el nou cicle d'homologació d'emissions WLTC obtenint els paràmetres tèrmics i elèctrics de funcionament del nou TEG fent èmfasi sobretot en el consum del vehicle amb i sense el dispositiu. Finalment, concloent aquesta tesi doctoral, amb els resultats experimentals obtinguts i amb els coneixements adquirits en els estudis previs l'autor proposa una metodologia per a avaluar el rendiment del TEG i poder predir l'estalvi de combustible esperat.

## Resumen

Desde los inicios de la automoción propulsada con motores de combustión interna todos los ciclos empleados en los motores alternativos comparten una característica térmica, una gran cantidad de calor liberado por el combustible se pierde en forma de gases calientes que salen por el sistema de escape. Esta característica no sería muy relevante en motores llamados estacionarios o incluso en propulsión marítima, donde por las características del emplazamiento, de la instalación y sobre todo del modo de funcionamiento a carga casi constante del motor es posible recuperar de forma muy eficiente parte de esta energía y transformarla en un fluido caliente en estado líquido o vapor que puede ser utilizado para otros fines.

El aprovechamiento energético del calor residual de los gases de escape es un hito perseguido por muchos fabricantes e investigadores en el campo de la automoción, esta investigación se ha intensificado en los últimos años motivada por las consecuencias del cambio climático, y sobre todo, por la presión de las administraciones sobre los fabricantes de automoción en cuanto a la disminución de las emisiones contaminantes, especialmente el CO<sub>2</sub>.

Un sistema de aprovechamiento de calor residual instalado en un vehículo debe cumplir ciertos requisitos técnicos, debe pesar poco, debe ser compatible con el resto de sistemas del vehículo, debe necesitar poco mantenimiento y finalmente ha de encarecer muy poco el producto.

El sistema propuesto en esta tesis utiliza las ventajas que puede proporcionar la termoelectricidad, un generador termoeléctrico puede satisfacer los requisitos mencionados anteriormente. El ámbito de aplicación de los materiales termoeléctricos es muy grande, desde sensores de temperatura, pasando por refrigeradores portátiles, hasta generadores de energía solar. En general, estas aplicaciones se pueden clasificar según la dirección de la conversión energética. Mientras el efecto Peltier se utiliza en refrigeración en estado sólido, el efecto Seebeck es responsable de convertir las diferencias de temperatura en tensión eléctrica en sistemas de recuperación de energía.

El efecto Seebeck es el que interesa producir en un vehículo cuando se quiere recuperar energía calorífica, pues gracias a los materiales termoeléctricos la electricidad producida se puede inyectar en el sistema eléctrico del vehículo reduciendo la carga del alternador y por tanto el consumo global del motor térmico.

Esta tesis doctoral aborda aspectos que hasta ahora habían sido muy poco explorados por los investigadores: (i) los efectos sobre el comportamiento del motor cuando se introduce un sistema nuevo en la línea de escape, (ii) la utilización de software suficientemente potente para simular la integración del generador termoeléctrico en un vehículo completo y (iii) la cuantificación experimental del ahorro de consumo cuando se incorporan generadores termoeléctricos.

La primera parte de la tesis se divide en tres líneas de investigación principales, la primera es predominantemente experimental y se centra en estudiar un modelo de generador termoeléctrico (ATEG) que ya había sido utilizado en trabajos de investigación previos. En esta parte el ATEG se instala en un motor diesel PSA XUD7 y se obtienen datos experimentales en 7 puntos de funcionamiento estacionarios donde se varía la carga del motor, el caudal de gases de escape y la temperatura de gases de escape, que nos permiten evaluar el comportamiento térmico y eléctrico del sistema generador. De forma complementaria, en esta línea se ve necesaria la construcción de un aparato de test de módulos termoeléctricos dado que los datos proporcionados por los fabricantes no coinciden con los observados en los experimentos.

En la segunda línea de investigación predomina el trabajo de simulación y ajustes de parámetros térmicos. El software utilizado es el GT-Suite, un software multi-físico que utilizan la mayor parte de fabricantes de motores y vehículos en todo el mundo. Es el único que nos puede ofrecer un módulo específico de simulación de generadores termoeléctricos y que luego se puede incorporar al modelo de un vehículo entero, incluyendo los sistemas periféricos tales como alternador, aire acondicionado, sistema de lubricación, sistema de transmisión y sistema de refrigeración.

Los resultados de la simulación de los 7 puntos de funcionamiento estacionarios muestran una muy buena correlación con los datos experimentales, mostrando una variación inferior al 5% en los datos de temperatura de salida de gases de escape, temperatura de agua de refrigeración del ATEG y producción eléctrica. La validación del modelo queda asegurada.

La ventaja de utilizar un software de estas características donde la construcción del modelo del ATEG es modulable, escalable y parametrizable permite investigar diferentes configuraciones del generador respecto a las del modelo físico. Se estudian diferentes caudales de agua de refrigeración, diferente área de contacto en el intercambiador de cara fría y diferentes diámetros de paso de gases calientes en el intercambiador de cara caliente. Por un lado cada uno de estos parámetros se optimiza para obtener la máxima potencia eléctrica del TEG y por el otro conseguir la mínima contrapresión a los gases de escape. Los resultados se combinan utilizando expresiones empíricas obtenidas por otros investigadores y se obtiene aquella configuración que resultaría en un mínimo consumo.

La investigación demuestra lo que ya se sospechaba y se estaba confirmando gracias a las investigaciones de otros miembros de nuestro grupo de investigación GREFEMA, el diseño de generadores termoeléctricos no puede centrarse exclusivamente en la obtención de la máxima potencia eléctrica y que los módulos termoeléctricos empleados en el diseño se deben escoger no en función de la máxima temperatura que soportan sino de la combinación entre su eficiencia de conversión y la temperatura soportable.

La tercera línea de investigación de esta primera parte pretende obtener mejores resultados gracias a un diseño de ATEG radial que se construye y se prueba experimentalmente sobre el mismo motor PSA XUD7. Los resultados experimentales muestran comportamientos muy similares a los que ya se habían observado en el estudio anterior, la contrapresión generada en la línea de escape debido a la incorporación de un TEG resulta determinante para obtener una reducción de consumo real. Se propone un parámetro  $P_n$ , ATEG / (VgDppb) que sirva para determinar la validez de un generador termoeléctrico si se quiere instalar en un vehículo.



La segunda parte de la tesis doctoral tiene dos líneas de investigación, en primer lugar se construye y se prueba experimentalmente sobre un BMW X1 de gasolina un nuevo generador termoeléctrico que ofrece menor contrapresión, utiliza módulos termoeléctricos más eficientes pero con menores temperaturas máximas admisibles y el diseño global pretende disminuir la inercia térmica del conjunto. Las pruebas se realizan bajo varias condiciones de funcionamiento estacionarias y también siguiendo el nuevo ciclo de homologación de emisiones WLTC obteniendo los parámetros térmicos y eléctricos de funcionamiento del nuevo ATEG pero sobre todo el consumo del vehículo con y sin el dispositivo. Finalmente concluyendo esta tesis doctoral, con los resultados experimentales obtenidos y con los conocimientos adquiridos en los estudios previos del autor propone una metodología para evaluar el rendimiento del ATEG y poder predecir el ahorro de combustible esperado.

## Chapter 1

### **Introduction**

---

## 1.1 Introduction

The mitigation of the effects of the consumption of fossil fuels is one of the main challenges that humanity is facing. In the European Union, 27% of carbon dioxide (CO<sub>2</sub>) emissions come from transport, which is also the main cause of air pollution in urban areas [1]. A value as high as 70% of these emissions come from road transport [2]. Therefore, the reduction of the level of emissions of road vehicles such as Light Duty Vehicles (LDVs), Light Commercial Vehicles (LCVs), Medium Duty Vehicles (MDVs) and High Duty Vehicles (HDVs) has a notable influence on public health, air quality and the consequences of climate change.

Environmental emission control regulations have made a significant change since 2000 to date with regard to the limits of regulated pollutants: CO<sub>2</sub>, non-burned hydrocarbons (HC), nitrogen oxides (NO<sub>x</sub>) and particulate matter (PM<sub>n</sub>) [3]. Manufacturers were able to adapt reasonably well to environmental regulations until about 2014, which was the time when Euro 6 regulations came into play in Europe [3]. In comparison with previous norms, the Euro 6 regulations were much stricter in terms of NO<sub>x</sub> and PM<sub>5</sub> light particles. This strongly questioned the long-term strategy planned years ago by many manufacturers based on downsizing [4], which, for an engine, means obtaining the same power but with less displacement. A common feature of the downsizing strategy is the addition of a supercharger in order to overcome the reduction in displacement. As a consequence, both pressure and temperature increase within the combustion chamber leading to substantial increases in NO<sub>x</sub> emissions. This is only an example of the current struggle between automotive technology and pollutant emissions.

Although the environmental benefits of stricter standards have been clearly demonstrated and technologies to achieve these benefits are readily available, there are still huge discrepancies about the timetables that should be applied in order to implement the increase of the severity of the emission limit values.

Among the reasons for postponing the application of these more stringent emission levels is the additional cost added to the vehicle due to the emission system control. For example, manufacturers estimate that for a LDV of 2.5 liters of total swept volume and diesel cycle, the economic cost of placing on the market a vehicle adapted to Euro 6 from Euro 5 supposes an increment of approximately 1500 € by unit [5].

It can be understood that vehicle manufacturers are looking for strategies with low technological cost in order to meet the new emission limits. Just a short time ago in a session of the "Fondo de Emprendedores" held at the headquarters of Repsol in Madrid, one of the speakers exposed a really impressive data: currently, the average cost in research to put on the market a given model of a LDV that lowers the level of emissions of 1 g / km of CO<sub>2</sub> only, is about 100 million euros. Since emission levels are directly related with fuel consumption, it is therefore interesting to find a technology that leads to fuel economy at a reasonable cost, with a fast implementation in the vehicle, a high compatibility with the rest of the vehicle systems, low maintenance and a low weight.

In internal combustion engines, approximately two thirds of the thermal energy of the fuel is lost as residual heat, with 40% of it in the form of exhaust gases [6]. Thus, only a small percentage of the energy provided by the fuel is used efficiently for the operation of the vehicle when it circulates in an urban or peri-urban environment although efficiency greatly improves when the vehicle can circulate to an almost constant load, such as HDVs on highways [7]. Some studies have shown that it would be possible to reduce fuel consumption by 10% if the conversion approximately 6% of the heat of exhaust in electrical energy [10]. As a result, the recovery of the residual heat of the internal combustion engine (ICE) shows a great potential in the energy saving and the reduction of emissions.

From the above, the recovery of residual heat from exhaust gases may play an important role in future strategies to reduce the fuel consumption and, hence, the pollutant emissions. Unfortunately, automobiles face two inherent problems: on the one hand, the operation at a variable load, especially on urban

routes, and, on the other hand, the fact of having a limited space to add novel technologies focused on maximizing the energy use.

The extraction of heat and/or of mechanical energy from the combustion gases that circulate through the exhaust system are not difficult tasks. In fact, they could be considered as simple problems of design of heat exchangers and turbomachines. For example, we can currently extract mechanical energy with high efficiency thanks to overcharging systems called turbochargers [8]. In these systems, and since the operating principle is based on taking advantage of the high pulse pressure and the high specific volumes of the combustion gases, the high energy remaining in the combustion gases is useful for the conversion of heat into electricity. The key question is whether the gain obtained with this energy recovery exceeds the loss caused by the incorporation of the system into the engine.

The energy recovery system proposed in this thesis is based on the thermoelectric effect. This phenomenon can be easily observed in commercial Thermal Electric Modules (TEMs). TEMs, as presented in Figure 1.1, are solid state systems that consist of a large number of p-type and n-type semiconductor elements that are electrically connected in series by metal interconnections. These semiconductors are physically located between two electrical insulators formed by ceramic substrates. TEMs can act as refrigerators (Peltier effect), heaters (Peltier effect), power generators (Seebeck effect) or thermal sensors (Seebeck effect) depending on its operation mode.

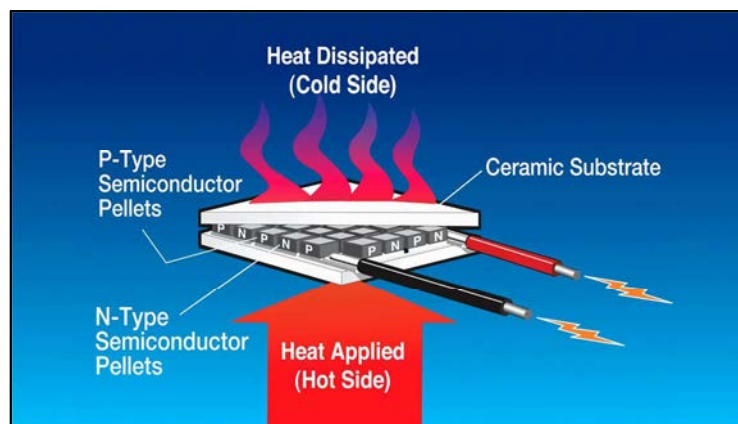


Figure 1.1: Parts of a TEM and the energy flow in Seebeck mode [9]

The application for energy use is done by installing an Automotive Thermal Electric Generator (ATEG) at the exhaust line of the vehicle. A thermoelectric generator is basically composed of a set of thermoelectric generators (TEGs) connected electrically in series, parallel or hybrid, and at the same time installed between two heat exchangers. The Hot Side Heat Exchanger (HSHE) is in charge of transmitting the heat from the exhaust gases to the warm face of the TEG and the Cold Side Heat Exchanger (CSHE) transports the heat towards a dissipation system. Thus, we obtain a temperature difference between the two faces of the TEGs that form the ATEG. The thermoelectric modules act in the generation mode and the electrical energy can be injected into the electric system of the vehicle. This allows the reduction of the operating time of the alternator and as a consequence a fuel consumption decrease is expected. In addition, ATEGs do not contain moving parts, are very reliable and silent, and TEGs are a mature technology. Therefore, converting this residual heat into electricity through thermoelectric generators seems, in principle, a very interesting option.

In recent years, numerous studies involving the development of ATEGs have been carried out in cooperation with several vehicle manufacturers, as described in Chapters 2 and 3. Most of them are theoretical studies and only a few have done experimental tests. Although these previous studies claim a great potential for the ATEG application in vehicles, there is still a substantial lack of information about its essential purpose: fuel economy. Indeed, most of the design studies of ATEGs made so far have only focused on generating the greatest possible amount of electrical energy, leaving the amount of fuel savings to speculation or simply ignoring it [11-14].

The general belief is that a greater generation of energy directly implies a greater saving of fuel, what we call "more is better". Based on recent studies carried out by the Research Group on Fluid, Energy and Environment (GREFEMA) of the University of Girona (UdG) [15-18], it has been shown that this statement is not entirely true. In some ATEG designs there is a clear incompatibility between increasing the electrical power obtained and increasing the fuel economy, as it is extensively explained in Chapters 2 and 3.

The main reason is that any system or device placed on the exhaust line of an alternative internal combustion engine produces an effect that is known by backpressure. This phenomenon arises due to the difficulty that the device creates to the exit of hot exhaust gases. The complete exhaust phase of the engines has two operating modes [6], initially when the exhaust valve opens, the gas output from the cylinder to the atmosphere is produced by the pressure difference between the internal gases and the environmental pressure. This is known as the spontaneous part of the exhaust period. Next, during the piston stroke between the bottom dead center (BDC) and the top dead center (TDC), the pressure inside the cylinder is very close to the atmospheric one and, therefore, the movement of the piston in its BDC-TDC travel pushes the gases towards the outside. This is known as the mechanical or forced mode of the exhaust period.

During the spontaneous exhaust period, the elements included in the exhaust line offer a restriction on the release of gases. In ATEGs, these elements include the HSHE. The effect on the engine during this period is diverse. In supercharged engines, the efficiency of the turbocharger is reduced and the capacity of the cylinder decreases. Therefore, a substantial amount of gases remains in the cylinder and a too high pressure is maintained inside it [6].

The effect of the backpressure during the period of mechanical exhaust results in a greater work needed by the piston when it comes to expelling the residual gases, which also leads to a lower efficiency of this emptying mode.

The deficiency of emptying capacity affects the volumetric performance of the engine, preventing the correct entry of fresh air and thus limiting the possibility of burning more fuel. This fact involves a decrease in power and, thus, it implies a greater fuel consumption.

The backpressure during the period of mechanical exhaust acts against the movement of the piston and thus reduces the efficiency of exhaust pumping, which also results in a decrease in power and an increase in fuel consumption.

Chapters 2 and 3 of this thesis show that choosing the best ATEG design is always a matter of compromise between producing as much electrical energy and the least possible backpressure. The design parameters of the ATEG such as

the exchange area, gas velocity, flow rate and coolant temperature or the heat transfer surface in the HSHE are key to achieve the best compromise. In addition, the parameters that affect the performance of the TEM such as the figure of merit  $ZT$ , the thermal contact resistance and the maximum admissible temperature also play an important role. The latter, however, mainly affect the properties of TEM and, therefore, the amount of electrical generation. The effects of the backpressure are independent of these factors since it only depends on the geometrical structure of the device.

From the above, we may conclude that: 1) most of previous studies of ATEGs have focused on obtaining the maximum power output, 2) the ATEG design that produces the maximum power output may not be the optimum in terms of reducing the fuel consumption and 3) the goal of an ATEG is to increase fuel economy while generating a non-negligible amount of electrical power. Thus, it was clear that we should analyze ATEG designs not only in terms of power generation but also in terms of fuel consumption.

The first ATEG design investigated in Chapter 2 is shown in Figure 1.2. It was installed at the exhaust line of a the XUD7 / K engine in the test bench of the Thermal Engine Laboratory of the Polytechnic School at the University of Girona (see Figure 1.2 (a)).

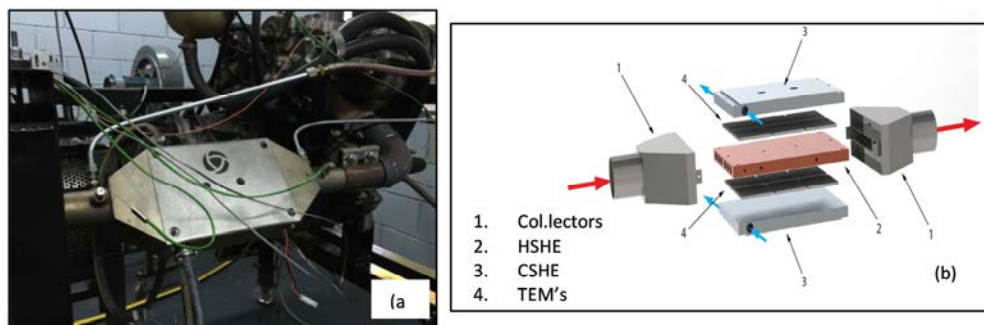


Figure 1.2: ATEG engine installed (a). Parts of the ATEG (b)

Figure 1.2 (b) shows the configuration of the ATEG tested according to the operating parameters specified in Chapter 2. The ATEG configuration is called a "sandwich type" since all the thermoelectric modules (# 4) located between the



HSHE (# 2) and the CSHE (# 3) were distributed in two parallel surfaces. The HSHE consisted of cylindrical holes.

Since the number of parameters involved in the design and subsequent assessment of the consumption savings of an ATEG installed in a vehicle is so large, we made use of a simulation tool that was validated with our experimental data. Simulations in Chapter 2 were carried out with the software GT-SUITE [20], which is a multi-physical CAE system with a broad implementation in industries of the automotive sector. GT-SUITE is made up of a set of libraries whose combination allows the simulation of fluid flows and their interactions with solid bodies, including the calculation of heat transfer mechanisms. This software has been used by other researchers in the study of the behavior of exhaust gases in ICEs analyzing, for example, the effects of the exhaust gas recirculation system in internal combustion engines, and investigating a variety of technologies of recovery of residual heat such as Organic Rankine Cycles (ORC), turbo-compounding and recently ATEGs [18, 21-23].

GT-SUITE's modeling methodology is based on linking several sub-models each one focused on solving a specific problem. Using combinations of these sub-models and libraries, one can build precise models of virtually any vehicle, including all of their subsystems under stationary or transient conditions, including homologation cycles.

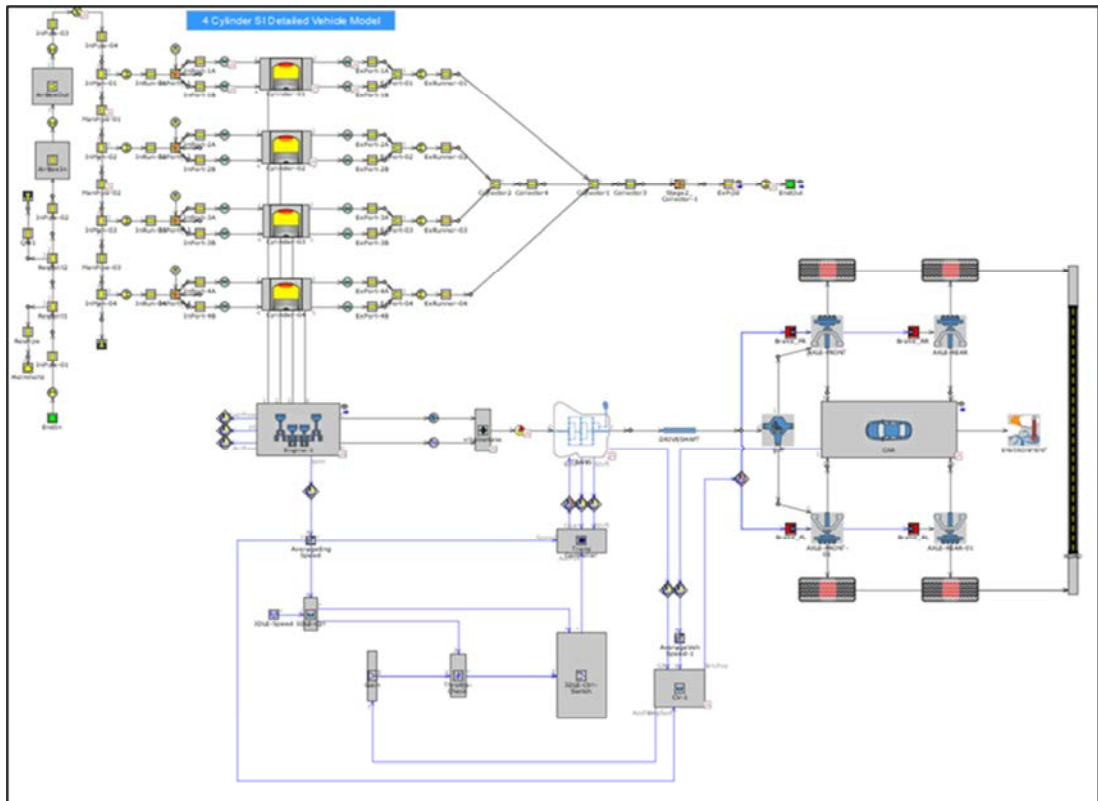


Figure 1.3: GT-SUITE model for a complete SUV vehicle

As an example of the GT-SUITE capabilities, Figure 1.3 shows the set of sub-models that form the complete model of a vehicle. The ATEG system is included as a part of the sub-model corresponding to the exhaust system and can be integrated perfectly into the whole set (linked, for example, to the electrical system). This simulation strategy gives an enormous advantage in terms of carrying out a global assessment of the consequences of installing an ATEG.

Here, we remark that the evaluation of fuel savings in a vehicle due to the implementation of an ATEG requires the knowledge of the behavior of the engine, the dynamics of the transmission system and the energy management of charging the battery.

The model in Figure 1.3 was used to integrate the ATEG described in Figure 1.2 in a vehicle. Although the model worked correctly, the simulation time in our computer facilities was extremely long (several weeks for a simulation of a single engine load operating point) due to the limited number of available licensees. Therefore, we opted to execute the ATEG model in "island" mode in

Chapter 2 (i.e., exhaust gas system). Under these conditions, simulations were faster and showed a very remarkable match with experimental data (temperatures, voltage, electrical current and power). Unfortunately, the “island” mode does not permit to evaluate fuel savings so these values were obtained after applying formulas extracted from [15-16]. The analysis was done varying different geometrical parameters of the ATEG.

Results from Chapter 2 indicated that backpressure effects were very important in HSHE with cylindrical holes, finally leading to negative fuel savings in almost all of the feasible geometrical configurations. In addition, temperatures at the hot side of the TEMs could be substantially high during some engine regimes and this could damage them.

Therefore, the next step was to design an ATEG that overcome the issues detected in Chapter 2. In chapter 3 we developed a new concept of ATEG specifically designed to work with low temperature TEMs. This radial ATEG allowed the use of environmental friendly TEMs (without Pb) and at the same time reduce the thermal stress of the device. On the other hand, the HSHE of this radial ATEG used fins instead of cylindrical holes in order to decrease the backpressure values. This new radial generator was experimentally tested in our test bench with the same engine used in Chapter 2 (XUD7 / K engine type). Figure 1.4 shows the thermoelectric device installed in the test engine.



Figure 1.4: Radial ATEG XUD7/K engine installed.

We selected 8 engine load stationary regimes that were representative of the expected working points. Experimental data were used to validate a numerical model that, now, was based on Computational Fluid Dynamics (CFD) technique. The CFD chosen was ANSYS-CFX®, commercial finite volume software that has the ability to correctly simulate the heat transfer between fluid flows and solid parts in complex 3D geometries. In comparison, GT-SUITE software (used in Chapter 2) adopts a 1D strategy that is suitable in simple geometries (such as the case of heat exchangers in cylindrical holes) but not so in relatively complex ones as in the radial ATEG where exhaust gases may circulate through the center of the duct without being in contact with the fins of the heat exchanger. The ANSYS-CFX® model developed in Chapter 3 was initially validated with our experimental data. Then, we modified some of the design parameters of the radial ATEG in order to investigate their effects on the electrical power output and fuel savings. The simulation technique reduced a lot the time spend in the analysis of alternative designs and allowed us to carry out sensitivity analyses of the main parameters that form the ATEG.

The global results found in Chapter 3 confirmed that a study of feasibility of an ATEG must implicitly accept two requirements: 1) electric output power above a given threshold value and 2) fuel savings above a given threshold value. The fulfilment of the last condition (fuel economy) implies, almost certainly, to satisfy the first one (achieve a minimum value of the electrical power). However, fulfilling the first condition (power) does not necessarily imply achieving a maximum of fuel savings. In comparison with Chapter 2, the ATEG design developed in Chapter 3 behaved much better with substantially smaller values of backpressure and, in some designs, generating fuel savings in few of the 8 operational points analyzed. Although the finned geometry employed in the hot heat exchanger was definitely a better option than the cylindrical holes of Chapter 2, the size of the radial ATEG was quite big and it did not include any active control of the exhaust gases in order to improve the power obtained. Besides that, a simulation of two radial ATEGs in series configuration along the exhaust pipe revealed a low efficiency in the total energy recovered, so this

configuration made sense with ATEGs with very few TEMs only. In addition, our previous studies did not integrate the electrical power into the car's electrical system.

Therefore Chapter 4 developed a new version of an ATEG aimed to overcome the problems detected in Chapters 2 and 3 taking advantage of the learnings gained from the previous experiences. We also searched for the integration of the ATEG into the car's electrical system since it has been estimated that with the technology currently available, an ATEG could reduce consumption by 1.5% [15] by means of reducing the alternator demand (which is responsible of the 3% - 11% of the total fuel consumption in a vehicle [5]). Thus, we tested a new ATEG whose generated power was injected into the electric energy management system of the vehicle.

The new ATEG design incorporated two fundamental design elements that we had already described above. On the one hand, the use of TEMs that works at a lower temperature on the hot side and have a better thermal-electric conversion performance. On the other hand, a hot heat exchanger design that offers a lower backpressure. This new design allowed the operation within the range of maximum energy conversion of the TEM, because it incorporated a by-pass system with a valve that graduated the flow at the exhaust gases. The valve operation depended on the value of the hot side TEM temperature. At the same time, the by-pass system derived all the gas flow through the center of the device in case that the hot side TEM temperature reached its upper limit, thus avoiding the destruction of the modules.



Figure 1.5: New prototype of ATEG tested at IDIADA.

The device was installed in a vehicle of the SUV category, a BMW X1 sDrive18i. It was tested at the facilities of IDIADA Automotive Technology S.A. The results of the tests carried out in 4 stationary operating points showed that the ATEG presented in chapter 4 achieved a maximum fuel savings value of 0.72%. The positive values of the fuel economy were obtained in the range of 4 to 70 mbar of backpressure value, with a generation of electrical energy of 30 W and above. From the experimental results, we were able to develop an analytical model for predicting the fuel economy provided by a given ATEG in terms of key design parameters. This model allows to easily obtaining the optimum design point that corresponds to the situation when the fuel economy of the vehicle reaches its maximum value. This model makes use of very interesting correlation between backpressure values and fuel savings, being validated with the experimental data here obtained.

## 1.2 Objectives

Until now, most of the previous researches on ATEGs have been focused on electrical power generation. However, the automotive sector seeks fuel savings, which is not necessarily correlated with electrical output power. Therefore, the main objective of the present thesis is to investigate the feasibility of ATEGs as devices to reduce the fuel consumption in automobiles.

This main objective has been pursued by 1) developing ATEG prototypes of increasing complexity that resolve the main drawbacks of the preceding studies and 2) proposing a general method to predict the capabilities of an ATEG to reduce the fuel consumption.

Thus, the first specific objective of this doctoral thesis has been to thoroughly study an ATEG with a hot side heat exchanger consisting of cylindrical holes in order to determine its capabilities not only in terms of power generation but also on fuel savings. In this case, we have focused on studying the thermal behavior, the fluid flow dynamics, the electrical output power and the variation of the fuel consumption of the ATEG prototype. Experimental data have been obtained from an experimental test on a XUD7 / K diesel engine.

The first specific objective has also included the validation of a 1D model of the ATEG developed with GT-SUITE software, which is a widely employed code in the automobile sector. The possibility to use GT-SUITE as a simulation tool of the ATEG device opens the possibility to carry out any change of the prototype with the aim of increasing the electrical generation and, particularly, the fuel economy.

The main drawbacks of the first ATEG developed have been 1) the high backpressure values reached and 2) the uncontrolled temperatures reached at the hot side of the thermoelectric modules (that can seriously damage the device and compromised its durability). Therefore, the second specific objective is to project and to build an ATEG with a different design than the first cylindrical prototype, which has a lower backpressure and also that it can work with lower temperature TEM modules. This new radial device has also been tested on the test bench with the same engine. Since the flow dynamics involved complex 3D features, the software used to simulate the behavior of this ATEG is ANSYS-CFX.

From the previous developments of an ATEG, the final specific objective is twofold: 1) to provide a method of calculation of the consumption of vehicles associated with the incorporation of an ATEG system in order to be able to discern if its installation is feasible and 2) to use specialized programs of simulation, to improve existing devices and to provide design recommendations for new ATEG devices.

### 1.3 Thesis organization

The background, objectives and organization of this thesis are included in Chapter 1. Then, as this thesis has been prepared as a compendium of publications reviewed by experts, Chapters 2, 3 and 4 contain a copy of the following published articles:

- (i) "Effects of Design Parameters on Fuel Economy and Output Power in an Automotive Thermoelectric Generator".
- (ii) "Power and Fuel Economy of a Radial Automotive Thermoelectric Generator: Experimental and Numerical Studies".
- (iii) "Validation of a fuel economy prediction method based on thermoelectric energy recovery for mid-size vehicles".

All of them follow a single thematic unit related to the study of the field of thermoelectricity applied to the automotive sector. The focus of this field is from an applied point of view, trying not only to understand the phenomenon in depth, but also to optimize it in each of its final applications. This thesis is introduced into two branches of this field, such as heat flow control and energy recovery in vehicles equipped with internal combustion engines.

The first article explores the possibilities of the use of specialized software for the resolution of one of the least studied fields on the subject, the actual saving of consumption and all the parameters involved.

The second article also focuses in the recovery of the residual heat of the automobile in order to increase fuel economy. Using the knowledge of previous studies, a radial ATEG was installed and tested on the test bench in a diesel-fueled combustion engine. Here the use of CFD-3D simulation software is also revealed as an important tool to obtain reliable results on reduction of consumption in the vehicle. Different virtual device configurations are studied in this chapter, with some of them implying reductions in fuel consumption.

The last article published (iii) is the logical result of the two previous ones. All the investigations carried out can be shaped and validated in a study that carries out a real experimentation in a vehicle where the energy produced by an ATEG of The last generation can be injected into the vehicle's electrical system. This



vehicle, also of last generation with regard to motorization and management of the intelligent charge of the battery, is a perfect platform to test our theories and investigations carried out until now.

Finally, Chapter 5 corresponds to the results and discussion section whereas the conclusions are found in Chapters 6.

## 1.4 References

- [1] European Environment Agency. <https://www.eea.europa.eu/data-and-maps/indicators/transport-emissions-of-greenhouse-gases/transport-emissions-of-greenhouse-gases-11> (accedida el 24 de noviembre de 2018)
- [2] European Commission. [https://ec.europa.eu/clima/policies/transport\\_en](https://ec.europa.eu/clima/policies/transport_en)
- [3] Blanco-Rodriguez, David. 2025 Passenger Car and Light Commercial Vehicle Powertrain Technology Analysis. FEV – Project-No. P33597/ Issue v03/ Report-No. 1/ ICCT
- [4] P. Leduc, B. Dubar, A. Ranini, and G. Monnier, "Downsizing of gasoline engine: An efficient way to reduce CO<sub>2</sub>emissions," *Oil Gas Sci. Technol.*, 2003.
- [5] F. P. Sanchez, A. Bandivadekar, and J. German, "Estimated cost of emission reduction technologies for LDVs," *Int. Counc. Clean Transp.*, no. March, pp. 1–136, 2012.
- [6] J. B. Heywood, "Internal Combustion Engine Fundamentals", vol. 21. 1988.
- [7] A. F. Agudelo, R. García-Contreras, J. R. Agudelo, and O. Armas, "Potential for exhaust gas energy recovery in a diesel passenger car under European driving cycle," *Appl. Energy*, vol. 174, pp. 201–212, 2016.
- [8] H. L. Talom and A. Beyene, "Heat recovery from automotive engine," *Appl. Therm. Eng.*, vol. 29, no. 2–3, pp. 439–444, 2009.
- [9] <https://www.youtube.com/watch?v=YhynSkFIJOs>
- [10] Vázquez, J.; Palacios, R.; Sanz-Bobi, M.A. "State of the art of thermoelectric generators based on heat recovered from the exhaust gases of automobiles". 7th European Workshop on Thermoelectrics, Pamplona, Spain, October 2002.
- [11] Stobart, R.; Wijewardane, M.A.; Yang, Z. "Comprehensive analysis of thermoelectric generation systems for automotive Applications". *Appl. Therm. Eng.* 2017, 112, 1433-1444.

- [12] Matsubara, K. "Development of a high efficient thermoelectric stack for a waste exhaust heat recovery of vehicles". 21st International Conference on Thermoelectronics, Proceedings ICT, 2002, 418-423.
- [13] Kim, T.Y.; Kwak, J.; Kim, B-W. "Energy harvesting performance of hexagonal shaped thermoelectric generator for passenger vehicle applications: An experimental approach". *Energ. Convers. Manage.* 2018, 160, 14-21.
- [14] Orr, B.; Akbarzadeh, A.; Lappas, P. "An exhaust heat recovery system utilizing thermoelectric generators and heat pipes". *Appl. Therm. Eng.* 2017, 126, 1185-1190.
- [15] A. Massaguer, E. Massaguer, M. Comamala, T. Pujol, L. Montoro, D. Carbonell, and A. Bueno, "Transient behavior under a normalized driving cycle of an automotive thermoelectric generator," *Appl. Energy*, vol. 206, pp. 1282–1296, 2017.
- [16] A. Massaguer, E. Massaguer, M. Comamala, T. Pujol, J. R. González, M. D. Cardenas, D. Carbonell, and A. J. Bueno, "A method to assess the fuel economy of automotive thermoelectric generators," *Appl. Energy*, vol. 222, no. March, pp. 42–58, 2018.
- [17] E. Massaguer, A. Massaguer, L. Montoro, and J. R. Gonzalez, "Modeling analysis of longitudinal thermoelectric energy harvester in low temperature waste heat recovery applications," *Appl. Energy*, vol. 140, pp. 184–195, 2015.
- [18] Cózar, I.R.; Pujol, T.; Lehocky, M. "Numerical analysis of the effects of electrical and thermal configurations of thermoelectric modules in large-scale thermoelectric generators". *Appl. Energ.* 2018, 229, 264-280.
- [19] Karri, M.A.; Thacher, E.F.; Helenbrook, B.T. "Exhaust energy conversion of thermoelectric generator: Two case studies". *Energ. Convers. Manage.* 2011, 52, 1596-1611.
- [20] Gamma Technologies LLC. <https://www.gtisoft.com>
- [21] Su, J.; Xu, M.; Li, T.; Gao, Y.; Wang, J. "Combined effects of cooled EGR and a higher geometric compression ratio on thermal efficiency improvement of a downsized boosted spark-ignition direct engine". *Energ. Convers. Manage.* 2014, 78, 65-73.

[22] Zhao, R.; Li, W.; Zhuge, W.; Zhang, Y.; Yin, Y. "Numerical study on steam injection in a turbo compound diesel engine for waste heat recovery". *Appl. Energ.* 2017, 185, 506-518.

[23] Zhao, M.; Wei, M.; Song, P.; Liu, Z.; Tian, G. "Performance evaluation of a diesel engine integrated with ORC System". *Appl. Therm. Eng.* 2017, 115, 221-228.

[24] Ming, T.; Wang, Q.; Peng, K.; Cai, Z.; Yang, W.; Wu, Y.; Gong, T. "The influence of non-uniform high heat flux on thermal stress of thermoelectric power generator". *Energies* 2015, 8, 12584–12602.

## Chapter 2

# Effects of Design Parameters on Fuel Economy and Output Power in an Automotive Thermoelectric Generator

---

This chapter is the transcription of the content of the following article:

M Comamala, I Ruiz, A Massaguer, E Massaguer, T Pujol. **Effects of design parameters on fuel economy and output power in an automotive thermoelectric generator.** *Energies*, 11, 3274, 2018. ISSN 1996-1073 (Impact factor 2.676; Journal 48 of 97; 2nd quartile; Energy and Fuels)  
<https://doi.org/10.3390/en11123274>





Article

# Effects of Design Parameters on Fuel Economy and Output Power in an Automotive Thermoelectric Generator

Martí Comamala <sup>1</sup>, Ivan Ruiz Cózar <sup>1</sup>, Albert Massaguer <sup>2</sup>, Eduard Massaguer <sup>1</sup> and Toni Pujol <sup>1,\*</sup>

<sup>1</sup> Department of Mechanical Engineering and Industrial Construction, University of Girona, 17003 Girona, Spain; marti.comamala@udg.edu (M.C.); ivan.ruiz@udg.edu (I.R.C.); eduard.massaguer@udg.edu (E.M.)

<sup>2</sup> Nabla Thermoelectrics, c/Llibertat 71, 17820 Banyoles, Spain; albert@nablatherm.com (A.M.)

\* Correspondence: toni.pujol@udg.edu; Tel.: +34-686-724-750

Received: 4 November 2018; Accepted: 21 November 2018; Published: 23 November 2018

**Abstract:** The need for more sustainable mobility promoted research into the use of waste heat to reduce emissions and fuel consumption. As such, thermoelectric generation is a promising technique thanks to its robustness and simplicity. Automotive thermoelectric generators (ATEGs) are installed in the tailpipe and convert heat directly into electricity. Previous works on ATEGs mainly focused on extracting the maximum amount of electrical power. However, the back pressure caused by the ATEG heavily influences fuel consumption. Here, an ATEG numerical model was first validated with experimental data and then applied to investigate the effects that modifying the main ATEG design parameters had on both fuel economy and output power. The cooling flow rate and the geometrical dimensions of the heat exchanger on the hot side and the cold side of the ATEG were varied. The design that produced the maximum output power differed from that which maximized fuel economy. Back pressure was the most limiting factor in attaining fuel savings. Back pressure values lower than 5 mbar led to a <0.2% increase in fuel consumption. In the ATEG design analyzed here, the generation of electrical output power reduced fuel consumption by a maximum of 0.5%.

**Keywords:** thermoelectric generator; ATEG; waste heat recovery; fuel economy

## 1. Introduction

Approximately 60% of the primary energy consumed in an internal combustion engine (ICE) is dissipated through the exhaust gases and the cooling system [1]. If 6% of the exhaust heat were converted into electricity, fuel consumption would be reduced by 10% [2]. Therefore, policies toward greener and more sustainable mobility are actively promoting research programs into increasing fuel savings through heat recuperation [3]. This strategy is especially important when dealing with heavy-duty vehicles because, for long-distance transport, ICEs will continue to be the main powertrain for the mid-term future.

Among different waste heat recovery techniques, thermoelectric generators (TEGs) have many advantages: light weight, simple structure, high reliability, and quiet operation. The core of a TEG is composed of thermoelectric modules (TEMs) that directly convert heat flow rate into electric power. Heat exchangers found on both the hot and cold sides of the TEMs guarantee heat transfer. TEGs installed in ICEs use one heat exchanger that absorbs heat from the exhaust gases and another that delivers it either to the engine coolant fluid or to an independent cooling system.

Automotive thermoelectric generators (ATEGs) are TEGs built into road vehicles. ATEGs are an optimistic prospect as waste heat recovery systems [4]. Several vehicle manufacturers cooperated with researchers to study the potential ATEGs have in terms of fuel savings and emission reductions (e.g., the heavy-duty vehicle data in Table 1). The additional supply of energy from ATEGs to the

vehicle’s electrical system shortens alternator demand time and this reduces the engine torque employed to move auxiliaries. Therefore, fuel consumption is expected to decrease. Consequently, experimental tests on ATEGs mainly focused on the amount of electrical power that is generated (Table 1, References [5–17], listed in order of engine displacement, from smallest to greatest). A detailed discussion of the major findings of these previous studies, including the main gaps detected in the state of the art, is outlined in a separate section (Section 2).

**Table 1.** Exhaust gas temperature at automotive thermoelectric generator (ATEG) inlet  $T_{g,i}$ , coolant temperature at ATEG inlet  $T_{w,i}$ , ATEG mass  $m_{ATEG}$ , ATEG electrical output power  $P_{ATEG}$ , and fuel economy  $F_e$  attributable to the ATEG at its best performance point in experimental studies.

Engine <sup>1</sup>	ATEG Design <sup>2</sup>	Number of TEMs <sup>3</sup>	$T_{g,i}$ (°C)	$T_{w,i}$ (°C)	$m_{ATEG}$ (kg)	$P_{ATEG}$ (W)	$F_e$ (%)	Reference
1.4 L SI	2 PP	12	709	74	7	111		[5]
1.6 L SI	2 PP	80	719	50		137	1.1*	[6]
1.8 L CI	Radial	10	540	28	4.8	40	0.0*	[7]
1.8 L CI	2 PP	12	526	34	7	64	0.0*	Present
1.9 L CI	4 SSP	8	427	7		30		[8]
2.0 L SI		20	650	25		266		[9]
2.0 L SI	HexS	18	611	80		99		[10]
3.0 L SI	HP	8	350	30		38		[11]
3.7 L CI		6	650	30		42		[12]
3.9 L CI	2 PP	240	290	80	200	618		[13]
5.3 L SI	2 PP	16	550	88	40	177	2.0 ± 1.5	[14]
6.6 L CI	2 PP	4	200	10		8		[15]
HDV CI	2 PP	224		80		416		[16]
14 L CI	OctS	72				1068		[17]

<sup>1</sup> SI = spark ignition; CI = compression ignition; HDV = heavy-duty vehicle (engine not specified). <sup>2</sup>

2PP = two parallel plates; 4SSP = four square section plates; HexS = hexagonal section; OctS = octagonal section; HP = heat pipes. <sup>3</sup>TEM = thermoelectric module. \*Data obtained from numerical calculations

However, other factors also affect fuel savings, the most important one being the increase in back pressure caused by the partial blockage of the flow of exhaust gases due to the heat absorber [18]. As a result, engine efficiency decreases because extra mechanical energy is required to overcome this restriction. Since the main purpose of an ATEG is to increase fuel savings, the best ATEG design will be found in a compromise between high power generation and low back pressure.

Experimental results rarely provide information on fuel economy due to the inherent difficulties in measuring it accurately enough to be conclusive (see, e.g., Table 1). Nevertheless, Karri et al. [19] proposed a simplified method of calculating the expected fuel economy of an ATEG, and this can be used to estimate the fuel savings in laboratory tests or simulations.

Thus, determining how the main design parameters of an ATEG can modify fuel consumption is of great interest. Hence, the objective of the present work was to analyze what effect changing the hot- and cold-side exchange areas and the coolant flow rate have on both output power and fuel economy for different engine operating points. The final target was to provide a design rule for ATEGs, focused on maximizing fuel savings rather than output power.

The structure of the paper is as follows: Section 2 discusses the relevant literature in more detail. Section 3 describes the experimental study of an ATEG installed in an engine test bench. The numerical model of the ATEG is detailed in Section 4, where laboratory data were employed to validate it. The results of the numerical model obtained by varying the main design parameters of the ATEG are shown and discussed in Section 5. Finally, the main conclusions of the present work are listed in Section 6.

## 2. Thermoelectric Generators

Electrical generation by thermoelectricity has many fields of application [20]. TEGs were used as reliable sources of electrical energy in extreme environments [21] and in remote areas for off-grid micro generation [22]. Very recently, novel designs increased the energy efficiency of solar TEGs that

include solar concentrators with flat-plate micro-channel heat pipes [23]. This technology significantly reduces the cost of previous higher-performing solar TEG layouts [24]. These thermoelectric energy converters can be successfully integrated into photovoltaic panels [25], as well as low-temperature thermal solar collectors [26], as devices to harness dissipated heat, transform it into electrical energy and, hence, increase the system's overall efficiency.

However, it is in ICEs where TEGs are expected to play a major role as waste heat recovery devices [20]. Although there are some studies on TEGs in continuous combustion ICEs [27], the principal application is focused on reciprocating ICEs in automobiles. Studies on ATEGs are carried out both numerically and experimentally. The latter requires engine test benches and prototypes with designs that may be far from the optimum. Therefore, many efforts are devoted to providing information on how to improve ATEG design.

In their laboratory experiment, Fernández-Yañez et al. [6] used an optimized internal geometry of the hot-side heat exchanger, concluding that, among the four geometries analyzed, the flat plate with straight fins had the highest heat transfer ratio vs. back pressure values [28]. However, when this design was installed in the exhaust of a 1.6-L spark ignition (SI) engine, it generated excessive losses (>1 kW at engine speed >3500 rpm). As expected, these power losses behaved with a quadratic growth in terms of engine speed; thus, the authors proposed a partial by-pass as the most effective strategy of reducing back pressure values while maintaining a reasonably high value of ATEG energy generation [6]. A similar conclusion was drawn by Massaguer et al. [5], who employed the same ATEG design as the one used in the present paper, but in a 1.4-L spark ignition engine instead of the 1.8-L compression ignition engine tested here.

In the search for a methodology to correctly include the properties of the hot heat exchanger, Stobart et al. [8] validated a numerical model of an ATEG with experimental data and tested it under different conditions to develop a simplified model. The results showed different power production from the TEMs depending on the non-uniform heat flux received, as already noted by Li et al. [29]. These uneven values of absorbed heat flux occur in the direction of the exhaust flow because of the decrease in available exhaust gas energy and on a perpendicular plane to the direction of the exhaust flow due to the non-symmetrical design of the ATEG. Thus, although the plate-fin heat exchanger configuration for the heat absorber on the hot side appears as the preferred one in many studies [8,9], the temperature distribution at the flat surface in contact with the TEMs is far from being uniform [28]. Therefore, ATEG designs with cross-sectional areas of regular polygons were proposed (squared [8], hexagonal [10], and octagonal [17]).

The design of the heat exchanger must not only provide a high heat transfer, but also a low pressure drop. Kim et al. [10] determined that the pressure drop through a hexagonal cross-sectional ATEG with a finned hot heat exchanger was mainly due to the flow diversion at the ATEG inlet and outlet, causing more than 80% of the total energy loss at high engine regimes. Very low pressure drops can be achieved when heat pipes instead of fins are used as heat absorbers [11]. Orr et al. [11] recorded pressure differences of only 135 Pa through the ATEG at the maximum engine load (4000 rpm and mass flow rate not specified). However, the volume limitations of an assembly using heat pipes limit the application of this solution for high-output-power devices since tens or even hundreds of TEMs would be required.

Haidar and Ghojel [12] identified the relevance of the thermal contact resistance between TEMs' hot and cold sides and their corresponding heat exchangers. The use of thermal spreaders, as well as practical constraints in terms of the location where the ATEG can be effectively mounted in the engine, may reduce the available temperature anticipated on the hot side [12]. A strategy intended to maintain the uniformity of the working conditions for each one of the TEMs that forms an ATEG consists of dividing the whole system into identical subassemblies that are mounted in parallel along the exhaust line [13]. Wang et al. [13] applied this methodology to build an ATEG with four plate heat exchangers, each one with 60 TEMs. They reported that the inner structure that provided the best heat transfer with the lowest pressure drop, was the one that used dimples instead of fins. However, small differences in the manifold length, assembly, etc. may cause large variations in the



exhaust mass flow rate and exhaust gas temperature between each one of the four identical subATEGs, clearly compromising the overall performance of the system.

In addition to the hot heat exchanger, the design of the cold-side heat exchanger is also critical for reaching high electrical output power values. Thacher et al. [14] experimentally found that decreasing the cold-side temperature from 90 to 30 °C resulted in a 25% increase in electrical power. They also found that, when using the engine's own cooling system, the extra load added for cooling the ATEG was not significant [14]. These authors reported experimentally derived fuel savings, although the scatter of these experimental data was substantial (see Table 1).

Installing ATEGs in the exhaust gas recirculation (EGR) system (rather than in the exhaust pipe past the after-treatment system) is one alternative to recovering heat. Lan et al. [15] analyzed this possibility in a large displacement engine. In heavy-duty vehicles, ATEGs can be installed in both exhaust and EGR systems [16,30], with a combined output power of 1 kW in a system fully integrated into the electronic controls of the vehicle. However, fuel savings were not reported.

The above analyses of previous experiments clearly indicate that ATEG performance is highly dependent on the design of both the hot and cold side heat exchangers. That said, very few studies addressed the issue of developing a tool to optimize these designs. In some cases, a set of alternative options (i.e., heat exchanger designs) were predefined and analyzed by comprehensive numerical models [28]. Studies exclusively focused on simulations were also carried out (e.g., References [31–33]), although the numerical models developed are difficult to implement in a real ATEG environment (e.g., including feedback from the electric vehicle system, with the engine response to back pressure, etc.), thereby becoming, in some cases, mere academic studies.

Indeed, any methodology aimed at improving ATEG design should be focused on facilitating its implementation for the key players in the automotive sector. For this reason, some research groups validate models developed with the software solutions widely employed by vehicle manufacturers and automotive suppliers. This is also the aim of the present paper which develops a procedure using the GT-SUITE software (version 2018, Gamma Technologies LLC., Westmont, IL, USA) [34]. The methodology describes how to correctly define the ATEG device within the GT-SUITE environment and makes it possible to automatize the search for key design parameters that maximize fuel savings and/or electrical output power. We point out that, in contrast to the studies mentioned above that analyze several real ATEG design alternatives, our methodology fixes the design and searches for the values of the parameters that will meet our target. Here, these key design parameters correspond to the main geometrical dimensions of an ATEG with cylindrical holes in the hot heat exchanger (diameter) and a rectangular cross-sectional wavy channel in the cold heat exchanger (channel height), and to the coolant flow rate.

### 3. Experimental Analysis

#### 3.1. Automotive Thermoelectric Generator

The ATEG employed in our study was previously tested in experimental studies with a spark ignition engine under stationary [18] and normalized driving cycle conditions [5]. These previous studies led to the development of an analytical method to assess the variation in fuel consumption when an ATEG is installed in a vehicle [18]. However, the ATEG used in References [5,18] might have been working in far from optimum conditions since there was no information on how changes to its key design parameters would affect its performance. Therefore, our objective was to validate a numerical model of the ATEG to improve its design by investigating the consequences of varying the most relevant design parameters, as described next.

The heat absorber or hot-side heat exchanger (HSHE) of this ATEG consisted of a 210 × 140 × 15 mm (length × width × height) copper plate with six cylindrical holes 12 mm in diameter (#1 in Figure 1a). A total of 12 commercial TEMs (TELBP1-12656-0.45, Thermonamic Electronics Corp., Ltd., Nanchang, China)—six TEMs each for the upper and lower faces of the heat absorber (#2 in Figure 1a)—were installed in the ATEG. On each face, the six TEMs were distributed in two rows (aligned with the direction of the exhaust gases) and three columns (perpendicular to the direction of the

exhaust gases). The dimensions of a single TEM were  $56 \times 56$  mm (length  $\times$  width) with a total surface area of  $A_{TEM} = 3136$  mm<sup>2</sup> and total height of  $L_{TEM} = 5$  mm. Each TEM was formed by 116 small legs of thermoelectric material (PbTe and BiTe based). These TEMs can cope with hot-side temperatures of 360 °C and, occasionally, of 400 °C.

The cold side of the TEMs was in contact with an aluminum block or cold-side heat exchanger (CSHE; #3 in Figure 1a), that acted as a heat sink since water flowed in a wavy path within it (Figure 1b). The rectangular cross-sectional area of the water channel was  $12 \times 10$  mm (height  $\times$  width). Both the upper and lower cooling blocks were clamped together to provide the pressure required on the faces of the TEMs (1.27 MPa). Since the TEMs used a graphite sheet on both the cold and hot sides, no additional thermal interface material was required to improve heat transfer.

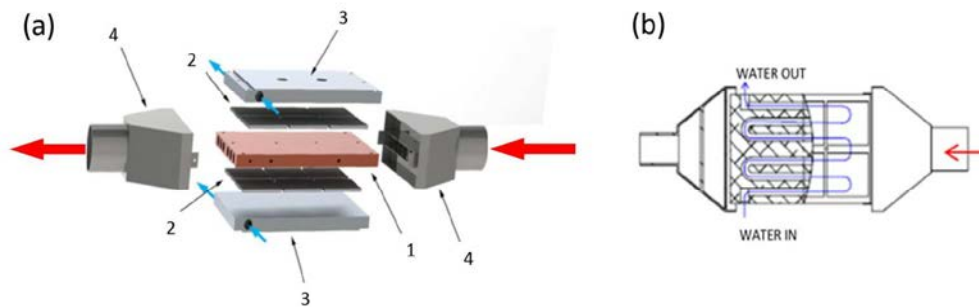


**Figure 1.** (a) Main elements of the automotive thermoelectric generator (ATEG; slightly modified from Reference [5]); (b) water channel path.

The HSHS was connected to the circular cross-sectional area of the exhaust pipes (50 mm in diameter) by expansion and contraction elements (#4 in Figure 1a) very similar to those employed in other types of ATEGs whose designs are based on TEMs located on two parallel plates (e.g., References [6,13,15]). The overall dimensions of the ATEG were  $440 \times 200 \times 20$  mm (length  $\times$  width  $\times$  height) and a total weight of 7 kg. The electrical connection of all the TEMs was in series as this was expected to provide higher electrical power output than in parallel [35]. The effect of using electrical hybrid connections was not analyzed here.

### 3.2. Experimental Set-Up

We used the same experimental set-up employed by Reference [35], who analyzed an ATEG formed by a single TEM. In essence, a PSA XUD7 version K (Peugeot S.A., Rueil-Malmaison, France) (an in-line four-cylinder 1.8-L naturally aspirated diesel engine of 44 kW of nominal power) was connected to a Schenck W130 dynamometer (Figure 2). The ATEG was installed very close to the exhaust manifold and in front of the muffler to ensure high temperature gases at the ATEG inlet (Figure 3). The engine coolant temperature was between 80 °C and 90 °C under regular functioning. The high temperature employed as a cooling flow in the CSHE would substantially reduce the performance of the ATEG. Therefore, to cool the ATEG we designed an independent closed-circuit water system with a 200-L tank and an electric pump. The range of flow rates varied from 140 to 580 L/h depending on the case tested. The series electrical configuration of the TEMs was connected to a variable external load resistance in order to attain the maximum output power.

We monitored the following information: engine torque, engine speed (rpm), exhaust mass flow rate, exhaust gas temperature at both ATEG inlet and outlet, water cooling volumetric flow rate, water cooling temperatures at both ATEG inlet and outlet, ambient temperature, ATEG output voltage, and output current (see Figure 2).

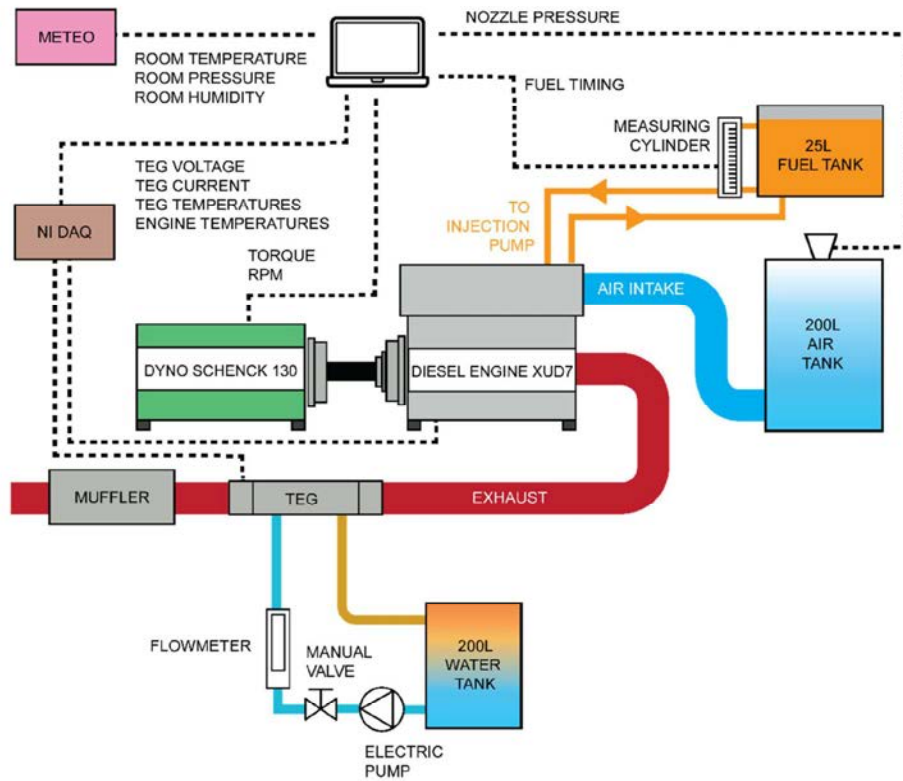


Figure 2. Schematic diagram of the laboratory set-up.

Temperatures were measured with type-K thermocouples using a National Instruments (NI) Compact RIO system with 9211 modules. Electrical information was also measured by an NI Compact RIO with 9215 (voltage) and 9227 (current) modules. Data were processed with LabVIEW software (version 2016, National Instruments, Austin, TX, USA). Engine torque, speed, and temperature were monitored with a Sportdevices SP4 unit. The mass flow rate of exhaust gases was calculated as the sum of the mass flow of air at the intake manifold plus the mass flow of consumed fuel. The volumetric flow rate of air at the inlet of the engine was measured with a calibrated Tecner TG40 nozzle installed at the inlet of a 200-L-capacity tank that damped the pulsating signal of the engine intake. The conversion of volumetric flow rate to mass flow rate used the air density calculated with the ideal gas law. At each stationary regime, the mass flow rate of fuel was obtained after measuring the time span needed to consume 30 cm<sup>3</sup> of net fuel (injected minus returned) in a calibrated measuring cylinder. The variation of fuel density with temperature was previously obtained with a thermostatic bath at different temperatures and a densimeter.

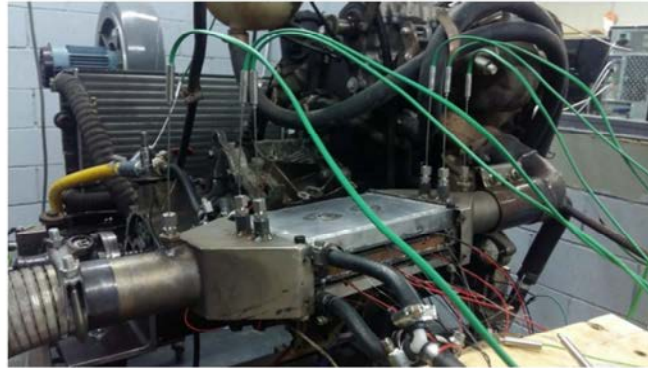


Figure 3. ATEG installed in the engine test bench.

The experimental uncertainty and the accuracy of the equipment used in the experimental tests followed the procedure detailed in Reference [35]. In essence, we assumed that the total uncertainty of a measured variable was the sum of an uncertainty related to the recorded time series plus an uncertainty related to the accuracy of the equipment.

Once the system reached stationary conditions, data were acquired during a time interval of 60 s minimum. Averaged values of the variables measured for these time series were calculated, and the uncertainty related to the mean values  $\varepsilon_s$  was expressed as

$$\varepsilon_s = \pm z_{\alpha/2} \frac{\sigma}{\sqrt{N}} \quad (1)$$

where  $z_{\alpha/2}$  was the confidence range (here chosen as 95%),  $\sigma$  was the standard deviation of the data series, and  $N$  was the number of samples in the data series.

On the other hand, the uncertainty of the equipment  $\varepsilon_e$  was obtained from

$$\varepsilon_e = \sum \left| \frac{\partial Y}{\partial x} \right| \Delta x, \quad (2)$$

where  $Y$  corresponded to the indirect variable,  $x$  referred to the direct measured variable, and  $\Delta x$  was the accuracy of the equipment in the measurement of the  $x$  variable.

Thus, the total uncertainty of data  $\varepsilon_t$  followed

$$\varepsilon_t = \sqrt{\varepsilon_s^2 + \varepsilon_e^2}. \quad (3)$$

The accuracy of the experimental equipment is listed in Table 2.

Table 2. Accuracy of the experimental equipment. NI—National Instruments.

Equipment	Accuracy	Ref.
Current (NI 9227)	$\pm (169.7 \text{ mA} + 5\% \text{ of reading})$	[36]
Voltage (NI 9215)	$\pm (85.3 \text{ mV} + 1.05\% \text{ of reading})$	[36]
Temperature (NI 9211)	$\pm 0.6 \text{ }^\circ\text{C}$	[36]
Type K thermocouple	$\pm 1.5 \text{ }^\circ\text{C}$	[37]
Sensus 405 S water meter	$\pm 0.05 \text{ L}$	[38]
Manometer	$\pm 10 \text{ Pa}$	
Fuel Calibrated volume cylinder	$\pm 0.5 \text{ cm}^3$	

### 3.3. Experimental Cases

Seven different engine operating points were investigated (see Table 3). These points were chosen according to the purpose of the present research, i.e., to investigate the effects of changing the main geometrical parameters of the ATEG and, also, the volumetric flow rate of the ATEG coolant ( $\dot{V}_w$ ). Since we tested a single ATEG, the objective was to experimentally obtain points varying the flow rate of the cooling water at different engine-shaft power  $P_e$  values. Thus, cases 1 to 3



corresponded to  $P_e \approx 18$  kW with different values of  $\dot{V}_w$ , ranging from the maximum (580 L/h) to almost the minimum (160 L/h). Cases 4 to 5 had  $P_e \approx 22$  kW and  $\dot{V}_w$  ranging from 580 L/h to 140 L/h, respectively. Finally, cases 6 to 7 had  $P_e \approx 25$  kW and  $\dot{V}_w$  ranging from 580 L/h to 180 L/h, respectively. Cases with  $P_e$  values lower than 18 kW were not tested since they were expected to provide low electrical output power [18]. Values of flow rate and temperature at the inlet of the ATEG for both the exhaust gases and coolant water, as well as air–fuel ratio, were later used as boundary conditions at the inlet of the ATEG in the numerical model. For each one of the seven different engine operating points, the external electrical resistance was tuned to achieve the maximum output power.

**Table 3.** Experimental data for engine regime, torque, exhaust gas mass flow rate  $\dot{m}_g$ , exhaust gas temperature at ATEG inlet  $T_{g,i}$ , water cooling volumetric flow rate  $\dot{V}_w$ , water coolant temperature at ATEG inlet  $T_{w,i}$  and air–fuel equivalence ratio  $\lambda$ .

Case	Regime (rpm)	Torque (N·m)	$\dot{m}_g$ (g/s)	$T_{g,i}$ (°C)	$\dot{V}_w$ (L/h)	$T_{w,i}$ (°C)	$\lambda$
1	2500	69.9 ± 0.1	43.4 ± 0.3	444.7 ± 2.0	580 ± 3	26.4 ± 2.0	1.68
2	2500	67.3 ± 0.1	42.8 ± 0.3	428.7 ± 2.0	280 ± 3	31.2 ± 2.0	1.68
3	2500	71.9 ± 0.1	43.0 ± 0.3	450.1 ± 2.1	160 ± 3	33.6 ± 2.0	1.63
4	2800	75.1 ± 0.1	46.1 ± 0.3	521.6 ± 2.1	580 ± 3	29.6 ± 2.0	1.50
5	2600	82.2 ± 0.1	44.4 ± 0.3	547.4 ± 2.0	140 ± 3	33.4 ± 2.0	1.43
6	3000	79.2 ± 0.1	48.3 ± 0.3	598.8 ± 2.0	580 ± 3	28.0 ± 2.0	1.34
7	3200	76.1 ± 0.1	51.0 ± 0.3	598.5 ± 2.0	180 ± 3	34.5 ± 2.0	1.36

### 3.4. Effective Thermal and Electrical Properties of the Thermoelectric Modules

The numerical model described in Section 4 adopted the strategy of interpreting each TEM as a single body with effective thermal and electrical properties. Therefore, we required the values of the effective Seebeck coefficient, the effective internal resistance, and the effective thermal conductivity. These effective properties were obtained with the test rig of thermoelectric modules that is schematically shown in Figure 4a.

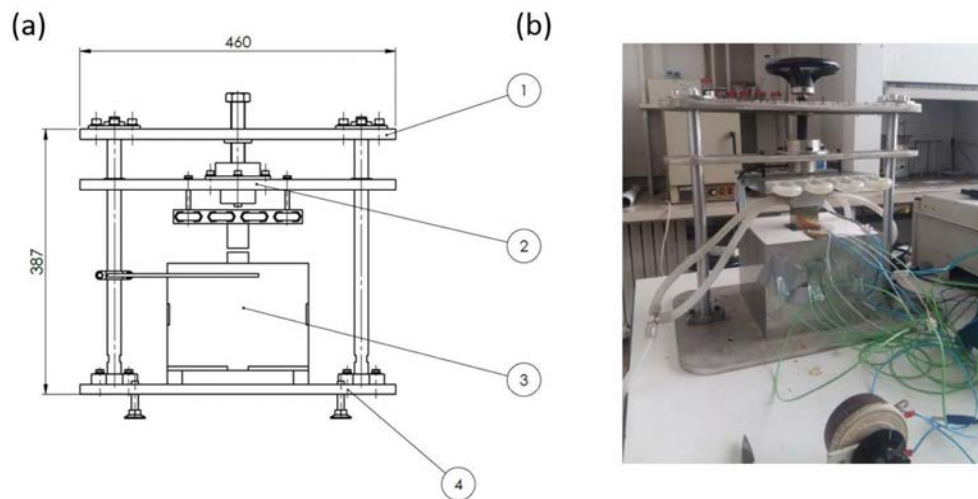


**Figure 4.** (a) Schematic drawing of the test rig of thermoelectric modules (TEMs; dimensions in mm); (b) test rig of TEMs in the laboratory.

In essence, the test rig consisted of a 400-W cartridge heater inserted into a 56 × 56 × 30 mm (length × width × height) bronze rectangular prism that was immersed inside a 200 × 200 × 150 mm (length × width × height) block filled with sheets of calcium silicate (#3 in Figure 4a). This thermal-insulating material has a thermal conductivity of only 0.072 W·m<sup>-1</sup>·K<sup>-1</sup> at 200 °C and guarantees thermal stability up to 1000 °C. An additional 56 × 56 × 36 mm (length × width × height) rectangular

bronze prism was placed on the top side of the bronze heated by the cartridge. This supplementary bronze block acted to delimit the path of the heat flow. The thermal conductivity of this block was  $k_b = 86.5 \text{ W}\cdot\text{m}^{-1}\cdot\text{K}^{-1}$  (C54400 85% Cu, 5% Sn, 5% Pb, 5% Zn composition). In this block, we inserted two K-type thermocouples vertically separated by a distance  $L_b = 30 \text{ mm}$ . Since the lateral sides of this block were in contact with thermal-insulating sheets of calcium silicate, we approximated the vertical heat flow  $Q_h$  through this element as

$$Q_h = \frac{k_b A_b \Delta T_b}{L_b}, \quad (4)$$

where  $A_b$  ( $= 56 \times 56 \text{ mm}$ ) was the cross-sectional area of the block, and  $\Delta T_b$  was the temperature difference between the two abovementioned thermocouples.

The upper face of the bronze block was in contact with the hot side of the TEM being tested (see Figures 4a–b). The cold side of the TEM was in contact with a  $56 \times 56 \times 30 \text{ mm}$  (length  $\times$  width  $\times$  height) aluminum block. The upper side of this aluminum block was, at the same time, in contact with a water heat exchanger. This heat sink was pressed against the TEM with a vertical screw (Figure 4a). A load cell (LCM305, Omega Engineering Ltd; #2 in Figure 4a) measured the force applied. Frame elements, including the vertical guide bars (#1 in Figure 4a) and the base plate (#4 in Figure 4a), were made of stainless steel.

The hot- ( $T_h$ ) and cold-side ( $T_c$ ) temperatures of the TEM were measured with thin K-type thermocouples 0.2 mm in diameter and located between the upper face of the supplementary bronze element and the TEM's hot side, and between the lower face of the aluminum block and the TEM's cold side, respectively. To ensure a uniform contact between surfaces, thermocouples were inserted in slits made of 0.2-mm-thick brass sheets with a  $56 \times 56 \text{ mm}$  cross-sectional area.

The TEM was electrically connected to an external variable resistance. Voltage and current were acquired with the same instruments as those described in Section 3.2. Results were obtained for a load pressure equal to 1.27 MPa in ambient conditions (equivalent to 3983 N force and equal to that applied in the ATEG) and a  $T_h$  temperature range from 140 °C to 226 °C and for  $T_c$  from 38 °C to 70 °C, expected to be similar to those obtained in the ATEG once installed in the engine test bench. Maximum electrical output power data were reported by suitably tuning the value of the external load resistance.

From the data obtained with the test rig, the effective Seebeck coefficient  $\alpha_e$  of the TEM was calculated as

$$\alpha_e = \frac{V_{oc}}{T_h - T_c}, \quad (5)$$

where  $V_{oc}$  was the open-circuit voltage.

On the other hand, the effective thermal conductivity  $k_e$  of the TEM was calculated as

$$k_e = \frac{L_{TEM} Q_h}{A_{TEM} (T_h - T_c)}, \quad (6)$$

where  $L_{TEM}$  ( $= 5 \text{ mm}$ ) was the total height of the TEM, and  $A_{TEM}$  ( $= 3136 \text{ mm}^2$ ) was its cross-sectional area.

Finally, the effective internal electrical resistance  $R_{ie}$  was calculated as

$$R_{ie} = \frac{V_{oc} - I_{TEM} R_L}{I_{TEM}}, \quad (7)$$

where  $I_{TEM}$  was the electrical current of the TEM when the external load resistance was  $R_L$ .

## 4. Numerical Model

### 4.1. Simulation Set-Up

Simulations were performed using the GT-SUITE software, which is a multi-physics CAE system widely used in the automotive sector [34]. GT-SUITE is composed of a set of libraries whose combination allows fluid flows and their interactions with solid bodies, including heat transfer mechanisms, to be simulated. This software was used to study the behavior of exhaust gases in ICes,

analyzing, for example, the effects the exhaust gas recirculation system has on internal combustion engines [39], and investigating waste heat recovery technologies such as the Organic Rankine Cycle [40], turbocompounding [41], and ATEGs [35].

GT-SUITE's modeling methodology is based on linking several submodels, each one focused on solving a specific problem. Figure 5 shows the schematic diagram of the whole model developed to reproduce our ATEG.

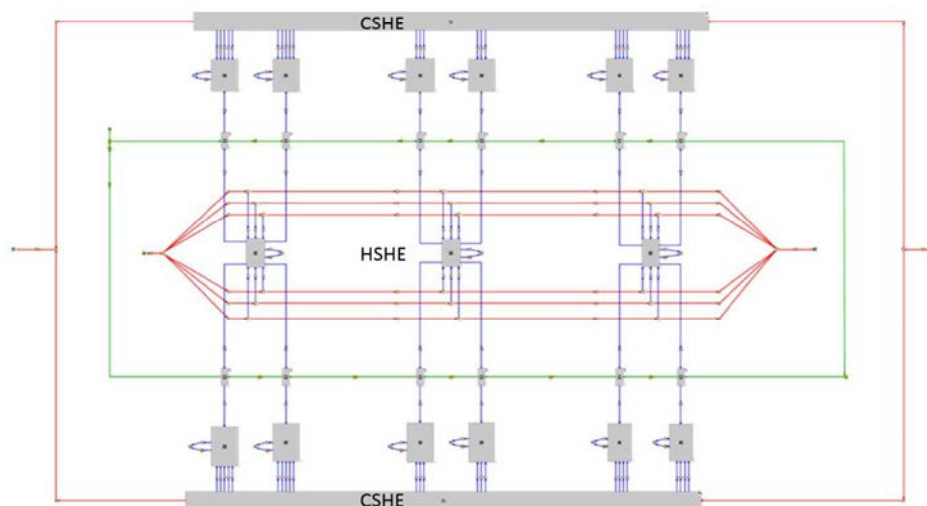


**Figure 5.** Block diagram of the ATEG model containing two cold-side heat exchangers (CSHEs), 12 TEMs, thermal connections (blue lines), flow connections (red lines), electrical connections (green lines), and the hot-side heat exchanger (HSHE).

The copper heat exchanger was divided into three thermal masses connected in series. Thus, each thermal mass corresponded to the part of the heat exchanger assigned to the four TEMs located in the same column (see Figure 1). This method of segmenting the hot heat exchanger along the exhaust flow direction allowed us to correctly simulate the disparity of cold- and hot-side temperatures among TEMs, one of the main drawbacks observed in ATEG designs. The surfaces of these thermal masses were appropriately connected to (1) the exhaust gases through six cylindrical surfaces, (2) the hot sides of TEMs, and (3) the ambient (see Figure 6). Heat transfer via conduction and convection was assumed and the external surface (contact with the environment) used a heat transfer coefficient  $h = 25 \text{ W}\cdot\text{m}^{-2}\cdot\text{K}^{-1}$  [42]. It also included losses via radiation with a gray body emissivity of the thermal mass surface equal to 0.9. The Colburn analogy was used for heat transfer via convection in fluids [42].

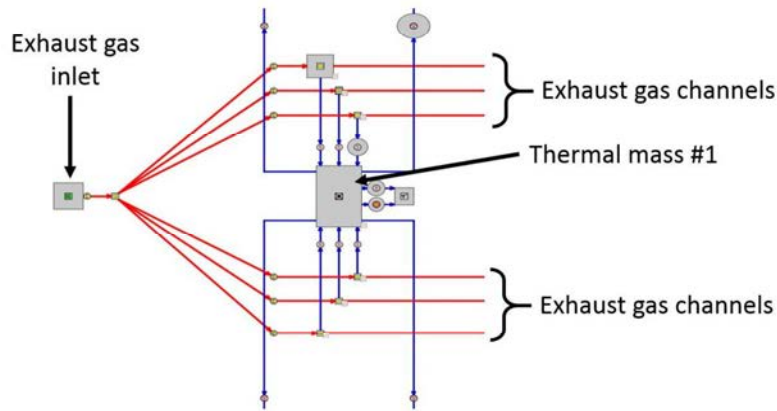


**Figure 6.** Block diagram of thermal mass #1 of the HSHE including exhaust gas channels (red) and thermal connections (blue).

TEMs were modeled by assuming them to be uniform bodies with the effective thermal and electrical properties obtained in Section 3.4. Thus, we avoided the task of simulating each and every thermoelement that formed the TEM. The hot side of each TEM was in contact with the corresponding thermal mass of the copper heat absorber or HSHE, whereas the cold side was in contact with the water heat sink or CSHE (Figure 7). The thermal connection between thermal masses and the TEMs' hot side and between water heat sink and the TEMs' cold side applied constant values for the thermal contact resistances  $R_h$  and  $R_c$ , respectively. These values were chosen as  $R_h = 5 \times 10^{-4} \text{ m}^2 \cdot \text{K} \cdot \text{W}^{-1}$  and  $R_c = 3 \times 10^{-4} \text{ m}^2 \cdot \text{K} \cdot \text{W}^{-1}$  in agreement with those used in similar ATEGs [5]. Changes of  $R_h$  and  $R_c$  with respect to temperature were not expected to substantially vary the results, as concluded in Reference [35], nor would they alter the conclusions of the present study.

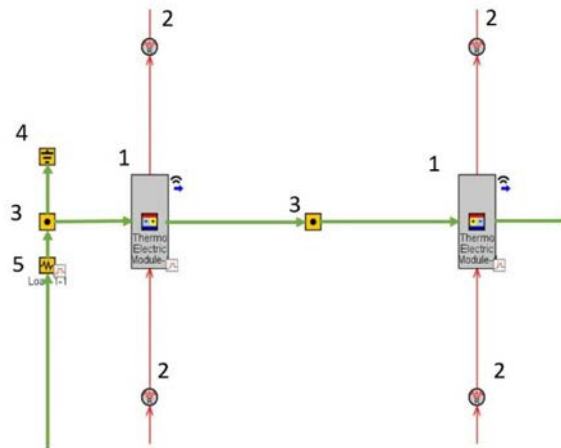


**Figure 7.** Block diagram of electrical and thermal connections of TEMs (1), indicating the thermal contact resistances (2), electrical node junctions (3), ground connection (4), and electrical load resistance (5).

The cold side of each TEM was in contact with heat sink zones corresponding to different water paths (see Figure 8a). To model this effect, we divided the heat sink into 24 sections depending on their location with respect to the TEMs below. Each one of these sections was thermally connected to the corresponding region of the aluminum heat sink that, at the same time, was thermally connected to the cold side of the pertaining TEM (adding a thermal contact resistance  $R_c$  as mentioned previously; see Figure 8b).



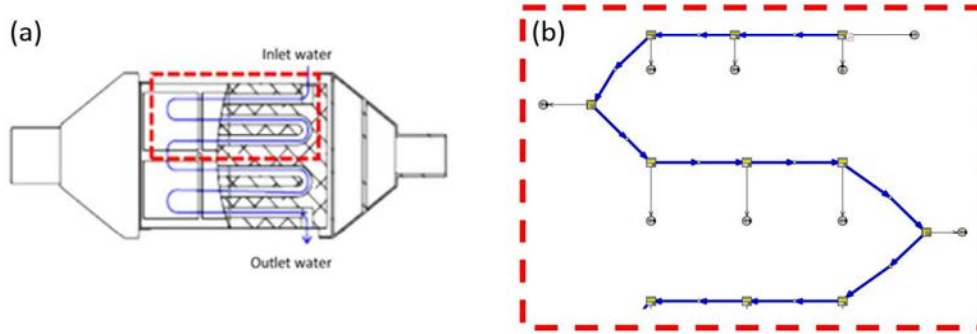


**Figure 8.** Example of a thermal connection between the CSHE and the TEMs. (a) Dashed lines enclose the example zone; (b) block diagram with connections within the example zone.

To correctly reproduce the experimental conditions, simulations used water as the coolant and the product of a combustion reaction as the exhaust gases. The latter assumption better represented actual laboratory conditions than imposing air as exhaust gases, as commonly adopted in other numerical models of ATEGs [7,18]. A complete combustion reaction of diesel fuel with an air–fuel ratio (AFR) higher than that of stoichiometric conditions ( $AFR_s$ ) was implemented and properties such as dynamical viscosity, thermal conductivity, specific heat, etc., as a function of the temperature of the mixed gas were used in the calculations. The actual air–fuel equivalence ratio values ( $\lambda = AFR/AFR_s$ ) for each experimental point were deduced from measurements, giving lean conditions ( $\lambda > 1$ ) in all of the engine operation points analyzed (see Table 3).

The electrical behavior of the ATEG was also simulated with GT-SUITE by electrically connecting all TEMs in a series configuration to an external electrical load resistance  $R_L$ . Effective values of the Seebeck coefficient, the thermal conductivity, and the internal resistance of each TEM followed those obtained in Section 3.4, and are listed in Table 4. The effective figure of merit was calculated as  $ZT_e = \alpha_e^2 \bar{T} / (\rho_e k_e)$  where  $\bar{T} = (T_h + T_c)/2$  and the effective electrical resistivity  $\rho_e = A_{TEM} R_{ei} / L_{TEM}$ .  $ZT_e$  was obtained for illustrative purposes only since the model did not require this value.

**Table 4.** Effective values of Seebeck coefficient ( $\alpha$ ), thermal conductivity ( $k_e$ ), internal electrical resistance ( $R_{ei}$ ), and figure of merit ( $ZT_e$ ) as a function of cold- ( $T_c$ ) and hot-side ( $T_h$ ) TEM temperatures.

$T_c$ (°C)	$T_h$ (°C)	$\alpha$ (V·K <sup>-1</sup> )	$k_e$ (W·m <sup>-1</sup> ·K <sup>-1</sup> )	$R_{ei}$ (Ω)	$ZT_e$
38	140	0.0255	3.17	0.759	0.157
39	160	0.0263	2.94	0.781	0.180
42	180	0.0272	2.90	0.814	0.192
50	160	0.0267	3.00	0.806	0.179
51	170	0.0274	3.02	0.838	0.183
55	181	0.0280	2.97	0.829	0.199
55	201	0.0280	2.84	0.834	0.212
65	201	0.0279	2.87	0.787	0.214
65	226	0.0296	2.73	0.922	0.232
70	140	0.0261	3.15	0.729	0.179
70	160	0.0267	3.11	0.760	0.186

The thermal and the electrical effective properties of each TEM as a function of temperature were determined by extrapolating the data of Table 4. This mathematical procedure was carried out by the GT-SUITE software, in which data were introduced in tabular form. Thermal properties of aluminum and copper as a function of temperature were taken into account using the own engineering libraries of the software.

The model took into account the coupling between the thermal and the electrical phenomena. Thus, the heat flow on the cold side of the TEM,  $Q_c$ , corresponded to that on the hot side,  $Q_h$ , minus the generated electrical power  $P_{TEM}$ :

$$Q_c = Q_h - P_{TEM}, \quad (8)$$

and both the cold and hot heat flows were calculated as

$$Q_c = \alpha_e I_{TEM} T_c + \frac{k_e A_{TEM}}{L_{TEM}} (T_h - T_c) - \frac{1}{2} I_{TEM}^2 R_{ie}, \quad (9)$$

$$Q_h = \alpha_e I_{TEM} T_h + \frac{k_e A_{TEM}}{L_{TEM}} (T_h - T_c) + \frac{1}{2} I_{TEM}^2 R_{ie}, \quad (10)$$

where  $I_{TEM}$  was the current flowing through the TEM, and was the same as that of the whole ATEG since the electrical connections were in pure series. The sum of the electrical power of all individual TEMs gave the total power generated by the ATEG  $P_{ATEG}$ .

In Equations (9)–(10), the first term corresponds to the Seebeck contribution (i.e., the thermoelectric effect), the second to Fourier's law, and the last to Joule heating. The Thomson effect was neglected since its contribution was expected to be of minor importance in comparison to the other three terms [35].

The global boundary conditions of the simulation were the following: exhaust gas at ATEG inlet, fixed temperature and mass flow rate (see Table 3); exhaust gas at ATEG outlet, fixed pressure (set to the atmospheric one); cooling water at ATEG inlet, fixed temperature and volumetric flow rate of cooling water (Table 3); cooling water at ATEG outlet, fixed pressure (set to the atmospheric one); fixed ambient temperature at 24 °C. The value of the external electrical load resistance was tuned to maximize a goal function (in this case, the electrical output power of the ATEG to validate the model). The optimization procedure is explained in Reference [35].

#### 4.2. Model Validation

The results from the model were compared with the experimentally measured values. For the thermal behavior, the prediction of the temperature at the outlet of both fluid flows (exhaust gas and water cooling) is shown in Figure 9. Simulation results coincided with the experimental values (within their uncertainty ranges) with small discrepancies only in the water outlet temperature for cases 5 (<1.5%) and 7 (<5%). The agreement of the simulations with the exhaust gas temperature measured at the ATEG outlet was quite remarkable since the experimental cases covered a broad range of values (i.e., gas temperature at ATEG inlet from 428 °C to 599 °C). Therefore, the results indicated that the model correctly predicted the heat transfer in the ATEG (i.e., from the exhaust gas to the water cooling).

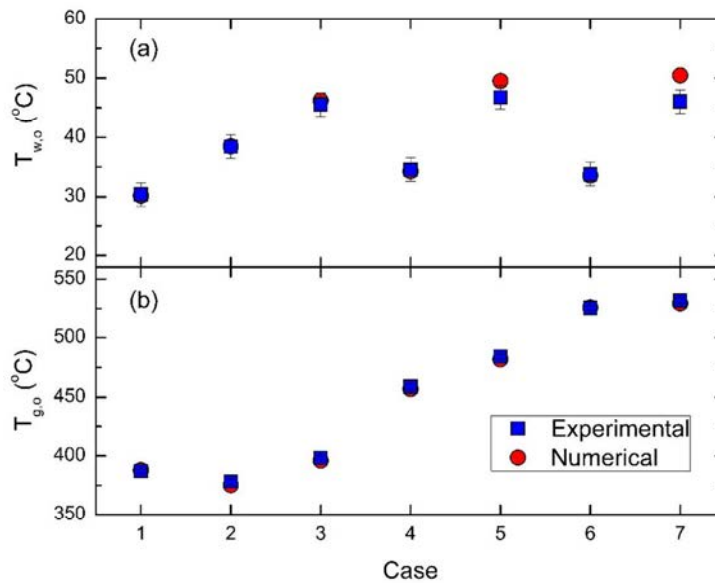


**Figure 9.** Experimental and simulated results of (a) water cooling temperature at ATEG outlet ( $T_{w,o}$ ), and (b) exhaust gas temperature at ATEG outlet ( $T_{g,o}$ ), for those cases listed in Table 3.

The conversion of heat into electricity by the TEMs' effective properties mentioned above also reproduced very well the electrical values obtained experimentally (Figure 10). The simulated voltage and current values matched the laboratory data within their uncertainty ranges. Note that the highest voltage values (>23 V) were obtained at very demanding engine speeds. The agreement of the results with the measured data confirmed the validity of the methodology implemented for determining the external resistance load that would maximize the output power.

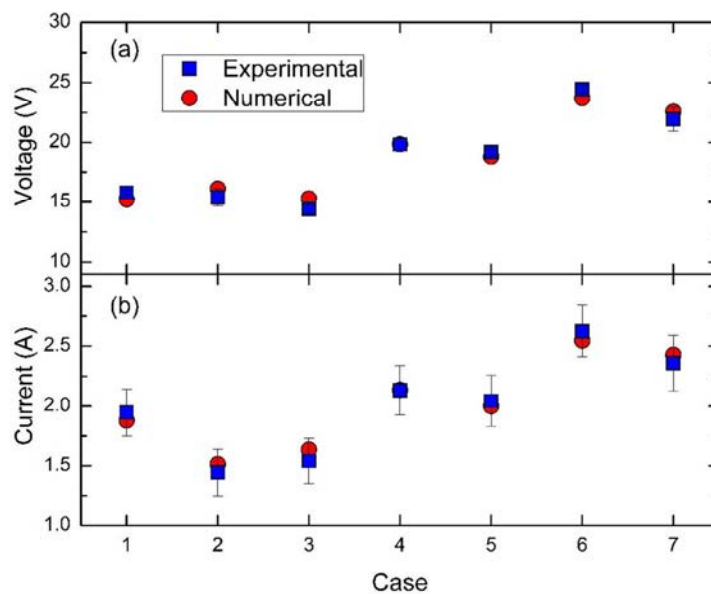


**Figure 10.** Experimental and simulated results of (a) ATEG voltage, and (b) ATEG current.

The electrical output power of the whole ATEG  $P_{ATEG}$  simulated by GT-SUITE for the cases listed in Table 3 were compared with the experimental ones (Figure 11). Case 6 obtained the maximum power value, reaching up to 64 W. This meant an average power production per TEM equal to 5.3 W. Since voltage and current were already well predicted by the model, simulated output power production followed the values observed. The trend obtained in the experimental cases was also replicated by the model.

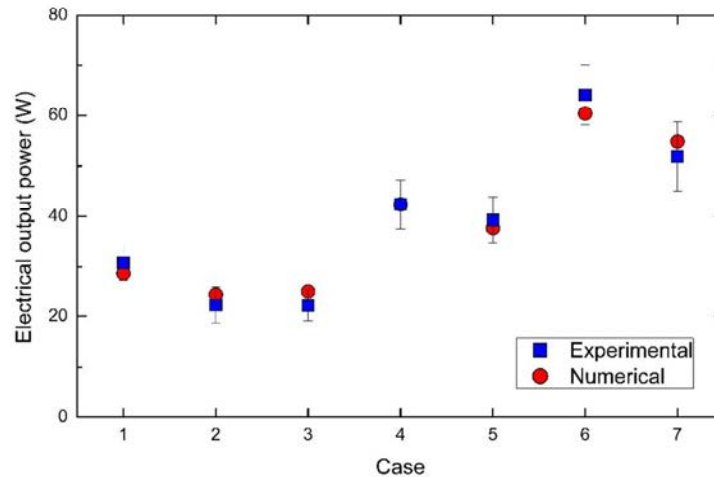


**Figure 11.** Experimental and simulated results of the electrical output power of the ATEG ( $P_{ATEG}$ ) for the cases listed in Table 3.

Thus, we accepted that our methodology correctly predicted the behavior of our ATEG (in both the thermal and electrical behavior). That said, in fuel consumption analysis, it is critical to correctly determine the energy losses through the ATEG. Indeed, the increase in the upstream pressure once the ATEG is installed in the exhaust (or, equivalently, the head losses experienced by the exhaust gas when moving through the ATEG) becomes one of the main ATEG design parameters [6,10,13]. These head losses can be directly related to the back pressure, which is defined as the pressure difference between the ATEG inlet (upstream, high pressure) and the ATEG outlet (downstream, low pressure).

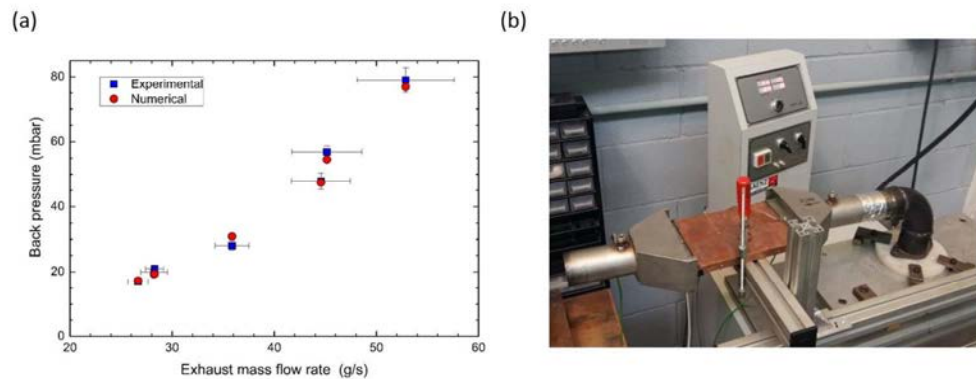


**Figure 12.** (a) Experimental and simulated results of back pressure obtained at the flow bench; (b) only the HSHE plus contraction and expansion cones of the ATEG were needed in the test.

Thus, an additional validation was required if the model were to be used as a tool to investigate the effect the ATEG has on fuel consumption. Due to laboratory limitations, pressure differences

through the ATEG could not be measured on the engine test bench. However, back pressure values were experimentally obtained when the ATEG was disassembled from the exhaust pipe and installed in a flow bench (Saenz D640). Seven different amounts of air mass flow rates and air temperatures were pumped through, and the results of the back pressure values were recorded (Figure 12). Simulations of the ATEG were carried out without a cooling system, but with the ATEG conditions at the inlet of the exhaust pipe the same as those applied in the flow bench. Results also matched the measured values within their uncertainty ranges, which implied that the flow dynamics of the exhaust gas in terms of energy losses (i.e., back pressure) were also being correctly simulated by the model (Figure 12a).

## 5. Results and Discussion

Our objective was to investigate the performance of our ATEG (output power and fuel economy) having changed the main design parameters of its heat exchangers (HSHE and CSHE). For a fixed distribution of TEMs (i.e., 12 TEMs and specified values for the temperature and mass flow rate of the exhaust gases), the main design parameter of the HSHE is the diameter of the cylindrical holes ( $D$ ), since length is determined by the dimensions of the TEMs. On the other hand, the main design parameters for the CSHE are the volumetric flow rate of cooling water and the value of the cross-sectional area of the water channel. The consequences of modifying these parameters are shown next.

### 5.1. Water Heat Sink: Effects of Changing the Geometry and Flow Rate

The height of the cooling channel  $L$  in the water heat sink was varied from 8 mm to 30 mm while the width (= 10 mm) was kept constant. This meant a variation from 80 mm<sup>2</sup> to 300 mm<sup>2</sup> in the cross-sectional area of the water channel. We also investigated the effects of changing the volumetric flow rate of the cooling water,  $\dot{V}_w$ , varying it from 140 L/h up to 580 L/h. This represented an average water velocity within the channel ranging from 0.13 m/s (case with  $\dot{V}_w = 140$  L/h and  $L = 30$  mm) to 2.01 m/s (case with  $\dot{V}_w = 580$  L/h and  $L = 8$  mm). Note that not all the combinations of  $\dot{V}_w$  and  $L$  implied turbulent conditions. However, being based on the Colburn analogy, the calculations for the convective heat transfer assumed different equations depending on the flow regime (see Reference [42]).

Simulations for  $L$  ranged between 8 and 30 mm with 1-mm increments and, for  $\dot{V}_w$ , they ranged between 140 and 580 L/h with 20-L/h increments taking the boundary conditions of the maximum output power case achieved in the experimental test (case 6 in Table 3 but with a variable  $\dot{V}_w$ ). For each one of the configurations ( $L$  and  $\dot{V}_w$ ) simulated, the model applied a numerical algorithm to find the maximum output power by suitably varying the external load resistance,  $R_L$ . In Figure 13, the degree of intensity of the convective heat transfer between the heat sink's aluminum block and the cooling water flowing in its interior was analyzed by calculating the convective heat transfer coefficient,  $h$ , and the area of the aluminum channel in contact with the water,  $A$ . This  $hA$  product (which is, indeed, the inverse of the thermal resistance) was evaluated by taking  $h$  as the value calculated at the end of the water channel path. Results shown in Figure 13b confirmed that the maximum heat transfer was achieved with the maximum flow rate and minimum height, thereby maximizing the flow velocity. Although  $hA$  substantially varied in the range of flow rates and water channel heights analyzed, its influence on the maximum electrical power extracted from the exhaust gases (Figure 13a) was not important until its value was below 2.70 W·K<sup>-1</sup> (thermal resistance equal to 0.37 K·W<sup>-1</sup>; electrical output power of 57.5 W in comparison with the maximum obtained of 63.9 W). The CSHE had a remarkable impact on the reduction in output power as  $hA$  further decreased (at low flow rates and high cross-sectional areas of the water channel) and, consequently, the thermal resistance increased. A similar behavior was observed in Reference [43] when the behavior of a TEG designed for a different purpose (it used hot water instead of exhaust gases as the main heat source) was experimentally studied.



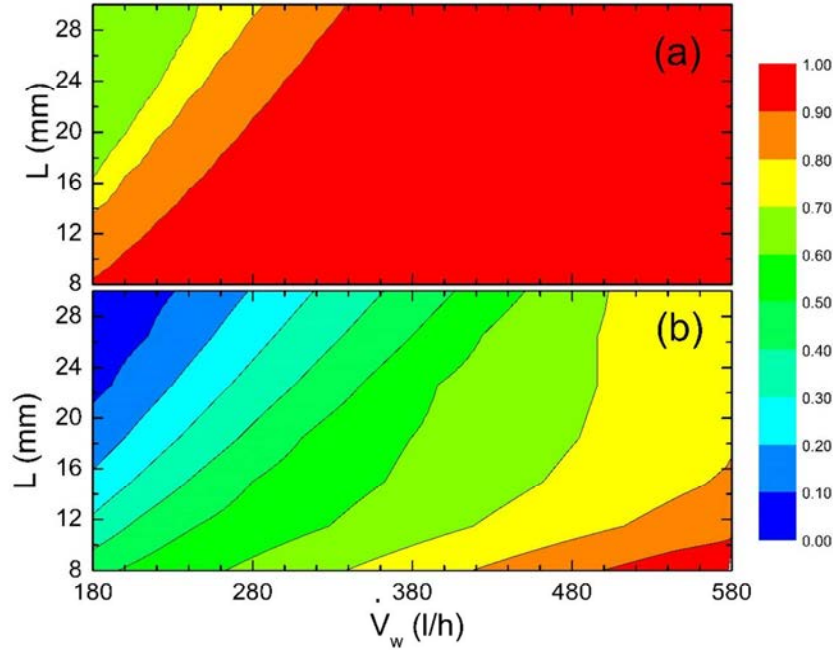


**Figure 13.** (a) Contours of electrical output power ( $P_{TEG}$ ) normalized to the maximum value obtained ( $P_{TEG}/P_{TEG,max}$ ;  $P_{TEG,max} = 63.9$  W); (b) contours of the product of the convective heat transfer multiplied by the area of the CSHE channel in contact with the water ( $hA$ ) normalized to the maximum value obtained ( $hA/hA_{max}$ ;  $hA_{max} = 9.54$  W·K<sup>-1</sup>) as a function of the water coolant flow rate  $\dot{V}_w$  and height of the coolant channel  $L$ . All other conditions are as in case 6 in Table 3.

While the results above focused on the power output, the final target of installing an ATEG in a vehicle is in fact to reduce fuel consumption. The  $P_{ATEG}$  value generated charges the battery of the vehicle. As previously mentioned, this reduces the time demand on the vehicle's electrical generator (i.e., the alternator) and, consequently, increases fuel economy. Nevertheless, because of the effect of the back pressure, due to the pressure increase upstream, the ATEG increases fuel consumption with respect to the pristine conditions of the vehicle. In addition, the ATEG has a non-negligible mass that should be added to the total mass of the vehicle. This weight increase also leads to increases in fuel consumption.

The impact of these three effects on fuel efficiency were estimated by Karri et al. [19], who proposed the following equations to estimate fuel economy resulting from the power generated by the ATEG ( $F_{e,ATEG}$ ), the increase in fuel consumption due to the power required to overcome the back pressure generated by the ATEG ( $F_{e,BP}$ ), and the increase in fuel consumption because of the increase in weight of the vehicle ( $F_{e,m}$ ):

$$F_{e,ATEG}(\%) = 100 \frac{\eta_{PCU}}{\eta_G} \frac{P_{n,ATEG}}{P_e}, \quad (11)$$

$$F_{e,BP}(\%) = -100 \frac{\dot{V}_g \Delta p_{bp}}{P_e}, \quad (12)$$

$$F_{e,m}(\%) = -100 \frac{\xi v m_{ATEG} g}{P_e}, \quad (13)$$

where  $\eta_{PCU}$  (= 0.84; see Reference [19]) is the efficiency of the power converter unit (PCU), which is a direct-current to direct-current converter to match the output voltage of the alternator,  $\eta_G$  (= 0.5; see Reference [19]) is the efficiency of the mechanical to electrical conversion of the alternator,  $P_e$  is

the engine-shaft power (torque multiplied by the engine regime in Table 3),  $P_{n,ATEG}$  is the net power produced by the ATEG (ATEG generation minus power required for pumping the water in the ATEG cooling system),  $\dot{V}_g$  is the volumetric flow rate of exhaust gases,  $\Delta p_{bp}$  is the back pressure increase due to the installation of the ATEG,  $\xi$  is the vehicle rolling resistance,  $v$  is the vehicle velocity (calculated from the transmission ratio, axle ratio, and tire diameter),  $m_{ATEG}$  is the mass of the ATEG, and  $g$  is the acceleration of gravity.

The total value of the fuel economy  $F_e$  was calculated as

$$F_e = F_{e,ATEG} + F_{e,BP} + F_{e,m}, \quad (14)$$

where the terms  $F_{e,BP}$  and  $F_{e,m}$  were negative values; thus, their contribution was to increase fuel consumption.

The value of  $P_{n,ATEG}$  in Equation (11) was obtained with the equation

$$P_{n,ATEG} = P_{ATEG} - P_{wp}, \quad (15)$$

where  $P_{wp}$  was the power consumed by the water pump of the ATEG's independent cooling system. This value was calculated by multiplying the water coolant volumetric flow rate by the head losses of the water cooling circuit (or, equivalently, the pressure drop through the cooling system). Since we used a water tank as a cold reservoir, there was no need to calculate extra energy losses different from those produced by the flow of water within the piping system and the CSHE. The values of the power pump were in the order of  $P_{wp} < 5$  W, which agreed with the coolant pumping power used in Reference [19] for similar flow rate values.

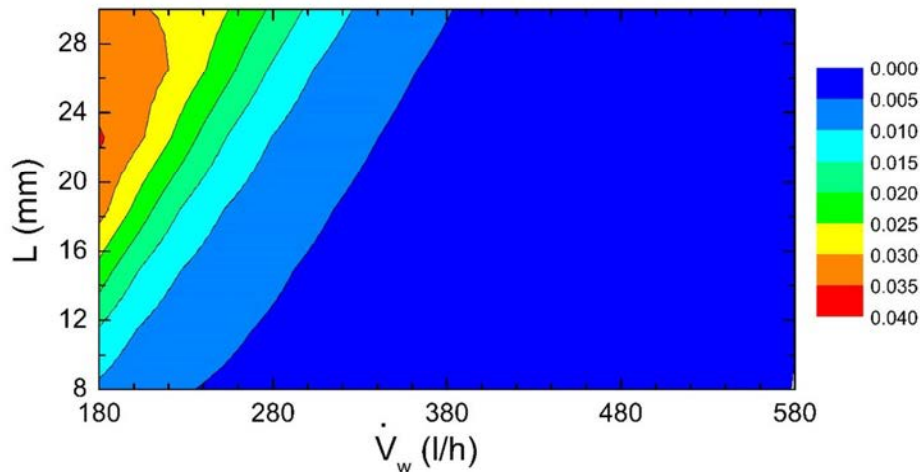


**Figure 14.** Contours of changes in fuel economy ( $F_e$ ) relative to the maximum value ( $F_e/F_{e,max} - 1$ ;  $F_{e,max} = -7.01\%$ ) as a function of water coolant flow rate  $\dot{V}_w$  and height of coolant channel  $L$ . All other conditions as in case 6 of Table 3.

The effect that changing the flow rate of coolant water and the height of the water cooling channel has on fuel consumption is shown in Figure 14 for engine operating conditions as in case 6 in Table 3. Note that values had relative changes with respect to the maximum fuel economy achieved, which was negative ( $= -7.01\%$ ) due to the considerable influence the back pressure term has. This meant that all the cases reported in Figure 14 produced an increase in fuel consumption higher than 7.01% in comparison with the base non-ATEG engine situation working under the same conditions as case 6. Since the back pressure value was independent of the heat sink design, the variation in fuel economy shown in Figure 14 was influenced by two terms only: (1) the positive effect due to the output power generated, and (2) the negative effect resulting from the increase in mass. Figure 14 clearly indicates that the way to improve fuel economy with the heat sink design is to enhance heat transfer (Figure 13b)

and, consequently, electrical output power (Figure 13a). Thus, the target would be to reduce the water channel height and to increase the volumetric flow of cooling water. However, this combination increased the flow velocity and, because of the major head losses by friction, pump power  $P_{wp}$ . This effect penalized situations in which the electrical output power  $P_{ATEG}$  was not very high ( $L$  above 20 mm and low flow rates  $\dot{V}_w$ ) and the pumping power,  $P_{wp}$ , played a relevant role in the value of  $P_{n,ATEG}$ . Thus, in contrast to the trend observed at high  $P_{ATEG}$ , we observed that an increase in  $L$  implied a reduction in  $P_{wp}$  and, therefore, better fuel efficiency (see, e.g., the trend of contour lines in Figure 14 at  $\dot{V}_w = 180$  L/h with higher fuel consumption at  $L = 23$  mm than at  $L = 28$  mm).

There are other techniques aimed at increasing the performance of thermoelectric generators which focus on improving heat transfer on the cold side, for instance, the use of nano fluid coolant [44]. However, as our objective was twofold (to focus on the effects of the structure (the geometry) and the flow rate), the option above was not analyzed here.

### 5.2. Heat Absorber: Effects of Changing the Diameter of the Cylindrical Holes

Previous results confirmed that back pressure is the main limiting factor to determining ATEG performance in terms of fuel consumption. Thus, actions intended to reduce the back pressure values should be focused on improving the design of the heat absorber. In our ATEG, the heat absorber was a copper block with six cylindrical holes of 12 mm inner diameter (Figure 1). As pointed out by other authors, this type of geometry generates more back pressure than heat absorbers based on fins, for example, Reference [7]. However, heat exchangers with cylindrical holes have some advantages over fin heat absorbers since the latter have constraints related to the type of material being used and the geometrical dimensions of the fin (minimum available fin spacing and fin thickness depending on the manufacturing techniques). The above implies that the cost of a fin-type heat absorber becomes higher than that with cylindrical holes. This is a very important issue when devices have to be mass produced. In addition, although not employed here, there are several passive methods to enhance heat transfer in heat absorbers with cylindrical holes such as, for example, inserting helical elements [45]. From the above, our goal was to investigate the potential heat absorbers with cylindrical holes had as heat transfer devices for the hot part of ATEGs, and how fuel consumption may be improved by changing a key design parameter: the diameter of the cylindrical hole.

The value of the convective heat transfer coefficient,  $h$ , multiplied by the exchange area,  $A$ , between the six inner cylindrical holes and the exhaust gas was calculated for different designs by varying the diameter  $D$  of the holes from 8 mm to 20 mm. Results with engine load operating conditions that gave the maximum  $P_{ATEG}$  value in the laboratory experiment (case 6 in Table 3) and with a low regime case ( $\dot{m}_g = 24.1$  g/s,  $T_{gi} = 454.8$  °C,  $T_{wi} = 20$  °C, and  $\dot{V}_w = 580$  L/h, as in Reference [7]) are shown in Figure 15a. The trend of  $hA$  as a function of  $D$  followed the same behavior as in Figure 13b. Heat transfer was enhanced when the diameter of the holes was reduced because the increment in flow velocity increased the value of  $h$  which, in turn, clearly compensated for the small decrease in the exchange surface area  $A$ . Varying the convective thermal resistance modified the power output (as observed in Figure 15b). High values of  $hA$  led to high values of  $P_{ATEG}$ . Furthermore, the heat flow extracted from the exhaust gases can be approximated as  $Q = hA(T_{ha} - T_g)$ , where  $T_{ha}$  and  $T_g$  are the temperatures of the heat absorber and exhaust gases, respectively. Thus, the  $P_{ATEG}/(hA)$  ratio can be understood as a measure of an energy conversion efficiency term of the ATEG multiplied by  $(T_{ha} - T_g)$ . For high values of  $D$  (>15 mm),  $P_{ATEG}/(hA)$  for both regimes was almost constant, especially in the low regime case, thus indicating a constant conversion efficiency  $\eta$ . This coefficient was evaluated as  $\eta = P_{ATEG}/Q_h$ . For an engine operating point as in case 6, the maximum power attained with  $D = 8$  mm was 73 W, whereas, with  $D = 20$  mm, the ATEG produced 45 W. For the low regime case,  $P_{ATEG}$  ranged from 26 W ( $D = 8$  mm) to 11 W ( $D = 20$  mm). The maximum ATEG conversion efficiency was achieved with  $D = 8$  mm, reaching  $\eta = 1.68\%$  under the same conditions as case 6 and only  $\eta = 1.1\%$  in the low regime case. The minimum ATEG conversion efficiency corresponded to simulations using  $D = 20$  mm, with values equal to  $\eta = 1.30\%$  for case 6 and  $\eta = 0.65\%$  for the low regime case.



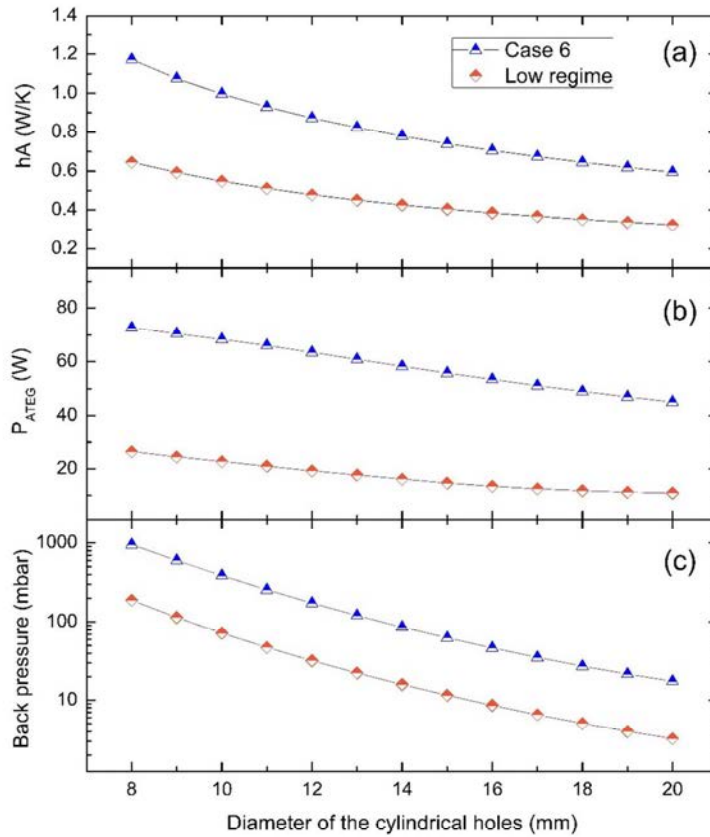


**Figure 15.** (a) Convective heat transfer coefficient multiplied by the contact area of gases with the heat absorber, (b) electrical output power, and (c) back pressure as a function of the diameter of the cylindrical holes for high (case 6 in Table 3) and low (see text) engine regime conditions.

However, the main effect that changing the diameter of the cylinders had was on the back pressure values (Figure 15c). The  $\Delta p_{bp}$  values changed by almost two orders of magnitude ( $\Delta p_{bp} = 955$  mbar at  $D = 8$  mm in comparison with  $\Delta p_{bp} = 17$  mbar at  $D = 20$  mm; case 6). The behavior of  $\Delta p_{bp}$  as a function of  $D$  almost perfectly fitted a power trend. Thus, the strategy of reducing the size of the diameters of the cylinders to increase heat transfer and, hence, electrical output power heavily penalized the back pressure. For example, a 14% increase in  $P_{ATEG}$  implied an increase in  $\Delta p_{bp} = 449\%$  (from  $D = 12$  mm to  $D = 8$  mm, case 6). Therefore, this action had dramatic consequences on the fuel economy values (Figure 16).

Individual contributions to the total fuel economy  $F_e$  (Equation (14)) are shown in Figure 16. The impact of  $P_{ATEG}$  on fuel consumption (Equation (11); Figure 16a) as a function of  $D$ , followed the trend observed in Figure 15b for the electrical output power. However, the differences between both cases (high- and low-load engine regimes) were not as important as in Figure 15b because the engine-shaft power in the low regime case was only 12.4 kW (24.9 kW in case 6). The effect of the power generated by the ATEG led to maximum fuel savings of 0.48% ( $D = 8$  mm, case 6) and 0.37% ( $D = 8$  mm, low regime). The contribution to the fuel economy (in %) due to the electric power generated was in the order of one-quarter of the value of the thermodynamic efficiency of the ATEG device. However, the consequences of the increasing back pressure at the exhaust pipe caused a massive increase in fuel consumption  $F_{e,BP}$  (Figure 16b), almost two orders of magnitude more important than the fuel savings from  $F_{e,ATEG}$  (Figure 16a) with an ATEG design that used  $D = 8$  mm.

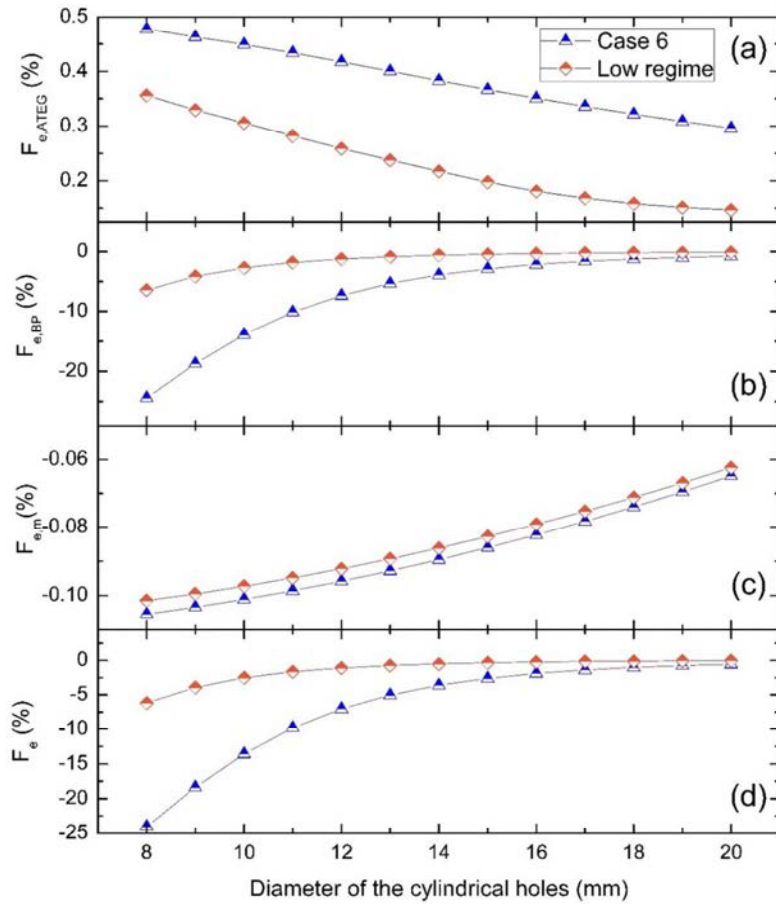


**Figure 16.** (a) Fuel economy (%) due to the electrical power generated by the ATEG (Equation (11)), (b) fuel economy (%) due to the back pressure created by the ATEG (Equation (12)), (c) fuel economy (%) due to the increase in vehicle mass (Equation (13)), and (d) overall fuel economy (%) (Equation (14)) as a function of the diameter of the cylindrical holes for high (case 6 in Table 3) and low (see text) engine regime conditions.

Values of less than a 1% increase in fuel consumption due to  $F_{e,BP}$  were only obtained in designs that offered a back pressure level below 23 mbar (designs with  $D > 18$  mm evaluated under case 6 conditions, and designs with  $D > 12$  mm in the low regime case). With our design, values of back pressure as low as 5 mbar were attained with  $D = 18$  mm in the low regime situation ( $F_{e,BP} = -0.19\%$ ).

On the other hand, the effect of the increase in vehicle mass due to the installation of the ATEG implied an increase in fuel consumption in the order of 22% of the  $F_{e,ATEG}$  value, varying slightly with  $D$  (Figure 16c). Values of  $F_{e,m}$  approached zero as  $D$  increased, because less material was required to build the ATEG's heat absorber; thus,  $m_{ATEG}$  decreased. Despite its low contribution to the overall fuel economy provided by the ATEG (Figure 16d), this term may be a critical contribution when  $F_{e,BP}$  is in the order of  $F_{e,ATEG}$ . This was the case for the low regime condition at  $D = 20$  mm, since  $F_{e,ATEG} = 0.15\%$ ,  $F_{e,BP} = -0.12\%$ , and  $F_{e,m} = -0.06\%$ , resulting in an overall fuel savings of  $F_e = -0.03\%$ . However, under stationary conditions (as in the laboratory experiment) the contribution of  $F_{e,m}$  is neglected and the very same design would produce a positive fuel economy value ( $F_e = 0.03\%$ ).

### 5.3. Configurations with Maximum Power and Maximum Fuel Economy

From the previous analyses, the back pressure emerged as the constraining factor for reaching fuel savings. However, the strategy to continuously reduce the back pressure may lead to designs that greatly reduce the amount of heat transferred to the ATEG, thus eventually obtaining very low electrical output power values. Although this may certainly imply positive numerical values of fuel economy, these savings are fictitious, since the amount of power injected into the system is so low that there is no sense in installing a whole ATEG device. This would be, for example, the case of the  $F_e = 0.03\%$  case discussed above.

Thus, an ATEG feasibility study must implicitly accept two requisites: (1) electrical output power above a given threshold value (e.g.,  $P_{ATEG} > 100$  W), and (2) fuel savings above a given threshold value (e.g.,  $F_e > 3\%$ ). Fulfilling the latter condition (fuel economy) would almost certainly imply achieving the first one (power). However, as we saw above, fulfilling the first condition (power) does not imply achieving minimum fuel savings.

Therefore, an interesting tool to assess the adequacy of the ATEG consisted of plots of output power and fuel savings corresponding to designs that maximized both terms (Figure 17 and 18). Obviously, output power values obtained with design parameters that maximized fuel economy ( $D = 20$  mm,  $\dot{V}_w = 580$  L/h,  $L = 8$  mm) became smaller than those corresponding to the design that maximized output power ( $D = 8$  mm,  $\dot{V}_w = 580$  L/h,  $L = 8$  mm) (Figure 17). The experimental design approached either the condition of  $P_{ATEG,max}$  or of  $F_{e,max}$  depending on the cooling flow rate used in the test and, therefore, on the amount of heat flow transferred. Cases with low heat flow yielded low output power, similar to those attained with a heat absorber whose cylindrical holes were of a higher diameter ( $F_{e,max}$  case). All in all, the differences in  $P_{ATEG}$  between the designs at  $P_{ATEG,max}$  and at  $F_{e,max}$  were less than 44% with respect to the values of the  $P_{ATEG,max}$  design.

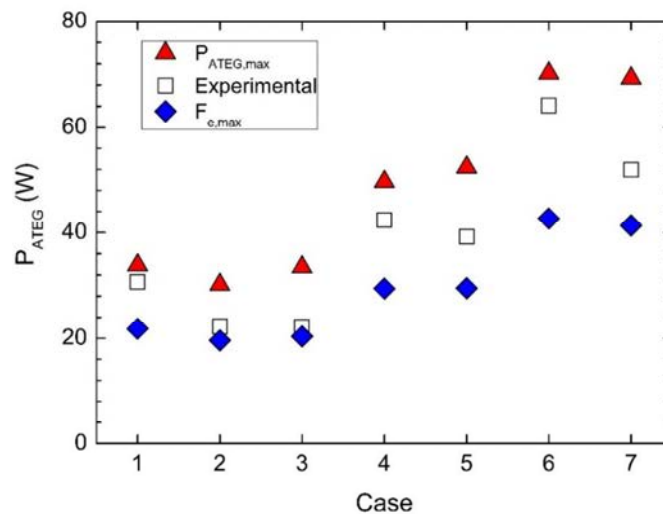


**Figure 17.** Output power of the ATEG obtained with the design that maximizes output power ( $P_{ATEG,max}$ ), the design that maximizes fuel economy ( $F_{e,max}$ ), and the design tested in the laboratory (Experimental) for the operational conditions given in Table 3.

However, differences in fuel consumption values for both designs were much higher (Figure 18). Note that all values in Figure 18 provided negative values of  $F_e$ , meaning that not one combination of the design parameters studied led to fuel savings. In contrast with output power, fuel economy was much more sensitive to the main ATEG design parameters and, particularly, to the design of the heat absorber. The reason is that back pressure was the dominant term when calculating fuel economy values.

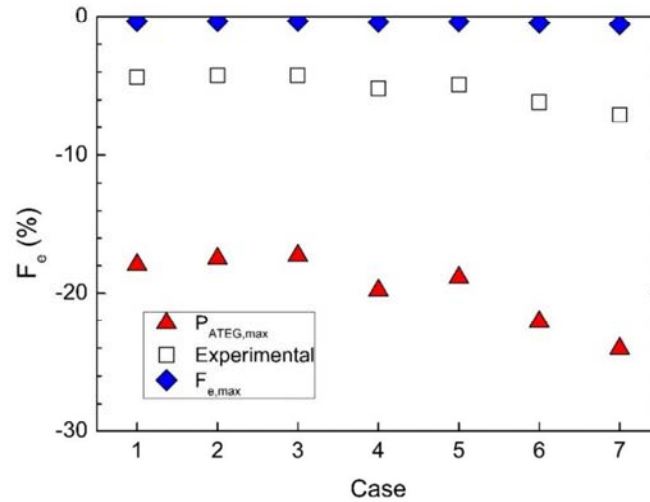


**Figure 18.** Fuel economy obtained with the design that maximizes output power ( $P_{ATEG,max}$ ), the design that maximizes fuel economy ( $F_{e,max}$ ), and the design tested in the laboratory (Experimental) for the operational conditions outlined in Table 3.

From Figure 18, we observed that the variability of the fuel consumption among the cases analyzed was not as high as among the output power values. For the  $P_{ATEG,max}$  design, for example,  $P_{ATEG} = 70$  W for case 6 and  $P_{ATEG} = 30$  W for case 2 (133% variation with respect to the latter case), whereas  $F_e = -24\%$  for case 6 and  $F_e = -17\%$  for case 1 (41% variation with respect to the latter case). A similar effect was observed for the  $F_{e,max}$  design. Thus, an initial estimation of the effect that back pressure values have on the fuel consumption does not require an evaluation of all the engine's operational points.

In addition to the effects of the structural design, improvements in ATEG performance can also be obtained by adopting state-of-the-art electronic techniques to maximize power generation in transient behaviors (e.g., maximum power point tracking control [46]). Finally, the ongoing research into new thermoelectric materials is expected to substantially increase the actual values of figure of merit in commercial modules in future years [47–48]. Thus, it is interesting to provide a simple tool to determine the increment of the actual  $ZT_e$  value in order to have positive fuel savings. This was carried out by analyzing data of Figure 16. Each one of the three terms that contributed to the fuel economy could be expressed with equations of the form  $F_{e,ATEG}(\%) = c_1 D^2 + c_2 D + c_3$ ,  $F_{e,BP}(\%) = c_4 e^{c_5 D}$ , and  $F_{e,m}(\%) = c_6 D^2 + c_7 D + c_8$  with  $c_1, \dots, c_8$  constants. For case 6, the values of the coefficients were  $c_1 = 0$  m<sup>-2</sup>,  $c_2 = -0.0156$  m<sup>-1</sup>,  $c_3 = 0.603$ ,  $c_4 = -254.6$ ,  $c_5 = -0.2948$  m<sup>-1</sup>,  $c_6 = 1.21 \times 10^4$  m<sup>-2</sup>,  $c_7 = -1.01 \times 10^6$  m<sup>-1</sup>, and  $c_8 = -0.1132$ , giving a square correlation coefficient greater than 0.998 in all of the three fits.  $F_{e,ATEG}(\%)$  was directly proportional to  $P_{ATEG}$  when neglecting the contribution of the increase of pumping power of the cooling water (11), and, hence, to  $ZT_e$  by assuming no changes in the thermal and in the electrical conductivity of TEMs. Thus, the condition  $rF_{e,ATEG} + F_{e,BP} + F_{e,m} = 0$  would provide the ratio  $r$  of the new figure of merit to the actual one needed to reach a null variation in fuel consumption. For  $D = 20$  mm in case 6, positive fuel savings would be achieved for  $r > 2.6$  (i.e., TEMs 260% more efficient than the actual ones), implying an electrical output power equal to 118 W.

## 6. Conclusions

A numerical model of an ATEG based on the GT-SUITE software was developed. The model was validated with experimental data and correctly predicted the electrical output power and the back pressure. The model was used to study the consequences of modifying the cooling flow rate and the cross-sectional areas of (1) hot gases conduits in the heat absorber, and (2) water flow in the heat



sink. Output power and fuel economy values were reported for different engine operating points. The main conclusions were as follows:

1. Engine operating points of maximum output power did not coincide with those of maximum fuel economy.
2. Designs that maximized output power differed substantially from those that maximized fuel savings.
3. While an increase in the cooling flow rate enhanced the output power, it also increased the power required to pump the cooling flow. Therefore, a compromise between gaining generated power and the loss of power needed to drive the water pump must be made. From the design point, a maximum value of flow velocity in the cooling system should be imposed to assure that energy losses are not excessive. Changes in the cross-sectional area of the water cooling channel had a similar effect. From the initial layout, a reduction in flow rate was preferred over an increase in the cross-sectional area of the channel, since the former implied greater decrements of the required pumping power.
4. The design of the heat absorber was critical in two opposing aspects: (1) to maximize the heat transfer, and (2) to minimize the back pressure. The back pressure was the main limiting factor in determining success in terms of fuel economy. Its value may vary several orders of magnitude depending on the type of heat absorber design. In order to have increments in fuel consumption <0.2% due to the effect of the back pressure, a value lower than 5 mbar should be attained.
5. A heat absorber with cylindrical holes is not a recommended geometry since it leads to large back pressure values. For this type of heat absorber, the main three terms that contributed to fuel savings could be analytically expressed as a function of the diameter of the cylindrical holes with a high degree of accuracy. The analytical equations could be used to determine the minimum efficiency of the thermoelectric modules (figure of merit) in order to obtain positive fuel savings.
6. The maximization of fuel savings cannot only rely on reducing back pressure values because this would result in trivial designs with very low back pressure and very low heat transfer being proposed. The feasibility of an ATEG requires a minimum value of electrical output power generated and this value should be kept as a constraint in the minimization study of the back pressure values.

Finally, it is worth noting that the present study had several limitations that can be resolved with future research. For example, the electrical connections were fixed in a series configuration since this was expected to provide the maximum output power. However, further investigation is required to determine whether or not hybrid (series/parallel) electrical configurations produce more electrical output power, especially in large ATEGs [35]. On the other hand, the fuel consumption calculations relied on analytical expressions that may deviate from observed data. Indeed, the goal of our ongoing research is to fully integrate the ATEG model into a complete simulation of a car within the GT-SUITE software and to validate its predictions with laboratory data. This full-vehicle model (including the ATEG) would provide very relevant information about the viability of this technology.

**Author Contributions:** M.C. conducted the experimental study including the entire set-up of the engine test bench and the flow bench. M.C. and I.R.C. conducted the detailed modeling and the validation study. M.C., E.M., and T.P. carried out the analyses of the results. M.C., A.M., and T.P. wrote the paper.

**Acknowledgments:** This work was partially funded by the University of Girona under the grant MPCUdG2016-4. The authors gratefully acknowledge the technical support provided by Sergi Saus and Jordi Vicens.

**Conflicts of Interest:** The authors declare no conflicts of interest. The funders had no role in the design of the study; the collection, analyses, or interpretation of data; the writing of the manuscript, or in the decision to publish the results.

## Nomenclature

$A$	area of the aluminum channel in contact with the water (m <sup>2</sup> )
$A_b$	block surface area (mm <sup>2</sup> )

$A_{TEM}$	TEM surface area (mm <sup>2</sup> )
$D$	diameter of the cylindrical holes (m)
$F_e$	fuel economy (%)
$F_{e,ATEG}$	fuel economy resulting from the power generated by the ATEG (%)
$F_{e,BP}$	fuel consumption (<0) due to overcome the back pressure (%)
$F_{e,m}$	fuel consumption due to increase in weight (%)
$g$	acceleration of gravity (m·s <sup>-2</sup> )
$h$	heat transfer coefficient (W·K <sup>-1</sup> ·m <sup>-2</sup> )
$I_{TEM}$	electrical current (A)
$k_b$	block thermal conductivity (W·K <sup>-1</sup> ·m <sup>-1</sup> )
$k_e$	TEM effective thermal conductivity (W·K <sup>-1</sup> ·m <sup>-1</sup> )
$L$	height of the cooling channel (mm)
$L_b$	block height (mm)
$L_{TEM}$	TEM height (mm)
$m_{ATEG}$	ATEG mass (kg)
$\dot{m}_g$	exhaust gas mass flow rate (g·s <sup>-1</sup> )
$N$	number of samples in the data series
$P_{ATEG}$	ATEG electrical output power (W)
$P_e$	engine-shaft power (W)
$P_{n,ATEG}$	net ATEG electrical output power (W)
$P_{TEM}$	TEM electrical output power (W)
$P_{wp}$	power consumed by the water pump (W)
$Q_c$	heat flow on the cold side of the TEM (W)
$Q_h$	heat flow on the hot side of the TEM (W)
$r$	ratio of figure of merits
$R_c$	thermal contact resistance (cold side) (m <sup>2</sup> ·K·W <sup>-1</sup> )
$R_h$	thermal contact resistance (hot side) (m <sup>2</sup> ·K·W <sup>-1</sup> )
$R_{ie}$	TEM effective internal electrical resistance (Ω)
$R_L$	external electrical load resistance (Ω)
$\bar{T}$	$(T_h + T_c)/2$ (K)
$T_c$	TEM cold side temperature (°C)
$T_g$	exhaust gas temperature (°C)
$T_h$	TEM hot side temperature (°C)
$T_w$	coolant temperature (°C)
$v$	vehicle velocity (m·s <sup>-1</sup> )
$V_{oc}$	open-circuit voltage (V)
$\dot{V}_w$	volumetric flow of the ATEG coolant (L·h <sup>-1</sup> )
$ZT_e$	effective figure of merit
$Z_{\alpha/2}$	confidence range
$\alpha_e$	TEM effective Seebeck coefficient (V·K <sup>-1</sup> )
$\Delta p_{bp}$	back pressure increase due to the ATEG (Pa)
$\varepsilon_e$	uncertainty of the equipment
$\varepsilon_s$	uncertainty of the mean values
$\varepsilon$	total uncertainty of data
$\eta$	ATEG efficiency
$\eta_G$	efficiency of the alternator
$\eta_{PCU}$	efficiency of the power converter unit
$\lambda$	air–fuel equivalence ratio
$\xi$	vehicle rolling resistance
$\rho_e$	effective electrical resistivity (Ω·m)
$\sigma$	standard deviation

### Subscripts

i	inlet
max	maximum conditions
o	outlet

### Abbreviations

AFR	air–fuel ratio
AFR <sub>s</sub>	stoichiometric air–fuel ratio
ATEG	Automotive thermoelectric generator
CAE	computer-aided engineering
CI	compression ignition
CSHE	cold-side heat exchanger
EGR	exhaust gas recirculation
HDV	heavy-duty vehicle
HexS	hexagonal cross-section
HP	heat pipes
HSHE	hot-side heat exchanger
ICE	internal combustion engine
OctS	octagonal cross-section
PCU	power converter unit
SI	spark ignition
TEG	thermoelectric generator
TEM	thermoelectric module
2PP	two parallel plates
4SSP	four square section plates

### References

1. Rahman, A.; Razzak, F.; Afroz, R.; Akm, M.; Hawlader, M.N.A. Power generation from waste IC engines. *Renew. Sustain. Energy Rev.* **2015**, *51*, 382–395.
2. Vázquez, J.; Palacios, R.; Sanz-Bobi, M.A. State of the art of thermoelectric generators based on heat recovered from the exhaust gases of automobiles. In Proceedings of the 7th European Workshop on Thermoelectrics, Pamplona, Spain, 3–4 October 2002.
3. European Commission. *Clean Power for Transport: A European Alternative Fuels Strategy. Communication from the Commission to the European Parliament, the Council, the European Economic and Social Committee and the Committee of the Regions*; COM (2013) 17; European Commission: Brussels, Belgium, 2013.
4. Karvonen, M.; Kapoor, R.; Uusitalo, A.; Ojanen, V. Technology competition in the internal combustion engine waste heat recovery: A patent landscape analysis. *J. Clean. Prod.* **2016**, *112*, 3735–3742.
5. Massaguer, A.; Massaguer, E.; Comamala, M.; Pujol, T.; Montoro, L.; Cardenas, M.D.; Carbonell, D.; Bueno, A.J. Transient behavior under a normalized driving cycle of an automotive thermoelectric generator. *Appl. Energy* **2017**, *206*, 1282–1296.
6. Fernández-Yáñez, P.; Armas, O.; Kiwan, R.; Stefaopoulou, A.G.; Boehman, A.L. A thermoelectric generator in exhaust systems of spark-ignition and compression-ignition engines. A comparison with an electric turbo-generator. *Appl. Energy* **2018**, *229*, 80–87.
7. Comamala, M.; Pujol, T.; Cózar, I.R.; Massaguer, E.; Massaguer, A. Power and fuel economy of a radial automotive thermoelectric generator: Experimental and numerical studies. *Energies* **2018**, *11*, 2720.
8. Stobart, R.; Wijewardane, M.A.; Yang, Z. Comprehensive analysis of thermoelectric generation systems for automotive applications. *Appl. Therm. Eng.* **2017**, *112*, 1433–1444.
9. Matsubara, K. Development of a high efficient thermoelectric stack for a waste exhaust heat recovery of vehicles. In Proceedings of the 21st International Conference on Thermoelectronics, Proceedings ICT, Long Beach, CA, USA, 29 August 2002; pp. 418–423.
10. Kim, T.Y.; Kwak, J.; Kim, B-W. Energy harvesting performance of hexagonal shaped thermoelectric generator for passenger vehicle applications: An experimental approach. *Energy Convers. Manag.* **2018**, *160*, 14–21.

11. Orr, B.; Akbarzadeh, A.; Lappas, P. An exhaust heat recovery system utilizing thermoelectric generators and heat pipes. *Appl. Therm. Eng.* **2017**, *126*, 1185–1190.
12. Haidar, J.G.; Ghojel, J.I. Waste heat recovery from the exhaust of low-power diesel engine using thermoelectric generators. In Proceedings of the 20th International Conference on Thermoelectrics, Proceedings ICT, Beijing, China, 8–11 June 2001; pp. 413–417.
13. Wang, Y.; Li, S.; Xie, X.; Deng, Y.; Liu, X.; Su, C. Performance evaluation of an automotive thermoelectric generator with inserted fins or dimpled-surface hot heat exchanger. *Appl. Energy* **2018**, *218*, 391–401.
14. Thacher, E.F.; Helenbrook, B.T.; Karri, M.A.; Richter, C.J. Testing of an automobile exhaust thermoelectric generator in a light truck. *Proc. Inst. Mech. Eng. Part D* **2007**, *221*, 95–107.
15. Lan, S.; Yang, Z.; Chen, R.; Stobart, R. A dynamic model for thermoelectric generator applied to vehicle waste heat recovery. *Appl. Energy* **2018**, *210*, 327–338.
16. Frobenius, F.; Gaiser, G.; Rusche, U.; Weller, B. Thermoelectric generators for the integration into automotive exhaust systems for passenger cars and commercial vehicles. *J. Electron. Mater.* **2016**, *45*, 1433–1440.
17. Bass, J.C.; Elsner, N.B.; Leavitt, F.A. Performance of the 1 kW thermoelectric generator for diesel engines. *AIP Conf. Proc.* **1994**, *316*, 295–298.
18. Massaguer, A.; Massaguer, E.; Comamala, M.; Pujol, T.; González, J.R.; Cardenas, M.D.; Carbonell, D.; Bueno, A.J. A method to assess the fuel economy of automotive thermoelectric generators. *Appl. Energy* **2018**, *222*, 42–58.
19. Karri, M.A.; Thacher, E.F.; Helenbrook, B.T. Exhaust energy conversion of thermoelectric generator: Two case studies. *Energy Convers. Manag.* **2011**, *52*, 1596–1611.
20. Champier, D. Thermoelectric generators: A review of applications. *Energy Convers. Manag.* **2017**, *140*, 167–181.
21. Von Lukowicz, M.; Abbe, E.; Schmiel, T.; Tajmar, M. Thermoelectric generators on satellites—An approach for waste heat recovery in space. *Energies* **2016**, *9*, 541.
22. Lv, H.; Li, G.; Zheng, Y.; Hu, J.; Li, J. Compact water-cooled thermoelectric generator (TEG) based on a portable gas stove. *Energies* **2018**, *11*, 2231.
23. Li, G.; Zhang, G.; He, W.; Ji, J.; Lv, S.; Chen, X.; Chen, H. Performance analysis on a solar concentrating thermoelectric generator using the micro-channel heat pipe array. *Energy Convers. Manag.* **2016**, *112*, 191–198.
24. Li, G.; Feng, W.; Jin, Y.; Chen, X.; Ji, J. Discussion on the solar concentrating thermoelectric generation using micro-channel heat pipe array. *Heat Mass Transfer* **2017**, *53*, 3249–3256.
25. Li, G.; Chen, X.; Jin, Y. Analysis of the primary constraint conditions of an efficient photovoltaic-thermoelectric hybrid system. *Energies* **2017**, *10*, 20.
26. Li, G.; Ji, J.; Zhang, G.; He, W.; Chen, X.; Chen, H. Performance analysis on a novel micro-channel heat pipe evacuated tube solar collector-incorporated thermoelectric generation. *Int. J. Energy Res.* **2016**, *40*, 2117–2127.
27. Cheng, K.; Feng, Y.; Lv, C.; Zhang, S.; Qin, J.; Bao, W. Performance evaluation of waste heat recovery systems based on semiconductor thermoelectric generators for hypersonic vehicles. *Energies* **2017**, *10*, 570.
28. Fernández-Yañez, P.; Armas, O.; Capetillo, A.; Martínez-Martínez, S. Thermal analysis of a thermoelectric generator for light-duty diesel engines. *Appl. Energy* **2018**, *226*, 690–702.
29. He, W.; Zhang, G.; Li, G.; Ji, J. Analysis and discussion on the impact of non-uniform input heat flux on thermoelectric generator array. *Energy Convers. Manag.* **2015**, *98*, 268–274.
30. Risseh, A.E.; Nee, H.-P.; Goupil, C. Electrical power conditioning system for thermoelectric waste heat recovery in commercial vehicles. *IEEE Trans. Transp. Electrification* **2018**, *4*, 548–562.
31. Demir, M.E.; Dincer, I. Performance assessment of a thermoelectric generator applied to exhaust waste heat recovery. *Appl. Therm. Eng.* **2017**, *120*, 694–707.
32. He, W.; Wang, S.; Yue, L. High net power output analysis with changes in exhaust temperature in a thermoelectric generator system. *Appl. Energy* **2017**, *196*, 259–267.
33. Kempf, N.; Zhang, Y. Design and optimization of automotive thermoelectric generators for maximum fuel efficiency improvement. *Energy Convers. Manag.* **2016**, *121*, 224–231.
34. Gamma Technologies LLC. Available online: <https://www.gtisoft.com> (accessed on 1 October 2018).
35. Cózar, I.R.; Pujol, T.; Lehocny, M. Numerical analysis of the effects of electrical and thermal configurations of thermoelectric modules in large-scale thermoelectric generators. *Appl. Energy* **2018**, *229*, 264–280.



36. National Instruments. Available online: <http://www.ni.com> (accessed on 3 September 2018).
37. Omega. Available online: <http://www.omega.com> (accessed on 3 September 2018).
38. Sensus. Available online: <http://www.sensus.com> (accessed on 3 September 2018).
39. Su, J.; Xu, M.; Li, T.; Gao, Y.; Wang, J. Combined effects of cooled EGR and a higher geometric compression ratio on thermal efficiency improvement of a downsized boosted spark-ignition direct engine. *Energy Convers. Manag.* **2014**, *78*, 65–73.
40. Zhao, M.; Wei, M.; Song, P.; Liu, Z.; Tian, G. Performance evaluation of a diesel engine integrated with ORC system. *Appl. Therm. Eng.* **2017**, *115*, 221–228.
41. Zhao, R.; Li, W.; Zhuge, W.; Zhang, Y.; Yin, Y. Numerical study on steam injection in a turbocompound diesel engine for waste heat recovery. *Appl. Energy* **2017**, *185*, 506–518.
42. Incropera, F.P.; DeWitt, D.P.; Bergman, T.L.; Lavine, A.S. *Fundamentals of Heat and Mass Transfer*, 7th ed.; John Wiley & Sons, Inc.: Hoboken, NJ, USA, 2007.
43. Chen, J.; Li, K.; Liu, C.; Li, M.; Lv, Y.; Jia, L.; Jiang, S. Enhanced efficiency of thermoelectric generator by optimizing mechanical and electrical structures. *Energies* **2017**, *10*, 1329.
44. Li, Z.; Li, W.; Chen, Z. Performance analysis of thermoelectric based automotive waste heat recovery system with nano fluid coolant. *Energies* **2017**, *10*, 1489.
45. Alam, T.; Kim, M-H. A comprehensive review on single phase heat transfer enhancement techniques in heat exchanger applications. *Renew. Sustain. Energy Rev.* **2018**, *81*, 813–839.
46. Twaha, S.; Zhu, J.; Maraaba, L.; Huang, K.; Li, B.; Yan, Y. Maximum power point tracking control of a thermoelectric generation system using the extremum seeking control method. *Energies* **2017**, *10*, 2016.
47. Xie, D.; Xu, J.; Liu, G.; Liu, Z.; Shao, H.; Tan, X.; Jiang, J.; Jiang, H. Synergistic optimization of thermoelectric performance in p-type Bi<sub>0.48</sub>Sb<sub>1.52</sub>Te<sub>3</sub>/graphene composite. *Energies* **2016**, *9*, 236.
48. Zhao, D.; Wu, D.; Bo, L. Enhanced thermoelectric properties of Cu<sub>2</sub>SbSe<sub>4</sub> compounds via gallium doping. *Energies* **2017**, *10*, 1524.



© 2018 by the authors. Licensee MDPI, Basel, Switzerland. This article is an open access article distributed under the terms and conditions of the Creative Commons Attribution (CC BY) license (<http://creativecommons.org/licenses/by/4.0/>).

## Chapter 3

# Power and Fuel Economy of a Radial Automotive Thermoelectric Generator: Experimental and Numerical Studies

---

This chapter is the transcription of the content of the following article

M Comamala, T Pujol, I Ruiz, E Massaguer, A Massaguer. **Power and Fuel Economy of a Radial Automotive Thermoelectric Generator: Experimental and Numerical Studies**. *Energies*, 11, 2720, 2018. ISSN 1996-1073 (Impact factor 2.676; Journal 48 of 97; 2nd quartile; Energy and Fuels)  
<https://doi.org/10.3390/en11102720>





Article

# Power and Fuel Economy of a Radial Automotive Thermoelectric Generator: Experimental and Numerical Studies

Martí Comamala , Toni Pujol \* , Ivan Ruiz Cózar, Eduard Massaguer and Albert Massaguer <sup>†</sup>

Department of Mechanical Engineering and Industrial Construction, University of Girona, c/Universitat de Girona 4, 17003 Girona, Spain; marti.comamala@udg.edu (M.C.); ivan.ruiz@udg.edu (I.R.C.); eduard.massaguer@udg.edu (E.M.); albert@nablatherm.com (A.M.)

\* Correspondence: toni.pujol@udg.edu; Tel.: +34-686-724-750

<sup>†</sup> Current address: Nabla Thermoelectrics, c/Llibertat 71, 17820 Banyoles, Spain.

Received: 30 September 2018; Accepted: 10 October 2018; Published: 11 October 2018



**Abstract:** Recent developments of high performance thermoelectric (TE) materials have increased the interest of using this technology to directly convert waste heat into electricity. In the automotive sector, many automotive thermoelectric generators (ATEGs) designs use TE modules (TEMs) with high hot side temperatures to cope with high engine load regimes. Here, we develop a new concept of a radial ATEG that is specifically designed to work with low temperature TEMs, which enables the use of Pb-free modules and reduces the thermal stress of the device. A prototype is built and tested at different regimes in an engine test bench. A numerical model of the ATEG is developed and validated. The consequences of modifying (1) the exchange area between the heat absorber and the exhaust gases and (2) the effective figure of merit of TEMs on the electrical output power and fuel economy are investigated by means of simulations. Results indicate that the maximum fuel economy (1.3%) is not attained at the point of maximum output power (228 W). In terms of fuel economy, the back pressure at the exhaust penalizes high mass flow regimes. We use a dimensionless parameter to analyze the potential of the ATEG for reducing fuel consumption.

**Keywords:** thermoelectric generator; ATEG; waste heat recovery; fuel economy

## 1. Introduction

Transport contributes to more than 20% of carbon dioxide (CO<sub>2</sub>) emissions worldwide [1]. In Europe, this contribution rises up to 27%, becoming the biggest source of carbon emissions and the main cause of air pollution in cities [2]. Since road transport accounts for more than 70% of all transport emissions, the European Union (EU) has defined green (i.e., low-emission) mobility as one of the main challenges of our society [3]. The transition to a low-carbon mobility involves a strategy with several priority actions. One of them is the development of more efficient vehicles that use internal combustion engines (ICEs), since this technology is not expected to decline at mid-term in long-distance transport with heavy-duty vehicles [4].

In ICEs, approximately 1/3 of the consumed primary energy is lost through the exhaust gases [5]. Several technologies aim to recover part of this waste heat to reduce fuel consumption. The most promising ones are organic Rankine cycles (ORCs) and automotive thermoelectric generators (ATEGs) [6].

ATEGs are devices located at the exhaust pipe, and they consist of commercial thermoelectric modules (TEMs) sandwiched between heat absorbers (in contact with exhaust gases) and heat sinks (in contact either with air or with liquid coolant) with the purpose of maintaining a given temperature difference or, equivalently, a heat flux, across them. TEMs directly convert this heat into electricity. The electrical energy generated is stored in batteries and shortens the time of alternator demand.

As a consequence, the engine torque that is intended to drive the alternator reduces, and therefore, fuel consumption diminishes.

On the other hand, the heat absorbers of the ATEG may be circular tubes [7], straight fins [8–11], dimples [12], phase-change pipes [13], etc., and, to some extent, all of them increase the pressure upstream of the exhaust pipe. This back pressure alters the regular functioning of the engine and increases the fuel consumption. This effect may eventually counterbalance the energy savings produced by electrical generation. However, many previous studies on ATEGs have focused only on maximizing ATEG electrical output power, ignoring the effect of the back pressure, and consequently, overestimating its performance.

Table 1 lists very recent experimental studies of ATEGs. The most common design employed in ATEGs distributes commercial TEMs in a way where their hot side surfaces are in contact with longitudinal (with respect to the flow direction) plates that contour the perimeter of the device cross-section (rectangular [7,8,10,12–14], square [11] or hexagonal [9]). The main problem of this layout is the high temperature that is achieved during a driving cycle, since hot gases at full load regimes may exceed 500 °C. Since the maximum allowable hot side temperature in bismute telluride TEMs is on the order of 250 °C, several authors have devised mechanisms to avoid damaging TEMs, which are mainly focused on bypassing the ATEG [8,10]. Alternative designs may involve heat pipes [13], so TEMs can be easily assembled without interfering with the exhaust manifold, or cylindrical non-commercial TEMs mounted in a transversal plane inside the exhaust system [15].

**Table 1.** Exhaust gas temperature at automotive thermoelectric generators (ATEG) inlet  $T_{g,i}$ , coolant temperature at ATEG inlet  $T_{c,i}$ , ATEG mass  $m_{ATEG}$ , ATEG electrical output power  $P_{ATEG}$ , ATEG backpressure  $\Delta p_{bp}$  and fuel economy  $F_e$  due to the ATEG at the best performance point in recent experimental studies.

Engine <sup>1</sup>	ATEG Design <sup>2</sup>	#TEMs	$T_{g,i}$ (°C)	$T_{c,i}$ (°C)	Heat Absorber	$m_{ATEG}$ (kg)	$P_{ATEG}$ (W)	$\Delta p_{bp}$ (Pa)	$F_e$ (%)	Reference
1.4 L SI	2PP	12	709	74	Circular tubes	7	111	3653		[7]
HDV	2PP	224		80	Fins		416			[8]
2.0 L SI	HexS	18	611	80	Fins		99	2100		[9]
1.6 L SI	2PP	80	719	50	Fins		137	318	1.1 *	[10]
1.9 L CI	4SSP	8	427	7	Radial fins		30	149		[11]
3.9 L CI	2PP	240	290	80	Fins/dimps	200	618	1348		[12]
3.0 L SI	HP	8	350	30	Heat pipes		38	135		[13]
6.6 L CI	2PP	4	200	10			8			[14]
1.8 L CI	Radial	10	540	28	Fins	4.8	40	524 *	0.0 *	Present

<sup>1</sup> SI = Spark ignition; CI = Compression ignition; HDV = heavy duty vehicle (engine not specified); <sup>2</sup> 2PP = two parallel plates; 4SSP = four square section plates; HexS = hexagonal section; HP = heat pipes; \* Data obtained from numerical calculations.

Maximum values of fuel economy due to ATEGs are commonly not reported (see Table 1), although values on the order of 1% have been estimated [10]. These are slightly lower values than those claimed by using ORCs (up to 7% [16]), although back pressure and weight effects in real on-vehicle tests may substantially reduce this figure, even leading to increments in fuel consumption [17]. In comparison with ORCs, ATEGs possess the advantages of being simpler, lighter, and more silent, compact, and reliable [6].

Thus, the research in ATEGs is in constant development. Especially in recent years, when ongoing research on new bulk thermoelectric materials has led to a continuous increase of the values of the figure of merit ( $ZT$ ) that determines the potential to convert heat into electricity. However, there still exists a gap between the efficiency of these bulk materials and commercial TEMs, which are formed by hundreds of  $p$ -type and  $n$ -type thermoelectric legs, electrically conductive junctions, and electrically isolating plates [18]. TEMs also suffer from thermal stress due to the continuous exposure to low and high temperature cycles [18]. This applies not only to each individual component of the TEM, but also to the overall module because of the mismatch in the thermal expansion coefficient of the materials used. Thus, in order to avoid TEM failure and to assure long-term mechanical stability, the



temperature variations applied to the TEM should be minimized [19]. However, and in order (1) to extract the maximum available heat of exhaust gases, and (2) to avoid not being overheated, some previous ATEG designs use high temperature TEMs (nominal hot side temperature on the order of 500 °C) [7]. These high temperature TEMs often use Pb in the semiconductors, unable to be present in commercial devices due to environmental reasons.

Thus, the purpose of the present paper aims to address the two issues regarding ATEGs that have been stated above: (1) to develop a novel ATEG design able to work with low temperature Pb-free commercial TEMs, and (2) to analyze the ATEG performance in terms of fuel consumption rather than on electrical output power.

The design consists of a radial ATEG whose main novelty is that the TEMs are not faced towards the exhaust pipe, but they are distributed in a transversal plane to the flow. This layout avoids the overheating of TEMs in high engine load regimes without adding any mechanical part, and allows us to use low-temperature TEMs. This radial ATEG is explained in detail in Section 2, where we also carry out an experimental study in an engine test bench. Section 3 describes and validates the numerical model that is used to simulate the ATEG. Numerical simulations under different scenarios (changes in TEMs performance and in fin dimensions of the heat absorbers) are analyzed in Section 4, which also includes a discussion focused on the fuel economy. Finally, the main conclusions are found in Section 5.

## 2. Experimental Analysis

### 2.1. Radial ATEG

The radial ATEG mounts five identical cooling-TEM-heat absorber units (see Figure 1). The core of each unit is the heat absorber. It is made of a single block of copper with 15 precision machined fins at one end (Figure 1a). These fins are 1 mm thick and 30 mm long. The fin height is 10 mm in all fins except in fins #1 and #15 (5 mm high) and #2 and #14 (7.5 mm high), in order to avoid interferences with neighbor units. The heat absorbers were custom made by a local machining company according to our requirements. These copper units are inserted in a pentagonal pipe after applying a sealant at its contact base (Figure 1b). The total system of five copper heat absorbers accounts for an exchange surface area with the exhaust gases equal to  $A_{t,o} = 418 \text{ cm}^2$ . Each one of the heat absorbers is milled to 0.5 mm depth in a  $40 \times 46 \text{ mm}$  surface area in both upstream and downstream faces for housing low temperature thermoelectric modules (H-199-14-06-L2, Crystal LTD [20]). Thermal grease was applied at both hot and cold sides of the TEMs for improving the heat transfer. The cold side of each TEM was in contact with a  $40 \times 40 \text{ mm}$  BXQINLENX water heat sink. Two aluminum rings clamped together the water heat sinks located at both opposite faces, finally exerting on the TEMs a pressure that was equal to 0.9 MPa (Figure 1c).

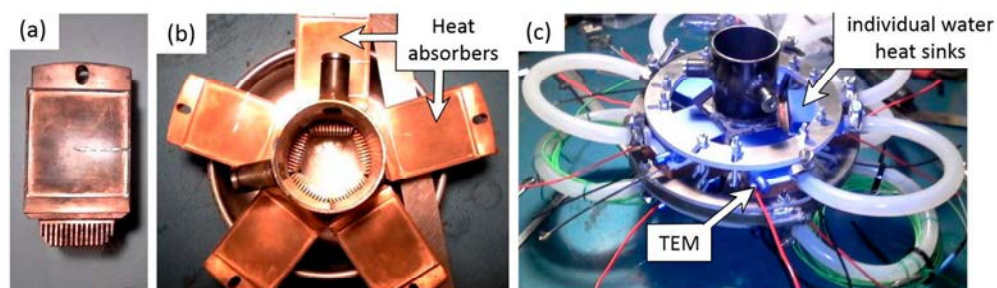


**Figure 1.** (a) Copper heat absorber (note the milling to insert the thermocouple); (b) radial distribution of the copper heat absorbers; (c) final assembly of the radial TEG including 5 heat absorbers, 10 individual water heat sinks and 10 TE modules (TEMs). For dimensions, see text.

Due to water pump limitations, each row of five water heat sinks are hydraulically connected in series. All 10 TEMs are electrically connected in series, since this connection is expected to produce higher output power than either parallel or hybrid ones [21]. The total weight of the system, including the 50 mm diameter pipes at both ATEG inlet and outlet, is only 4.8 kg. In addition, the system was very compact, with an overall diameter of 20 cm (excluding water pipes) and a length of 20 cm.

In comparison with other ATEGs, this design has several advantages. First, all TEMs possess a very similar temperature difference, since all of them absorb energy at the same point. Small differences appear due to the hydraulic connection in series but, as will be observed next, these are of low relevance. Thus, the external electrical load resistance can be tuned to match the optimum value that is valid for all TEMs. Second, the use of high volume heat absorbers avoids the overheating of TEMs without using any mechanical system. This allows us to use economic, free-Pb, low temperature TEMs. At the same point, this implies a high heat capacity of the heat absorbers, preventing fast fluctuations from being obtained in the output power as the regime changes in transient cycles. Finally, the radial distribution facilitates the individual monitoring of TEMs and their removal in case of malfunction.

## 2.2. Experimental Set Up

The engine test bench uses a PSA XUD7 1.8 L diesel engine connected to a Schenck W130 dynamometer (Figure 2). Water initially at 19 °C from an external reservoir of 400 L capacity was used for cooling the ATEG. The flow rate was 4.4 liters/minute per each row of five water heat sinks that were hydraulically connected in series. In an ICE, the engine coolant temperature under regular functioning is in the order of 80 °C. This implies that our testing conditions were equivalent to include an independent cooling system for the ATEG in the case of being installed in a road vehicle. This strategy may be more suitable than redesigning the engine cooling system (radiator and pump) in order to operate with engine coolant, since the use of low temperature coolant for the heat sinks located at TEMs cold side is expected to substantially increase the electrical output power [22]. As already commented, the TEMs are electrically connected in series with a variable external load resistance.

Data from the dynamometer, ICE, and ATEG were simultaneously recorded. Exhaust gas temperatures at the ATEG inlet and outlet, the cold and hot side temperatures of TEM #1 (at water inlet) and #5 (at water outlet), the water temperatures at the ATEG inlet and outlet, and the ambient temperature were acquired with type K thermocouples by a National Instruments (NI) Compact RIO system with 9211 modules. In the electrical circuit, voltage and current were acquired by a NI Compact RIO with 9215 and 9227 modules. These data were processed with LabVIEW software.

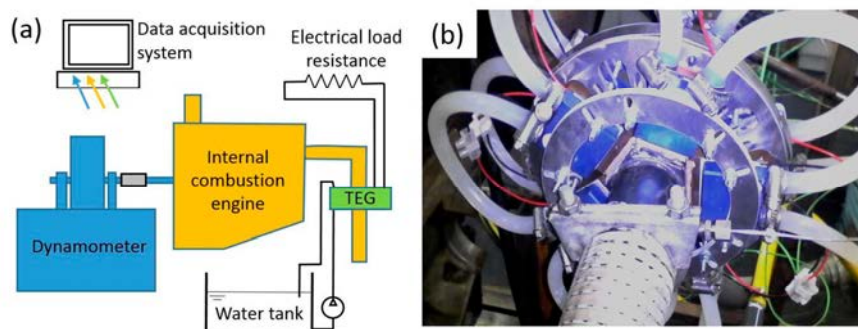


Figure 2. (a) Schematic laboratory set up; (b) TEG installed at the exhaust pipe.

The treatment of the experimental uncertainty and the accuracy of the equipment used in the experimental tests are described in detail in [21], where a similar laboratory layout was applied in the study of an ATEG with a single TEM. As a summary, the total uncertainty was calculated from the uncertainty of the data series  $\varepsilon_{ds}$  recorded by the data acquisition system:



$$\varepsilon_{ds} = \pm z_{\alpha/2} \frac{\sigma}{\sqrt{N}}, \quad (1)$$

where  $z_{\alpha/2}$  is the confidence range,  $\sigma$  is the standard deviation and  $N$  is the number of samples, and the uncertainty of the equipment  $\varepsilon_{eq}$ :

$$\varepsilon_{eq} = \sum \left| \frac{\partial Y}{\partial x} \right| \Delta x, \quad (2)$$

where  $Y$  corresponds to the indirect value,  $x$  refers to the direct measured value, and  $\Delta x$  is the accuracy of the equipment in the measurement of the  $x$  value. Table 2 lists the main  $\Delta x$  values of our equipment.

**Table 2.** Accuracy of the experimental equipment.

Equipment	Accuracy	Reference
Current (NI 9227)	$\pm(169.7 \text{ mA} + 5\% \text{ of reading})$	[23]
Voltage (NI 9215)	$\pm(85.3 \text{ mV} + 1.05\% \text{ of reading})$	[23]
Temperature (NI 9211)	$\pm 0.6 \text{ }^\circ\text{C}$	[23]
Type K thermocouple	$\pm 1.5 \text{ }^\circ\text{C}$	[24]
Sensus 405 S water meter	$\pm 0.05 \text{ L}$	[25]
Manometer	$\pm 10 \text{ Pa}$	
Calibrated volume cylinder	$\pm 10 \text{ cm}^3$	

Thus, the total uncertainty of data  $\varepsilon_{total}$  follows:

$$\varepsilon_{total} = \sqrt{\varepsilon_{ds}^2 + \varepsilon_{eq}^2}. \quad (3)$$

### 2.3. Experimental Cases

Eight different engine operating points were tested (see Figure 3). These points cover a broad working zone. Points 1 to 3 corresponded to scenarios at three different loads at a turning velocity equal to 1500 rpm; points 4 to 6 at a turning velocity of 2000 rpm, and points 7 and 8 at a turning velocity of 2500 rpm. Note that the exhaust mass flow rate was almost constant in points with equal turning velocity (see Table 3). In terms of load, almost no-load conditions were applied in points 1 and 4. An intermediate load were applied in points 2, 5 and 7, and a heavy load in points 3, 6 and 8. The temperature of the exhaust gases at the ATEG inlet was basically a function of the load applied to the engine. For each one of the eight different regimes, the external electrical resistance was tuned to achieve the maximum output power.

**Table 3.** Experimental data of torque, exhaust gas mass flow rate  $\dot{m}_g$ , temperature of the exhaust gas at ATEG inlet  $T_{g,i}$ , temperature of water coolant at ATEG inlet  $T_{w,i}$ , and ambient temperature  $T_{amb}$ .

Case	Regime (rpm)	Torque (N m)	$\dot{m}_g$ (g/s)	$T_{g,I}$ ( $^\circ\text{C}$ )	$T_{w,I}$ ( $^\circ\text{C}$ )	$T_{amb}$ ( $^\circ\text{C}$ )
1	1500	$21.4 \pm 0.1$	$24.1 \pm 0.6$	$158.5 \pm 1.6$	$19.1 \pm 1.6$	$20.0 \pm 1.6$
2	1500	$50.0 \pm 0.1$	$24.0 \pm 0.6$	$259.7 \pm 1.6$	$20.2 \pm 1.6$	$20.9 \pm 1.6$
3	1500	$79.1 \pm 0.1$	$24.1 \pm 0.7$	$454.8 \pm 1.6$	$20.3 \pm 1.6$	$23.4 \pm 1.6$
4	2200	$14.4 \pm 0.1$	$34.5 \pm 0.4$	$159.5 \pm 1.6$	$21.8 \pm 1.6$	$24.6 \pm 1.6$
5	2200	$45.0 \pm 0.1$	$34.2 \pm 0.5$	$282.9 \pm 1.6$	$22.2 \pm 1.6$	$25.5 \pm 1.6$
6	2200	$72.3 \pm 0.1$	$34.1 \pm 0.7$	$510.5 \pm 1.6$	$22.9 \pm 1.6$	$27.6 \pm 1.6$
7	2700	$43.3 \pm 0.1$	$44.7 \pm 0.4$	$285.8 \pm 1.6$	$25.1 \pm 1.6$	$27.7 \pm 1.6$
8	2700	$76.2 \pm 0.1$	$44.8 \pm 0.7$	$539.1 \pm 1.6$	$24.8 \pm 1.6$	$29.4 \pm 1.6$



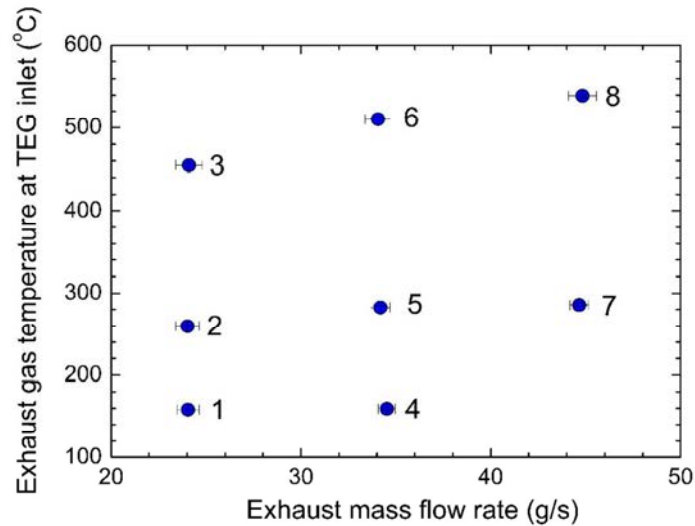


Figure 3. Exhaust gas temperature at ATEG inlet as a function of the exhaust mass flow rate for the eight experimental points analyzed.

### 3. Numerical Model

#### 3.1. Simulation Set Up

A numerical model is developed in order to provide results when some of the design parameters of the radial ATEG are changed. The simulation technique reduced costs and time in the analysis of alternative designs, and it allowed us to carry out sensitivity studies to variations in the main properties of the ATEG elements. The commercial computational fluid dynamics (CFD) software ANSYS-CFX<sup>®</sup> was used, since it has the capability to correctly simulate the heat transfer between fluid flows and solid parts. Several researchers have applied this software to successfully predict heat transfer problems involving both fluid and solids (e.g., [26]).

The computational domain consisted of one-fifth of the whole radial ATEG, since it takes advantage of radial symmetry conditions (Figure 4). Six solids and two fluids were involved in the simulation. For the sake of simplicity, Figure 4a shows the solid elements only, namely: the heat absorber (copper), pipe (steel), seal (aluminum), two identical heat sinks (aluminum), two identical rings (aluminum), and two TEMs. The fluids were liquid water that flowed in the heat sinks and air (ideal gas law) that simulated the exhaust gases. The latter approximation is common in studies of ATEGs (e.g., [27]), since it is known to produce small discrepancies in comparison with the real exhaust flow behavior. A schematic drawing of the main heat flow path is shown in Figure 4b, where we included both the conduction and convection processes.

The actual radial ATEG tested in the engine bench did not strictly possess a radial symmetry, since rows of five water heat sinks (all upstream and all downstream ones) were connected in series due to water pump limitations. However, the experimental values of both hot and cold side temperatures at the first and last (#5) TEMs were very similar (see Section 3.2), which confirmed the validity of simulating one-fifth of the entire device only. On the other hand, the longitudinal dimension of the domain was chosen so as to reproduce the experimental ATEG from the position of the inlet temperature sensor to the position of the outlet temperature sensor (Figures 1 and 2). Simulations with a pipe that was 50 mm longer at the exit have been also carried out. In the latter model, hot and cold side TEM temperatures and pressure changes across the ATEG differed less than 0.7% and 0.3%, respectively, in comparison with the results of the reference case. Therefore, the conclusions were expected to be independent of the simulation domain.

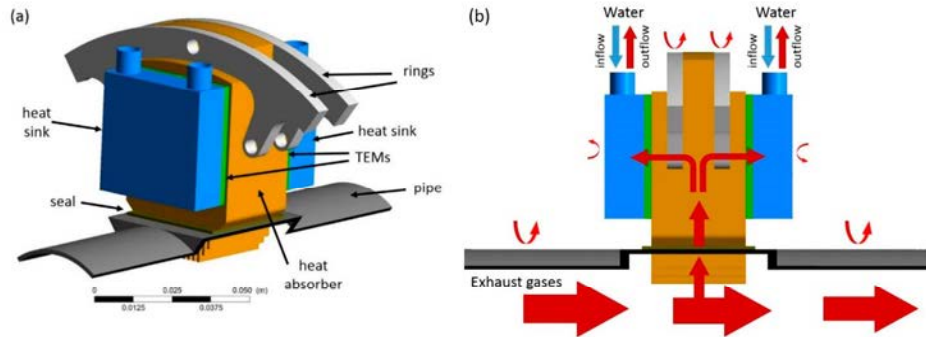


**Figure 4.** (a) Visualization of the domain applied in the simulations (solid parts only); (b) schematic drawing of the heat flow path.

The mesh was created with ANSYS-Meshing<sup>®</sup>. Quadrilaterals with 1 mm maximum length were used to mesh the heat absorber, rings, and seal. TEMs were meshed with quadrilaterals of 0.5 mm maximum length. Tetrahedrons were used to mesh complex geometries such as the pipe (1 mm maximum length) and, especially, the heat sinks (0.6 mm maximum length), since they contained five small inner passages. Fluids were also meshed with tetrahedrons of 0.5 mm maximum length for water, and of 0.7 mm maximum length for the exhaust gas. In the latter case, a refiner mesh near the fins of the heat absorber was defined (0.2 mm maximum length). Four layers of prisms were created in contact with the solid surface (Figure 5). A total number of  $8.8 \times 10^6$  elements were needed to mesh all the domains, with  $6.5 \times 10^6$  elements dedicated to the gas subdomain. The maximum skewness and aspect ratio values were 0.89 and 23.3, respectively. This was equivalent to  $44 \times 10^6$  elements for the entire ATEG device. Several coarser meshes were also simulated to evaluate the sensitivity of the results to changes in the mesh, as explained in Section 3.2. The finer mesh provided a wall-normal resolution  $y^+$  less than 5 (<15 for the coarser mesh), which agreed with the criterion employed in [12].

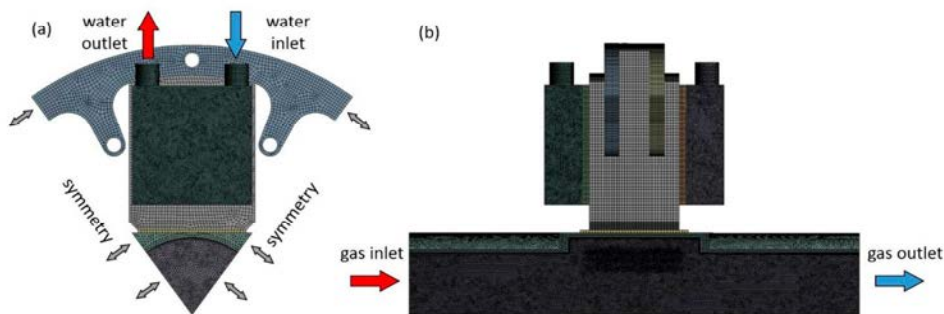


**Figure 5.** Mesh and non-wall boundaries with a different color scheme than in Figure 4 for a better visualization. (a) Frontal view; (b) longitudinal view.

Boundary conditions fixed the values of mass flow and temperature at both gas and water inlet surfaces. These values corresponded to the experimental data obtained in the previous section. Constant pressure was set at both the water and gas outlets. All other boundaries were defined as either symmetrical or smooth walls. Heat transfer was allowed in all surfaces (see Figure 4b). Contact thermal resistances  $R_c$  were added between the heat absorber and the TEM hot side, and between the TEM cold side and the heat sink. A constant value of  $R_c = 10^{-4} \text{ m}^2 \text{ K W}^{-1}$  was assumed, since it was representative of solid/solid interfaces [28] and similar values have satisfactorily been used in other studies of ATEGs [7]. Convection to the ambient air was allowed in all bodies, using

a convective heat transfer coefficient for natural convection  $h_c = 2 \text{ W m}^{-2} \text{ K}^{-1}$  [28]. The effect of including radiative fluxes in the simulation was analyzed, and it produces modifications in hot and cold side TEM temperatures less than 1%. Therefore, radiation was ignored since it substantially slowed down the calculation time and its inclusion did not alter the main conclusions of our research.

Heat transfer by conduction uses the thermal conductivity of solid and fluid elements. Here, each one of the TEMs was included as a single solid, so that effective thermal and electrical properties for the whole module were used. The effective thermal conductivity of the whole TEM was used in order to correctly capture the thermal behavior of the ATEG in the simulation process. The effective thermoelectric properties of the whole TEM (essentially the effective Seebeck coefficient) were not included in the simulations. This property was used in the analytical calculation of the maximum output power that the ATEG design could provide. This is a common strategy that is adopted to numerically analyze the behavior of large scale ATEGs [11,12,21]. Note that each individual TEM is formed by hundredths of *p*-type and *n*-type semiconductors that are connected in series with small sheets of copper that act as junctions of two dissimilar thermoelements and that are packed with two electrically isolating ceramic plates. The simulation of a single TEM taking into account all of these components would involve domains with characteristic sizes that differ in more than three orders of magnitude, and therefore, it would require very high computational resources.

Here, the effective thermal conductivity of the whole TEM  $k_e$ , has been extracted by using the manufacturer's datasheet of output power that is generated at a matched electrical load, expressing it as a function of temperature differences at both hot  $T_h$  and cold  $T_c$  sides of the TEM ( $\Delta T = T_h - T_c$ ), being  $k_e = -1.455 \times 10^{-4} \Delta T^2 + 0.0674 \Delta T + 0.0269$ .

Both exhaust gases and cooling water flow regimes are turbulent. The RNG *k*- $\epsilon$  turbulence model with 10% turbulence intensity at the inlet of exhaust gases and 5% turbulence intensity at water inlets has been adopted. High resolution schemes for both advection and turbulence are chosen, with a convergence criterion of RMS residuals of less than  $10^{-5}$ .

The previous set up of the CFD model simulates heat transfer and flow behaviors only. Electrical output power  $P_{ATEG}$  of the ATEG is calculated by assuming optimum conditions:

$$P_{ATEG} = n \frac{\alpha_e^2 \Delta T^2}{4R_i}, \quad (4)$$

where  $n$  ( $=10$ ) is the number of TEMs,  $\alpha_e$  is the effective Seebeck coefficient, and  $R_i$  corresponds to the electrical load resistance that, per unit TEM, maximizes the output power. In Equation (4), we implicitly assume small variations among the  $\Delta T$  measured in each individual TEM, since they are thermally connected in parallel. Due to the series connection of the water cooling system in the experimental study, there exist some deviations in the individual values of  $\Delta T$ , although these are smaller than 5% for all regimes. On the other hand, the effective Seebeck coefficient  $\alpha_e$  employed in the calculation of the output power is chosen to match the experimental value determined from Equation (4). Thus, measured TEM hot and cold side temperature differences  $\Delta T$ , electrical load resistance  $R_i$ , and output power  $P$  from the eight experimental cases detailed in Table 3 when substituted into Equation (4) provide values of the effective Seebeck coefficient. The mean value of these experimentally found effective Seebeck coefficients is  $\alpha_e = 0.052 \text{ V K}^{-1}$  with a standard deviation equal to  $0.003 \text{ V K}^{-1}$ .

The conversion of simulated  $\Delta T$  into the power generated by the ATEG applies Equation (4) with a TEM-effective Seebeck coefficient that is equal to the mean value experimentally estimated from laboratory data ( $\alpha_e = 0.052 \text{ V K}^{-1}$ ) and an internal resistance per TEM that is equal to the value at nominal conditions indicated by the manufacturer ( $R_i = 1.86 \Omega$ ). This value agrees with the average external resistance  $R_{exp}$  (divided by the number of TEMs of the ATEG) that is experimentally obtained when it is tuned to achieve the maximum output power in the engine bench (the average value for all eight experimental cases is  $R_{exp} = 1.96 \Omega$  with a standard deviation of  $0.20 \Omega$ ). Indeed, both the effective Seebeck coefficient and the TEM internal resistance are slightly temperature-dependent within the temperature range that is observed in cases 1 to 8. However, we applied constant values of  $\alpha_e$  and



$R_i$  in Equation (4), since these temperature dependences were not provided by the manufacturer, and as in other studies with similar temperature ranges, they are expected to have little effect on the results (see, e.g., [12]). In our comparative analyses, this assumption did not invalidate the conclusions.

### 3.2. Model Validation

Experimental points 1 to 9 (Figure 3) were simulated with a set up that applies the boundary conditions detailed in Table 3. For fluids flows, the output results to compare with laboratory data were temperatures of exhaust gases at the ATEG outlet ( $T_{g,o}$ ) and of the water coolant at the ATEG outlet ( $T_{w,o}$ ). Since we studied one-fifth of the radial ATEG, the simulated value of  $T_{w,o}$  was multiplied by five in order to properly perform the comparison with measurements. For the solid bodies, temperatures predicted at both TEMs hot ( $T_h$ ) and cold ( $T_c$ ) sides were compared with the experimental data (Figure 6).

From Figure 6, we observed that temperatures of both water and exhaust gases were very well reproduced by the model. It was very remarkable that the agreement of these temperatures was reached under very different engine operating points (ranging from low rpm at almost no load to high rpm and very high loads). On the other hand, hot and cold side TEM temperatures were also very well predicted in most of the cases.

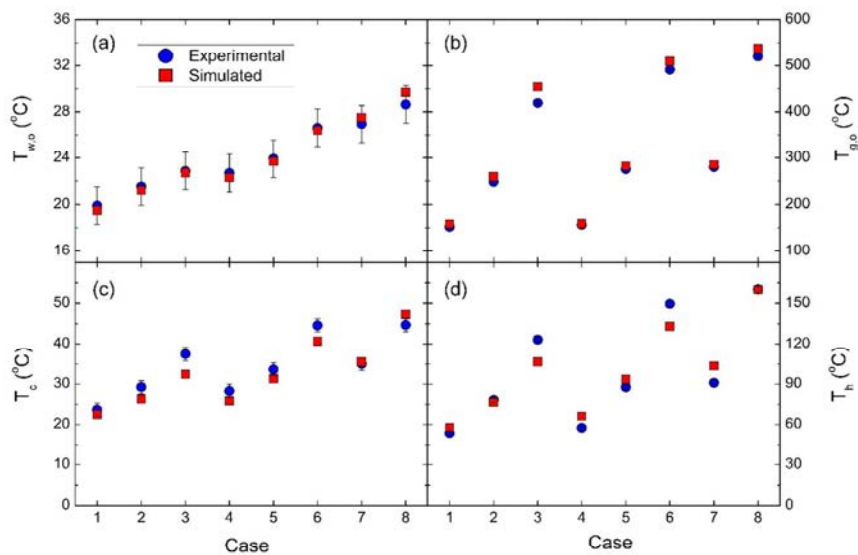


**Figure 6.** Experimental and simulated temperatures of (a) water at the ATEG outlet; (b) exhaust gas at the ATEG outlet; (c) cold side TEM and (d) hot side TEM for the regimes shown in Table 3.

Figure 7 compares the electrical output parameters calculated from simulations with those obtained experimentally. Note that the voltage and current obtained from the numerical model correctly reproduced the laboratory data, with a maximum in voltage and current for Case 8. This corresponds to the point with maximum turning velocity and engine load (Table 3), implying a very high temperature of the exhaust gases (Figure 6). In this case, the experimental output power obtained was 40 W at a TEM hot side temperature equal to 158 °C, and at TEM cold side temperature 46 °C. These temperature conditions almost coincided with the optimum performance point exposed in the manufacturer’s datasheet ( $T_h = 150$  °C,  $\Delta T = 100$  °C), from which an output power production of 10.9 W per module was expected at the matched resistance load. However, the laboratory data produced 4 W per module only. The reason for such a discrepancy on the TEMs performance could not be attributed to a mismatch in the working conditions of the modules, since TEM #1 (located at

coolant inlet) is at  $T_h = 160\text{ }^\circ\text{C}$  and  $\Delta T = 115\text{ }^\circ\text{C}$  and TEM #5 (located at coolant outlet) is at  $T_h = 155\text{ }^\circ\text{C}$  and  $\Delta T = 108\text{ }^\circ\text{C}$ . The small difference in the TEM working conditions could not be responsible for reducing the expected power by more than half. In addition, the external resistance was tuned to reach the maximum output power during each stationary regime. The difference may be a consequence of the clamping force that was set to be equal to 1500 N per module, equivalent to a pressure of 0.9 MPa. This conservative value was chosen in order to prevent cracks in the module, especially in the zone that was free of semiconductor pellets where the electrical wires were soldered. This was observed to be the most fragile region of the TEM, since the inlet and outlet hoses of the individual water cooling pressed on it once we had assembled the ATEG. At higher loads (2000 N, as recommended in  $40 \times 40\text{ mm}$  TEMs by some manufacturers), some of the TEMs cracked and they had to be replaced, and the ATEG reassembled with a more conservative clamping load. However, this did not affect the validation procedure, since numerical calculations of the output power applied an effective Seebeck coefficient that was extracted from the experimental data.

We also carried out a grid independence study. The results shown here corresponded to the finer mesh ( $8.8 \times 10^6$  elements). However, simulations with coarser grids ( $6.4 \times 10^6$ ,  $5.1 \times 10^6$ ,  $4.2 \times 10^6$ , and  $3.7 \times 10^6$  elements) have been obtained. This has allowed us to calculate the Grid Convergence Index  $GCI_{\text{fine21}}$  for the main variables in the system by applying the methodology detailed in [29]. In a numerical simulation of fluid flows, the  $GCI_{\text{fine21}}$  index is accepted as an indicator of the discretization error. The mesh independency study gave:  $GCI_{\text{fine21}} = 2.7\%$  (order  $p = 0.4$ ) for  $T_h$ ,  $GCI_{\text{fine21}} = 6.7\%$  (order  $p = 1.0$ ) for  $T_c$ , and  $GCI_{\text{fine21}} = 1.2\%$  (order  $p = 3.4$ ) for  $\Delta p_{dp}$ .

From the above, and since the output power simulated for all cases agreed with laboratory data within the uncertainty range of the experiment (Figure 7), we accepted that the model was suitable to carry out comparative analyses of the ATEG performance when some of its design parameters were changed, as in Section 4.

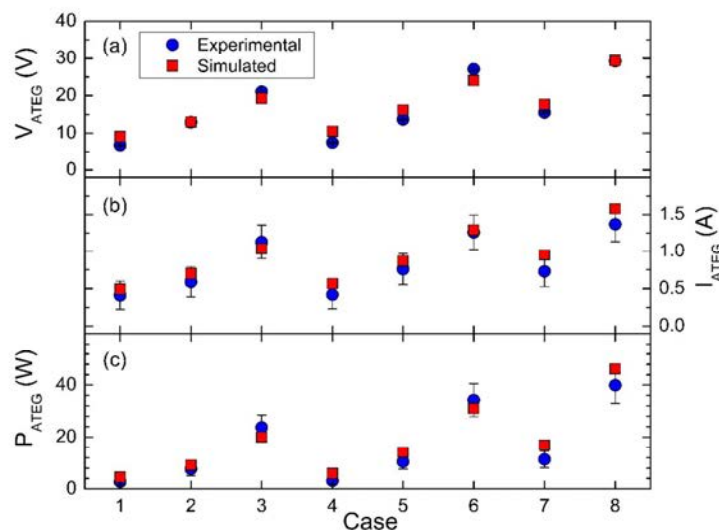


Figure 7. Experimental and simulated values of (a) ATEG voltage; (b) ATEG current; and (c) ATEG output power for the regimes shown in Table 3.

#### 4. Results and Discussion

The continuous research for developing ATEGs faces two challenging tasks: (1) the design of heat exchangers that increase the heat transfer without penalizing the fuel consumption, and (2) the improvement of the heat-to-electricity conversion rate of thermoelectric materials. Here, we analyzed the effects of modifying both the heat exchanger and the efficiency of the thermoelectric modules.

Each one of the five heat absorbers that form the ATEG tested in the engine bench used straight fins that were 1 mm wide with a total surface area  $A_{t,o} = 418 \text{ cm}^2$  (Figure 1). In the present comparative analysis, we increased the surface area of the heat absorber by increasing the height of the fins while maintaining the width (=1 mm) and the fin-to-fin distance (=1 mm). Figure 8 shows the four cases analyzed that correspond to heat absorbers with an effective increase in the surface area of the heat absorber equal to 20%, 40%, and 60% with respect to  $A_{t,o}$ .

On the other hand, the effective figure of merit  $ZT_e$  of the TEM module was calculated with the following equation:

$$ZT_e = \frac{\alpha_e^2 \bar{T}}{\rho_e k_e}, \quad (5)$$

where  $\bar{T}$  is the average temperature of  $T_h$  and  $T_c$ , and  $\rho_e$  is the TEM-effective electrical resistivity, with all previous data calculated at nominal conditions. Following the manufacturer's datasheet, at nominal conditions,  $\bar{T} = 373.15 \text{ K}$ ,  $\rho_e = 0.902 \text{ }\Omega\text{m}$ ,  $k_e = 5.33 \text{ W K}^{-1} \text{ m}^{-1}$  and  $\alpha_e = 0.090 \text{ V K}^{-1}$ . This gives a value of the effective figure of merit  $ZT_e = 0.63$ . However, under laboratory conditions, the actual effective Seebeck coefficient is  $\alpha_e = 0.052 \text{ V K}^{-1}$ , as already discussed at the end of Section 3.1. In this case, the effective figure of merit of the TEMs, once installed in our ATEG, was  $ZT_e = 0.21$  only, being three times smaller than the expected value. Since we applied the effective value of the Seebeck coefficient extracted from the laboratory data in order to convert heat into electricity, the power generated was also three times lower than expected.

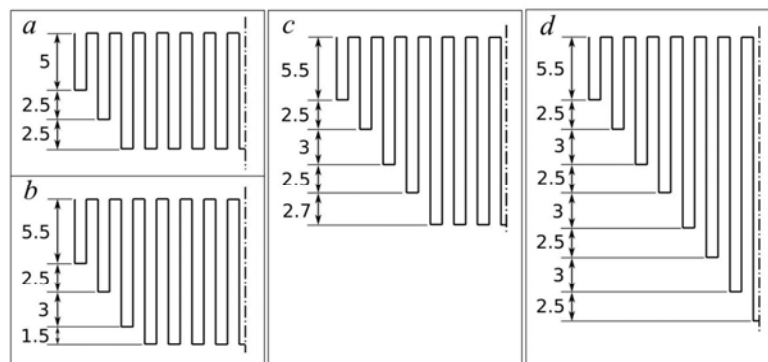


**Figure 8.** Fin geometries of heat absorbers simulated. (a) Dimensions of the original case tested and validated in Section 3 (ATEG total heat exchanger surface area  $A_t = A_{t,o} = 418 \text{ cm}^2$ ); (b)  $A_t = 1.2A_{t,o}$ ; (c)  $A_t = 1.4A_{t,o}$ ; (d)  $A_t = 1.6A_{t,o}$ . Fin thickness: 1 mm. Fin-to-fin distance: 1 mm. Fin length = 30 mm. Dimensions in mm.

In the following subsections, a comparative analysis of the effect of using different heat absorbers on the electrical power output, as well as on the fuel economy, was carried out by means of the numerical model.

#### 4.1. Electrical Power Output

Temperature differences between both the hot and cold sides of the TEM obtained when using heat absorbers with different total surface areas for each one of the cases studied in Figure 3 are shown in Figure 9. The average increase in  $\Delta T = T_h - T_c$  with respect to the reference design (heat absorber with total surface area equal to  $A_{t,o}$ ) was 11%, 22%, and 33% when increasing the total fin surface area by 20%, 40%, and 60%, respectively. The maximum increase in  $\Delta T$  is observed in case 3, being 13%, 25%, and 37% corresponding to heat absorbers with 20%, 40%, and 60% more total fin surface area than that of the reference design. In general, the increase in the total surface area of the heat exchange zone with the exhaust gases favored the raise of  $\Delta T$  in those engine regimes with low mass flow rates



(cases 1, 2, and 3 in Figure 3). In comparison, the gain in  $\Delta T$  at high regimes (e.g., cases 7 and 8) was proportionally, not as pronounced.

Figure 10 shows the temperature variations that occurred in the heat absorber when changing the fin dimensions in case 8. The ATEG with heat absorbers with very high fins (Figure 10b) almost completely blocked the incoming flow that was forced to go through the fin exchanger. This substantially increased the temperature of the fins in comparison with the design tested in Section 2 (Figure 10a). Under the same incoming flow, temperatures may be higher than 100 °C of those found in the original design. This finally led to an increase in the temperature of the body of the heat absorber, and hence, a greater  $\Delta T$  of the TEM. Note that simulations clearly predicted a reduction of the heat absorber temperature from fins to the body, and even there, the temperature decays as it approaches the outer rings. This was a consequence of heat losses to the ambient surroundings, as well as to the heat flow through the different solid elements until reaching the water heat sinks located at the cold side of the TEMs. Note that although fin temperature was clearly higher in the upstream region, the high thermal conductivity of copper led to almost equal average temperatures in the hot side faces of both upstream and downstream TEMs (variations of less than 0.5 °C).

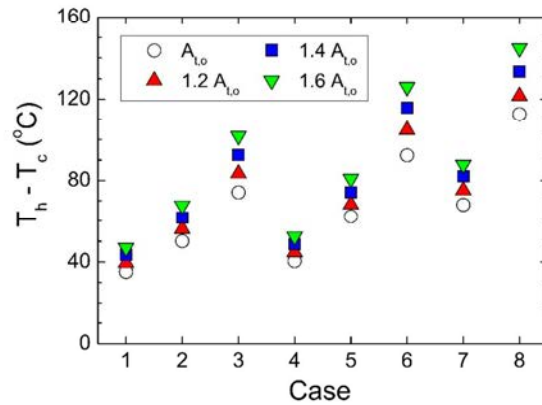


Figure 9. Temperature differences at both hot and cold sides of the TEM for the cases shown in Figure 3 when using heat absorbers with different total surface area  $A_t$ . Numerical results.

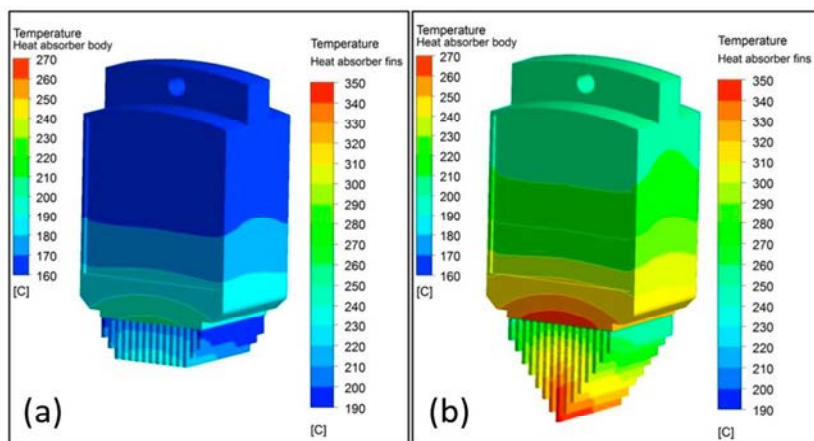
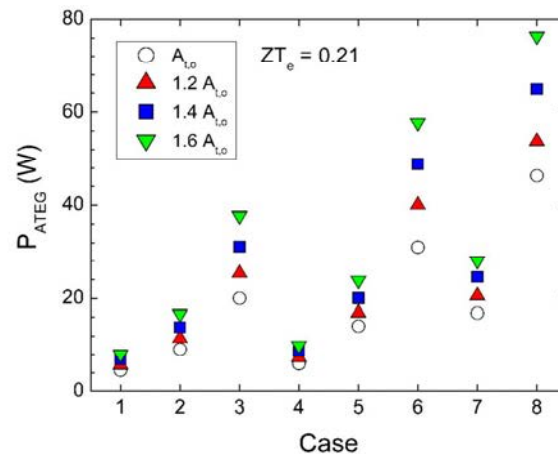


Figure 10. Temperature of the heat absorber (body and fins in different color scales for clarity) for case 8, with a total fin surface area equal to (a)  $A_{t,o}$  (=418 cm<sup>2</sup> for the whole ATEG) and (b)  $1.6A_{t,o}$ .

The maximum electrical output power  $P_{ATEG}$  per each case of Figure 9 is depicted in Figure 11. Since  $P_{ATEG}$  is proportional to  $\Delta T^2$ , the average increase in  $P_{ATEG}$  with reference to the initial design tested in the engine bench (Section 2) was 23%, 49%, and 75% when the total fin surface area of the absorber increased by 20%, 40%, and 60%, respectively. In case 8, the maximum output power for the  $1.6A_{t,o}$  heat absorber type reached 76 W, in comparison with the 46 W obtained with the  $A_{t,o}$  case. In case of using the modules with  $ZT_e = 0.63$ , the output power would rise up to 228 W and 138 W, respectively.



**Figure 11.** Electrical output power for the cases shown in Figure 3 when using heat absorbers with different total surface area  $A_t$ . Numerical results.

The efficiency  $\eta_{TEM}$  of the heat to electricity conversion can be calculated from the electrical output power of a single TEM  $P_{TEM}$  ( $=P_{ATEG}/10$ ) and the heat flow through its hot side  $Q_h$ :

$$\eta_{TEM} (\%) = 100 \frac{P_{TEM}}{Q_h} . \quad (6)$$

Under engine operating conditions equal to case 1, the heat flow of the original design is  $Q_h = 34.5$  W, leading to a TEM efficiency of  $\eta_{TEM} = 1.3\%$ . This value increases up to  $\eta_{TEM} = 1.9\%$  under conditions of case 8 (Figure 10a), where the heat flow increases up to  $Q_h = 242$  W. The modification of the heat absorber including higher fins, did not substantially increase the TEM efficiency. In the  $1.6A_{t,o}$  total surface area design, and for cases 1 and 8 (Figure 10b), the heat flow was  $Q_h = 58$  W and  $Q_h = 377$  W, respectively, increasing the efficiency by only 0.1%, in comparison with the original design. Thus, a maximum of  $\eta_{TEM} = 2.0\%$  was obtained, which was slightly below the values claimed by other authors in the study of ATEGs (on the order of 2.6% [9,13]). An increase in the  $ZT_e$  value up to 0.63, according with our TEMs datasheet, would imply TEM efficiencies on the order of 6.0% maximum.

The reduction of the available cross-sectional area for the exhaust flow implied an increase in the energy losses along the exhaust pipe. This phenomenon was equivalent to enhancing the value of the required pressure upstream the pipe in order to properly drive the flow to the exit (at atmospheric pressure). We defined the back pressure  $\Delta p_{bp}$  as the pressure change between both the inlet and outlet cross-sections of the ATEG. An increase in the back pressure may have adverse consequences on the regular functioning of the engine, leading to an increase in the fuel consumption. Therefore, not only output power, but also back pressure values are worthy of investigation when developing ATEG designs.

Figure 12 shows the value of the back pressure  $\Delta p_{bp}$  for all of the eight cases tested in the laboratory. As expected,  $\Delta p_{bp}$  increased as a function of the mass flow rate in those cases with almost equal gas



inlet temperatures. On the other hand,  $\Delta p_{bp}$  increased as a function of the gas inlet temperature when the mass flow rate was kept constant. The effect of enlarging the total surface area of fins  $A_t$  of the heat absorber dramatically increased the energy losses. An average of a 45%, 108%, and 192% increase in  $\Delta p_{bp}$  with respect to the  $A_{t,0}$  case was observed for those designs with  $A_t = 1.2 A_{t,0}$ ,  $1.4 A_{t,0}$ , and  $1.6 A_{t,0}$  respectively.

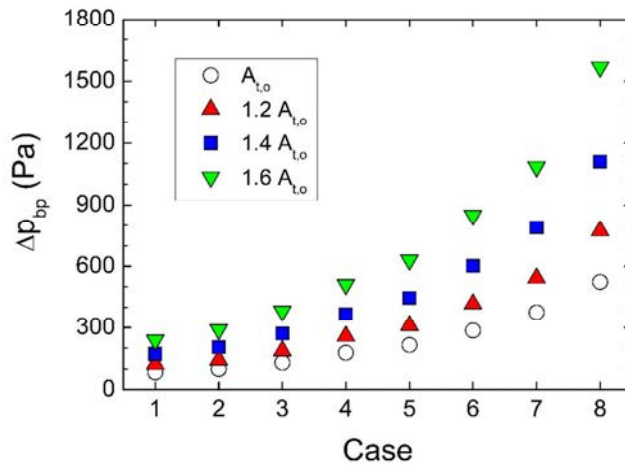


Figure 12. Back pressure  $\Delta p_{bp}$  of those cases analyzed in Figure 11. Numerical results.

It is very remarkable that, for a fixed exhaust gas temperature, the electrical output power could be directly related with the back pressure values for any of the designs proposed (Figure 13). This general behavior of our radial design would allow us to predict the output power once the value of the energy losses through the exhaust was estimated. This would be a very fast method to assess the potential of electrical generation of the ATEG without the need to carry out either complex simulations or experimental tests. We point out that a similar behavior has been recently observed in an ATEG with circular tubes as heat absorbers [30], being used for developing an analytical method to calculate the fuel economy.

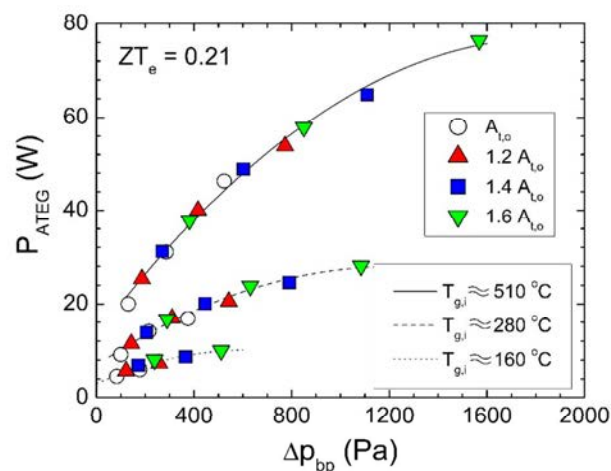


Figure 13. Electrical output power as a function of the back pressure for all cases analyzed. Numerical results.

Power production may be enhanced by adding another radial ATEG in series configuration. We numerically analyzed this case under conditions of case 8 with the original configuration of the heat absorber. Since the temperature of the exhaust gases at the output of the first radial ATEG decreased, the power of the second radial ATEG reached only 27 W, in comparison with the 46 W obtained in the upstream one. Therefore, the strategy of adding more and more TEMs in an ATEG with the purpose of increasing the output power may clearly fail, since the geometrical distribution of TEMs to maximize the available waste heat is a key factor of the ATEG performance [21].

#### 4.2. Fuel Economy

The electrical output power generated by an ATEG is useful information for deciding whether or not the design has the potential to supply a reasonable amount of power to the vehicle. Nevertheless, it is worth mentioning that the ultimate goal of an ATEG is to reduce the fuel consumption rather than to maximize power. Previous experimental studies on ATEGs provide data of electrical output power, since it is a straightforward measure. However, very few evaluate the implications on the fuel consumption. This is due to the fact that the conversion of power output to fuel savings is a very complex task where a myriad of factors may be relevant.

Here, we numerically estimate the impact of the ATEG on fuel consumption following the methodology developed by Karri et al. [31]. For simplicity, we account for only two terms, the contribution to the fuel economy due to (1), the power generated by the ATEG ( $F_{e,ATEG}$ ), and (2) the power required to overcome the back pressure that is generated by the ATEG ( $F_{e,BP}$ ):

$$F_{e,ATEG}(\%) = 100 \frac{\eta_{PCU}}{\eta_G} \frac{P_{n,ATEG}}{P_e} , \quad (7)$$

$$F_{e,BP}(\%) = -100 \frac{\dot{V}_g \Delta p_{bp}}{P_e} , \quad (8)$$

where  $\eta_{PCU}$  ( $\approx 0.84$  [30]) is the efficiency of the power converter unit (PCU), which is a direct-current to direct-current converter to match the output voltage of the electrical generator of the vehicle,  $\eta_G$  ( $\approx 0.5$  [30]) is the efficiency of the mechanical to electrical conversion of the electrical generator of the vehicle,  $P_e$  is the engine shaft power (equal to the torque multiplied by the turning velocity of Table 3, and assumed not to vary for each single case when using different ATEG designs),  $P_{n,ATEG}$  is the net power produced by the ATEG (ATEG generation minus the power required for pumping the water in the ATEG cooling system), and  $\dot{V}_g$  is the volumetric flow rate of exhaust gases. Note that  $F_{e,BP}$  is a negative contribution to fuel economy, as expected. The value of  $P_{n,ATEG}$  is here calculated as  $P_{n,ATEG} = P_{ATEG} - P_{wp}$  where  $P_{wp}$  is the power that is required by the water pump installed at the cooling system of the ATEG (see Figure 2a). In our experiment, we used a large reservoir for the cooling system so that the pumping power that was required simply reduced to the value needed to drive the water through water pipes and heat sinks. CFD simulations gave a pressure loss that was equal to 3.1 kPa (pressure difference between the exit and the inlet of the water heat sink). Since we have five heat sinks in a series configuration, and a constant volumetric flow rate of 4.4 liters/minute for all cases, the pumping power would be on the order of 1.2 W only. To this value, we must add the pumping power that is required to drive water through the cooling lines of the ATEG. For all cases, we have assumed a conservative value of  $P_{wp} = 10$  W, which agrees with the coolant pumping power that is proposed in [31] for a similar flow rate.

Thus, the fuel economy  $F_e$  is calculated as:

$$F_e = F_{e,ATEG} + F_{e,BP} . \quad (9)$$

We stress that Equation (9) gives the maximum possible value of fuel economy assigned to the ATEG device, since  $P_{n,ATEG}$ , as calculated in Equation (4), corresponds to the maximum power value, and Equation (9) neglects any additional terms that tend to reduce the fuel economy, such as the

increase of power that is needed to transport the ATEG weight. The latter contribution was neglected, since it required the speed of the vehicle, and since our test was on an engine bench, this velocity should be estimated with the transmission ratio, axle ratio, tire diameter, transmission efficiency, etc., which are data from components that were not available in our laboratory. All in all, the  $F_e$  value here calculated must be understood as the maximum possible value of fuel economy that was achieved with our ATEG design.

Figure 14 shows  $F_e$  for all of the cases previously analyzed using TEMs with an effective figure of merit  $ZT_e = 0.21$  or  $ZT_e = 0.63$ . Cases with  $ZT_e = 0.21$  and total fin surface area  $A_t = A_{t,0}$  correspond to the laboratory conditions described in Section 2. In these cases, only three of the eight regimes provided fuel savings. However, these fuel economy values were so small that we could conclude that the original ATEG design did not contribute to improving the engine fuel consumption.

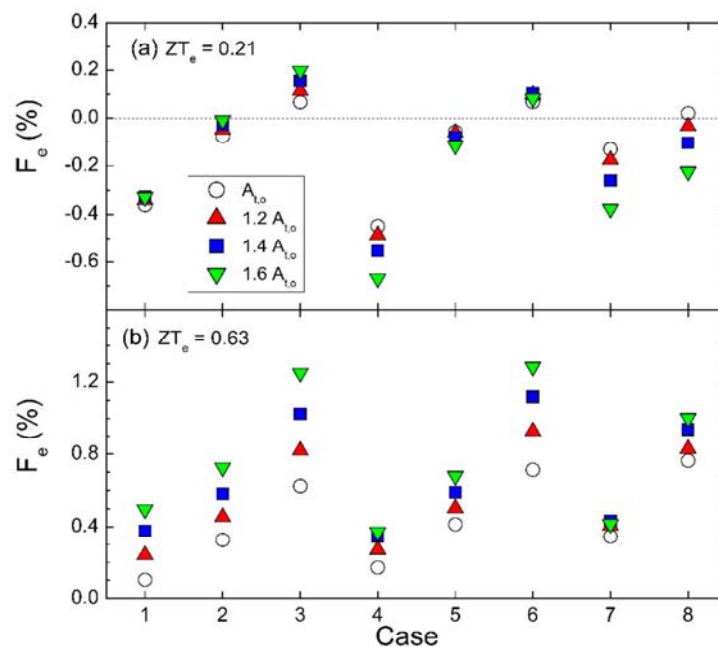


**Figure 14.** Fuel economy for those cases analyzed in Figure 11 using TEMs with an effective figure of merit (a)  $ZT_e = 0.21$  and (b)  $ZT_e = 0.63$ . Numerical results.

When increasing the total fin surface area, the back pressure effect was more adverse than in the base case. Thus, although electrical power increased, the overall contribution led to an increase of the fuel consumption for the  $1.6A_{t,0}$  case, especially at high engine regimes and high engine loads. At low regimes, since the back pressure was not excessive, the  $1.6A_{t,0}$  case gave slightly better results than the  $A_{t,0}$  case. In view of the fuel economy results, the overall conclusion was that the radial ATEG designs here proposed when using TEMs with  $ZT_e = 0.21$  were not feasible.

However, the improvement of the thermoelectric properties of the TEMs up to  $ZT_e = 0.63$  values under the same thermal properties as in those modules initially used, allowed positive fuel savings to be reached under all conditions (Figure 14b). The maximum fuel economy was achieved at intermediates regimes, since the high value of the back pressure strongly penalized the outcome under high regime conditions.

Results from Figure 14 confirmed that the condition of maximum fuel savings did not coincide with the maximum electrical output power. Therefore, studies on ATEGs should focus on how to improve fuel consumption, and not only on maximizing generated power. Besides power, key



information such as back pressure values and, in non-stationary engines, the ATEG mass value, should be provided to estimate the impact of the ATEG on fuel economy.

In Figure 13, we clearly identified a common trend of generated power as a function of back pressure in the form  $P_{ATEG} = a + b\Delta p_{bp} + c\Delta p_{bp}^2$ , with  $a$ ,  $b$  and  $c$  constants for a fixed value of the exhaust gas temperature at ATEG inlet. In terms of fuel economy, this unique dependency with the back pressure was not observed, as it can be seen in Figure 15. In this figure, different hatched areas correspond to cases with different exhaust gas temperatures at ATEG inlet. From Equations (7) and (8), fuel economy not only depends on  $\Delta p_{bp}$  but also on the volumetric flow rate of exhaust gases  $\dot{V}_g$  and on the engine shaft power  $P_e$ . Both terms cannot be expressed as a function of  $\Delta p_{bp}$  only. Thus,  $F_e/100 = d(a + b\Delta p_{bp} + c\Delta p_{bp}^2 - P_{wp})P_e^{-1} - \dot{V}_g\Delta p_{bp}P_e^{-1}$  with  $d$  a constant. At low values of the figure of merit of the TEMs, the energy production was low, and in most of the cases, the dominant term was the negative contribution of the back pressure. As  $ZT_e$  increased, the power generation term eventually led to positive fuel savings, reaching a maximum at intermediate back pressure conditions.

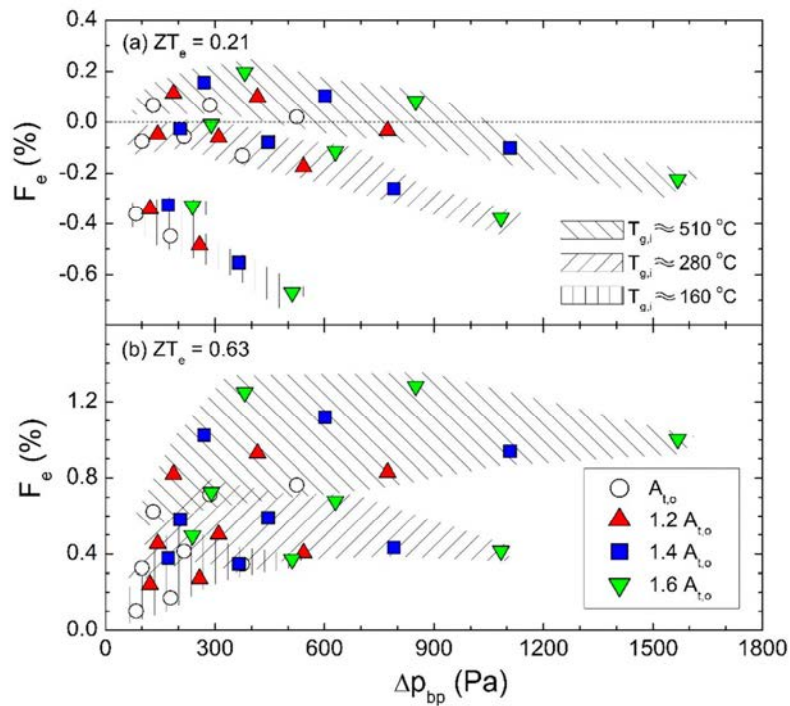


**Figure 15.** Fuel economy as a function of the back pressure for all cases when using TEMs with an effective figure of merit (a)  $ZT_e = 0.21$  and (b)  $ZT_e = 0.63$ . Numerical results.

At low engine load regimes (exhaust gas temperature at ATEG inlet on the order of 160 °C), the output power generated (with  $ZT_e = 0.21$ ) was even lower than that required for pumping water in the ATEG cooling system. As a consequence,  $P_{n,ATEG}$  was negative (Figure 16). This led to an increase of the fuel consumption of almost 0.7% in the design that had a total fin surface area  $A_t = 1.6 A_{t,0}$ , since in this case, there was also a high penalization due to the back pressure value. The latter played a key role in the determination of fuel consumption, since even with  $ZT_e = 0.63$  (Figure 16b), the maximum fuel saving did not coincide with the maximum net output power, except for the original design due to the comparatively low  $\Delta p_{bp}$  values reached.

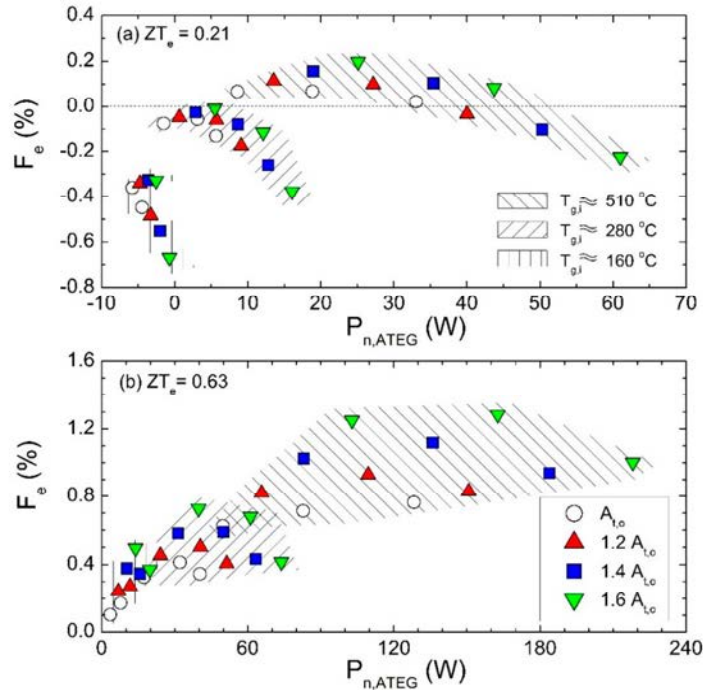


**Figure 16.** Fuel economy as a function of net ATEG power production for all cases when using TEMs with an effective figure of merit (a)  $ZT_e = 0.21$  and (b)  $ZT_e = 0.63$ . Numerical results.

ATEG designs able to generate the same output power but at lower engine loads substantially improved the fuel savings. When the figure of merit increased, the TEM power production enhanced, and larger differences of performance between designs were observed. For  $ZT_e = 0.63$ , the maximum degree of fuel savings was equal to 1.3% at intermediate regimes and high load, whereas the maximum power was equal to 228 W at the highest engine regime and load in both cases for the ATEG design with the greatest surface area of the heat absorber-gas exchange ( $d$  in Figure 8). However this layout was the worst one at high engine regimes, in terms of fuel efficiency, when the TEM's effective figure of merit  $ZT_e = 0.21$ .

It would be of interest to have a simple rule-of-thumb to determine whether or not an ATEG design is feasible in terms of fuel consumption. From Equation (9), the ratio  $F_{e,ATEG}/F_{e,BP} \approx P_{n,ATEG}/(\dot{V}_g \Delta p_{bp})$ , since  $\eta_{PCU}/\eta_G$  is on the order of 1. Thus, positive fuel savings are expected when  $F_{e,ATEG}/F_{e,BP} > 1$  or, equivalently,  $P_{n,ATEG}/(\dot{V}_g \Delta p_{bp}) > 1$ , as it is shown in Figure 17. The relevant point is that optimum conditions in terms of fuel economy are reached at intermediate values of  $P_{n,ATEG}/(\dot{V}_g \Delta p_{bp})$  (from 2 to 4 depending on the radial ATEG design). Note that points with maximum  $P_{n,ATEG}/(\dot{V}_g \Delta p_{bp})$  values correspond to those of the lower regime (1500 rpm), since  $\dot{V}_g \Delta p_{bp}$  takes low values. However, the reduction in fuel consumption when  $P_{n,ATEG}/(\dot{V}_g \Delta p_{bp}) \gg 1$  is not very high, since the electrical output power in these points is very modest.

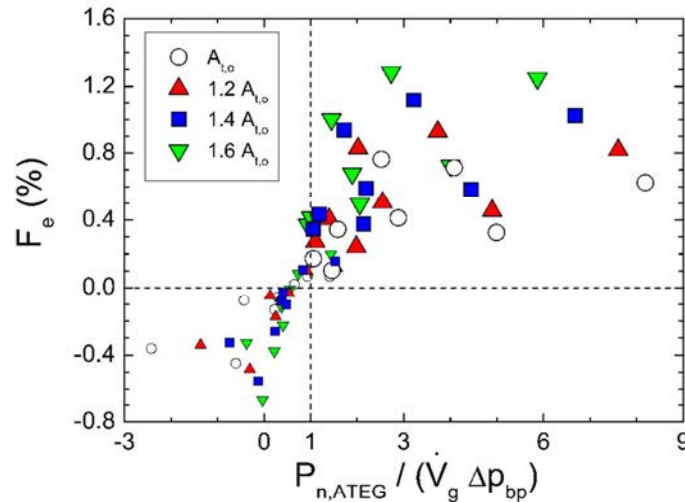


**Figure 17.** Fuel economy as a function of the net output power to exhaust gas flow power ratio for all cases analyzed. Small symbols:  $ZT_e = 0.21$ . Large symbols.  $ZT_e = 0.63$ . Numerical results.

## 5. Conclusions

We have designed a new type of ATEG with the purpose of using economic, lead-free, low-temperature commercial TEMs without adding any complex mechanical systems to regulate the flow of exhaust gases. A novel radial ATEG with 10 commercial TEMs has been built and tested in an engine bench under eight different engine operating conditions.

A numerical model based on commercial software ANSYS-CFX® has been developed, coupling fluid flows (exhaust gases and water cooling system) and solid bodies in the study of the heat transfer. This model has been validated with the experimental data obtained in the laboratory.

Several ATEG designs with different total surface area of exchange with the exhaust gases have been simulated. In addition, the effect of increasing the conversion rate of heat into electricity of the commercial modules has also been investigated. For all scenarios, values of electrical output power and fuel savings have been reported. Fuel savings values correspond to maximum figures due to the assumptions done in our calculations.

From our findings, we conclude that the electrical output power can be expressed as a parabolic function of the ATEG back pressure when working in conditions of equal exhaust gas temperature at the ATEG inlet. The maximum output power is reached at the highest engine regime with the highest engine load, since it implies conditions of maximum exhaust gas mass flow rate and exhaust gas temperature. However, even in these conditions, the temperature reached at the hot side of the TEM does not exceed its maximum operating temperature (200 °C), which assures the integrity of the system, even in the most demanding working regimes.

Results confirm that back pressure severely affects the fuel savings. This implies that the point of maximum electrical output power does not always coincide with that of maximum fuel economy. In our study, the maximum fuel economy for an effective figure of merit equal to that found in the experimental test, is reached at high engine loads but at low engine regimes. In addition, the strategy to increase the total surface area of the heat exchanger in contact with the exhaust gases may be counterproductive in some engine regimes, since the fuel consumption may greatly increase due to the increment in the back pressure. Thus, analyses of ATEGs should include not only studies on electrical output power, but also on fuel economy.

For a given ATEG configuration, there exists a threshold value of the effective figure of merit  $ZT_e$ , beyond which all the regimes analyzed produce positive fuel savings. In our designs, a value of  $ZT_e =$



0.63 leads to a maximum reduction of fuel consumption of 1.3%, with an efficiency of TEM energy conversion that is equal to 6%.

Finally, we propose the dimensionless expression  $P_{n,ATEG}/(\dot{V}_g\Delta p_{bp})$  as a simple parameter to determine the feasibility of the ATEG design. Only those cases with  $P_{n,ATEG}/(\dot{V}_g\Delta p_{bp}) > 1$  may be of interest in terms of fuel consumption. In our radial ATEG, maximum efficiency values are achieved when  $P_{n,ATEG}/(\dot{V}_g\Delta p_{bp})$  ranges from 2 to 4. Although other types of ATEG designs may have their own maximum ranges, the  $P_{n,ATEG}/(\dot{V}_g\Delta p_{bp}) > 1$  criterion still holds.

**Author Contributions:** M.C. conducted the experimental study, including all the setup of the engine test bench. M.C., T.P., I.R.C., and A.M. conducted the detailed modeling and the validation study. M.C. and E.M. carried out the analyses of the results. M.C. and T.P. wrote the paper.

**Funding:** This work has been partially funded by the University of Girona under grant MPCUdG2016-4.

**Acknowledgments:** The authors gratefully acknowledge the technical support provided by Sergi Saus and Jordi Vicens. Iker Garcia provided very helpful assistance in the CAD/CFD drawings.

**Conflicts of Interest:** The authors declare no conflict of interest. The funders had no role in the design of the study; in the collection, analyses, or interpretation of data; in the writing of the manuscript, or in the decision to publish the results.

## References

1. The World Bank. Available online: <https://data.worldbank.org/indicator/en.co2.tran.zs?end=2014&start=1960> (accessed on 5 September 2018).
2. European Environment Agency. Available online: <https://www.eea.europa.eu/data-and-maps/indicators/transport-emissions-of-greenhouse-gases/transport-emissions-of-greenhouse-gases-10> (accessed on 5 September 2018).
3. European Commission. Available online: [https://ec.europa.eu/clima/policies/transport\\_en](https://ec.europa.eu/clima/policies/transport_en) (accessed on 5 September 2018).
4. European Commission. *Clean Power for Transport: A European Alternative Fuels Strategy. Communication from the Commission to the European Parliament, the Council, the European Economic and Social Committee and the Committee of the Regions*; COM(2013) 17; European Commission: Brussels, Belgium, 2013.
5. Rahman, A.; Razzak, F.; Afroz, R.; AKM, M.; Hawlader, M.N.A. Power generation from waste IC engines. *Renew. Sustain. Energy Rev.* **2015**, *51*, 382–395. [CrossRef]
6. Karvonen, M.; Kapoor, R.; Uusitalo, A.; Ojanen, V. Technology competition in the internal combustion engine waste heat recovery: a patent landscape analysis. *J. Clean. Prod.* **2016**, *112*, 3735–3742. [CrossRef]
7. Massaguer, A.; Massaguer, E.; Comamala, M.; Pujol, T.; Montoro, L.; Cardenas, M.D.; Carbonell, D.; Bueno, A.J. Transient behavior under a normalized driving cycle of an automotive thermoelectric generator. *Appl. Energy* **2017**, *206*, 1282–1296. [CrossRef]
8. Frobenius, F.; Gaiser, G.; Rusche, U.; Weller, B. Thermoelectric generators for the integration into automotive exhaust systems for passenger cars and commercial vehicles. *J. Electron. Mater.* **2016**, *45*, 1433–1440. [CrossRef]
9. Kim, T.Y.; Kwak, J.; Kim, B.W. Energy harvesting performance of hexagonal shaped thermoelectric generator for passenger vehicle applications: An experimental approach. *Energy Convers. Manag.* **2018**, *160*, 14–21. [CrossRef]
10. Fernández-Yáñez, P.; Armas, O.; Kiwan, R.; Stefaopoulou, A.G.; Boehman, A.L. A thermoelectric generator in exhaust systems of spark-ignition and compression-ignition engines. A comparison with an electric turbo-generator. *Appl. Energy* **2018**, *229*, 80–87.
11. Stobart, R.; Wijewardane, M.A.; Yang, Z. Comprehensive analysis of thermoelectric generation systems for automotive applications. *Appl. Therm. Eng.* **2017**, *112*, 1433–1444. [CrossRef]
12. Wang, Y.; Li, S.; Xie, X.; Deng, Y.; Liu, X.; Su, C. Performance evaluation of an automotive thermoelectric generator with inserted fins or dimpled-surface hot heat exchanger. *Appl. Energy* **2018**, *218*, 391–401. [CrossRef]
13. Orr, B.; Akbarzadeh, A.; Lappas, P. An exhaust heat recovery system utilizing thermoelectric generators and heat pipes. *Appl. Therm. Eng.* **2017**, *126*, 1185–1190. [CrossRef]
14. Lan, S.; Yang, Z.; Chen, R.; Stobart, R. A dynamic model for thermoelectric generator applied to vehicle waste heat recovery. *Appl. Energy* **2018**, *210*, 327–338. [CrossRef]

15. Crane, D.; Lagrandeur, J.; Jovovic, V.; Ranalli, M.; Adldinger, M.; Poliquin, E.; Dean, J.; Kossakovski, D.; Mazar, B.; Maranville, C. TEG on-vehicle performance and model validation and what it means for further TEG development. *J. Electron. Mater.* **2013**, *42*, 1582–1591. [CrossRef]
16. Saidur, R.; Rezai, M.; Muzammil, W.K.; Hassan, M.H.; Paria, S.; Hasanuzzaman, M. Technologies to recover exhaust heat from internal combustion engines. *Renew. Sustain. Energy Rev.* **2012**, *16*, 5649–5659. [CrossRef]
17. Di Battista, D.; Mauriello, M.; Cipollone, R. Waste heat recovery of an ORC-based power unit in a turbocharged diesel engine propelling a light duty vehicle. *Appl. Energy* **2015**, *152*, 109–120. [CrossRef]
18. Dávila Pineda, D.; Rezanía, A. *Thermoelectric Energy Conversion. Basic Concepts and Device Applications*, 1st ed.; Wiley-VCH Verlag GmbH&Co.: Weinheim, Germany, 2017.
19. Ming, T.; Wang, Q.; Peng, K.; Cai, Z.; Yang, W.; Wu, Y.; Gong, T. The influence of non-uniform high heat flux on thermal stress of thermoelectric power generator. *Energies* **2015**, *8*, 12584–12602. [CrossRef]
20. Crystal Ltd. Available online: [www.crystaltherm.com](http://www.crystaltherm.com) (accessed on 4 May 2018).
21. Cózar, I.R.; Pujol, T.; Lehocky, M. Numerical analysis of the effects of electrical and thermal configurations of thermoelectric modules in large-scale thermoelectric generators. *Appl. Energy* **2018**, *229*, 264–280. [CrossRef]
22. Chen, J.; Li, K.; Liu, C.; Li, M.; Lv, Y.; Jia, L.; Jiang, S. Enhanced efficiency of thermoelectric generator by optimizing mechanical and electrical structures. *Energies* **2017**, *10*, 1329. [CrossRef]
23. National Instruments. Available online: <http://www.ni.com> (accessed on 2 May 2018).
24. Omega. Available online: <http://www.omega.com> (accessed on 2 May 2018).
25. Sensus. Available online: <http://www.sensus.com> (accessed on 2 May 2018).
26. Su, C.Q.; Tong, N.Q.; Xu, Y.M.; Chen, S.; Liu, X. Effect of the sequence of the thermoelectric generator and the three-way catalytic converter on exhaust gas conversion efficiency. *J. Electron. Mater.* **2013**, *42*, 1877–1881. [CrossRef]
27. Wang, Y.; Li, S.; Zhang, Y.; Yang, X.; Deng, Y.; Su, C. The influence of inner topology of exhaust heat exchanger and thermoelectric module distribution on the performance of automotive thermoelectric generator. *Energy Convers. Manag.* **2016**, *126*, 266–277. [CrossRef]
28. Bergman, T.L.; Lavine, A.S.; Incropera, F.P.; DeWitt, D.P. *Fundamentals of Heat and Mass Transfer*, 7th ed.; John Wiley & Sons, Inc.: Hoboken, NJ, USA, 2011.
29. Celik, I.B.; Ghia, U.; Roache, P.J.; Freitas, C.J.; Coleman, H.; Raad, P.E. Procedure for estimation and reporting of uncertainty due to discretization in CFD applications. *J. Fluids Eng.* **2008**, *130*. [CrossRef]
30. Massaguer, A.; Massaguer, E.; Comamala, M.; Pujol, T.; González, J.R.; Cardenas, M.D.; Carbonell, D.; Bueno, A.J. A method to assess the fuel economy of automotive thermoelectric generators. *Appl. Energy* **2018**, *222*, 42–58. [CrossRef]
31. Karri, M.A.; Thacher, E.F.; Helenbrook, B.T. Exhaust energy conversion of thermoelectric generator: Two case studies. *Energy Convers. Manag.* **2011**, *52*, 1596–1611. [CrossRef]



© 2018 by the authors. Licensee MDPI, Basel, Switzerland. This article is an open access article distributed under the terms and conditions of the Creative Commons Attribution (CC BY) license (<http://creativecommons.org/licenses/by/4.0/>).





## Chapter 4

# Validation of a fuel economy prediction method based on thermoelectric energy recovery for mid-size vehicles

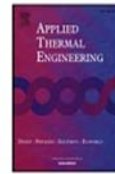
---

This chapter is the transcription of the content of the following article

M. Comamala, A Massaguer, E Massaguer, T. Pujol. **Validation of a fuel economy prediction method based on thermoelectric energy recovery for mid-size vehicles.** *Applied Energy*. Energies 2018, 11(10), 2720 ISSN 0306-2619 (Impact factor 7,182; Journal 6 of 92; 1st quartile; Energy and Fuels)

<https://doi.org/10.3390/en11102720>





Research Paper

Validation of a fuel economy prediction method based on thermoelectric energy recovery for mid-size vehicles



M. Comamala<sup>a</sup>, A. Massaguer<sup>b,\*</sup>, E. Massaguer<sup>b</sup>, T. Pujol<sup>a</sup>

<sup>a</sup> Department of Mechanical Engineering and Industrial Construction, University of Girona, C. Universitat de Girona, 4, 17003 Girona, Spain  
<sup>b</sup> Nablathermoelectrics SL, C. de la Libertat, 71, 17820 Banyoles, Spain

HIGHLIGHTS

- An automotive thermoelectric generator (ATEG) is built and tested experimentally.
- A method to predict the ATEG fuel economy is validated.
- ATEG backpressure, power generation, weight and coolant pumping power are considered.
- The maximum fuel economy point does not coincide with the ATEG maximum power generation.

ARTICLE INFO

**Keywords:**  
Thermoelectric generator  
TEG  
Fuel economy  
Automotive engine exhaust waste heat recovery  
ATEG

ABSTRACT

Automotive thermoelectric generators (ATEG) have become a promising technology for exhaust heat recovering in vehicles. Many models and prototypes have been developed and validated with very encouraging results. Most of them have been analyzed in both steady-state and transient conditions in engine test benches. However, only very few have been tested on a real vehicle while injecting the power generated by the ATEG to the electrical system. The first part of this work deals with a real test of a new concept of ATEG in a mid-size vehicle under different steady-state engine regimes. The second part, which goes beyond the state-of-the-art of ATEGs, is focused on the validation of a new mathematical method for predicting the expected fuel economy.

The ATEG presented allows for saving up to 1.08% of fuel and CO<sub>2</sub> emissions. In addition, the results show that the model enables the estimation of the ATEG savings accurately, with an average error of 11.27%. This data represents the accomplishment of the main objective of this paper providing original and unique data, and a useful tool for ATEG designers.

1. Introduction

Current internal combustion engines (ICEs) exhibit on average approximately 25% efficiency [1] under typical driving conditions (e.g., in an European driving cycle) but can range from 20% to 45% depending on the engine type and operating conditions. Between 55% and 80% of the remaining energy is wasted as heat in both the coolant and the exhaust gases. A waste heat recovery system has the potential to convert some of this waste heat into electricity and consequently reduce the fuel consumption of the car by decreasing the load demanded by the car alternator [2–5].

Recovering the exhaust gas energy in a diesel passenger car under the New European Driving Cycle (NEDC) can lead to potential fuel savings from 8% to 19% [6]. Thermoelectric generators are one of the most promising technologies to recover energy from the exhaust, due to

their small weight and size, low maintenance costs, silent operation and high reliability [3,4,7,8]. This electric recovery is especially useful in case of vehicles having a high degree of electrification, synergistically increasing the efficiency potential [9]. Unfortunately, heat recovery systems have an important drawback, they increase fuel consumption mainly due to an increase of the back pressure in the exhaust system [10–12].

In recent years, a large number of studies have been carried out in cooperation with several vehicle manufacturers. Most of them are theoretical studies and only a few have conducted experimental tests (see Table 1) [13–23]. The majority of them were focused on generating the maximum amount of electrical power, with the objective of reducing the load required by the car alternator. Consequently, and by applying a simplistic rule of thumb, this load reduction would imply a fuel economy, which is the main purpose of any ATEG development.

\* Corresponding author.  
E-mail address: [albert@nablatherm.com](mailto:albert@nablatherm.com) (A. Massaguer).

**Table 1**  
Summary of physical properties of ATEGs described in the literature.

Heat source	Max. ATEG power [W]		Temperatures [°C]		Cooling temperature [°C]		TE material	Exhaust flow rate [g/s]	Back pressure [mbar]	Fuel economy [%]	CO <sub>2</sub> emission reduction [%]	Ref
	Steady-state conditions	Transient conditions	TE hot side	TE AT side	Exhaust gases	Exhaust gases						
Cummins NTC350 141 300HP Diesel truck engine	1068	-	175	-	-	-	BiTe	-	-	-	-	[13]
Toyota 21	266	-	270	-	25	-	Skutterudites/BiTe	-	-	-	-	[14]
Ruston 3YDA 3.6l	42.3	-	237	-	650	650	BiTe	-	-	-	-	[16]
Ford Lincoln BMW X6	700	450 (US06 Driving Cycle)	-	-	625	625	Skutterudites	45	-	-	-	[17]
Combustor bench	35.6	-	396	-	25	595	SiGe	58	-	-	-	[18]
GMC Sierra 5.3l	177	-	283	-	88	550	BiTe	-	-	-	-	[19]
Chevy suburban	235	-	420	-	600	600	Skutterudites/BiTe	-	-	-	-	[20]
Engine simulator	350	-	-	-	10	600	BiTe	-	-	-	-	[21]
Experimental rig	250	-	-	-	600	600	Siicide	-	< 30	-	-	[22]
Light Duty Truck 2.3l diesel engine	500	150 (NEDC) 200 (WLTP)	-	-	450	450	BiTe	-	< 30	-	-	[23]
Golf 1.4 TSI	111	30	344	260	65	557	BiTe + PbTe	37	36	1.08	-	[15]
BMW X1	198	-	238	116	30	660	BiTe	-	46	1.08	-	[15]

\* Thermoelectric (TE).

\*\* Worldwide Harmonized Light vehicles Test Procedure (WLTP).

\*\*\* Present work.

Unfortunately, this deduction is not that straightforward, since parameters like the backpressure or the ATEG weight are involved in the variation of the fuel consumption. Very few studies [15,24–26] address the problem from the fuel economy point of view and even much less experimentally quantify it.

As Massaguer et al. state in [27], two key design parameters have to be considered in order to assure a convenient ATEG performance: the amount of power generation and backpressure. The relationship between them defines the feasibility of the design. In [15], the authors proposed a methodology to assess the ATEG performance and to predict the expected fuel economy. The study presents an equation based on three ATEG key design parameters; the amount of power generation, the backpressure and weight. It also provides insight about the optimal design point when the vehicle's fuel economy reaches its maximum value.

This paper is divided into two main parts. The first one is focused on testing, comparing and analyzing the performance of a new concept of ATEG installed in a BMW X1 under different steady-state conditions and under the Worldwide harmonized Light vehicles Test Procedure (WLTP) Class b. The amount of power generated and the total energy recovered on both experiments will be analyzed. This new thermoelectric generator makes use of a hot side heat exchanger geometry that reduces the thermal inertia and guarantees that the thermoelectric (TE) material will resist the highest exhaust temperatures. It is important to say that the practicality of the ATEG presented is not the main objective of this study, leaving the discussion of its feasibility to future studies.

The second part, which goes beyond the state-of-the-art of ATEGs with original and unique data, is dedicated to validate a new method for calculating the fuel economy described in [28]. This part represents the main objective of this paper.

## 2. Experimental setup

The ATEG presented in Fig. 1 is designed to transform the energy contained in the exhaust gases of automobiles into profitable electric energy. The goal is to feed the electrical system of the vehicle and to reduce the load on the car's alternator. This will lead to fuel and greenhouse gas emissions savings.

The size of the device is 170 × 420 × 170 mm (W × L × H) with a total weight of about 8 kg. It is composed of 34 thermoelectric modules (TEMs) (H-199-14-06L2, Crystal LTD) configured in two parallel branches (of 8 and 9 individual TEMs) each one electrically connected in series. TEMs are constructed with Bismuth telluride and stuck with thermal grease on their sides to provide low contact thermal resistance. These modules are arranged on the surrounding surfaces of an aluminum heat exchanger (element (4) in Fig. 2), through which the exhaust gas is carried, and four aluminum cold plates (element (2) in Fig. 2). Fig. 2 shows the schematic diagram of the ATEG.

As seen in Fig. 3, hot gases enter the ATEG through inlet (6) and they are forced to flow up to the outlet depending on the TEMs hot side



Fig. 1. ATEG prototype.

Chapter 4 : Validation of a fuel economy prediction method based on thermoelectric energy recovery for mid-size vehicles

M. Comanala, et al.

Applied Thermal Engineering 153 (2019) 768–778

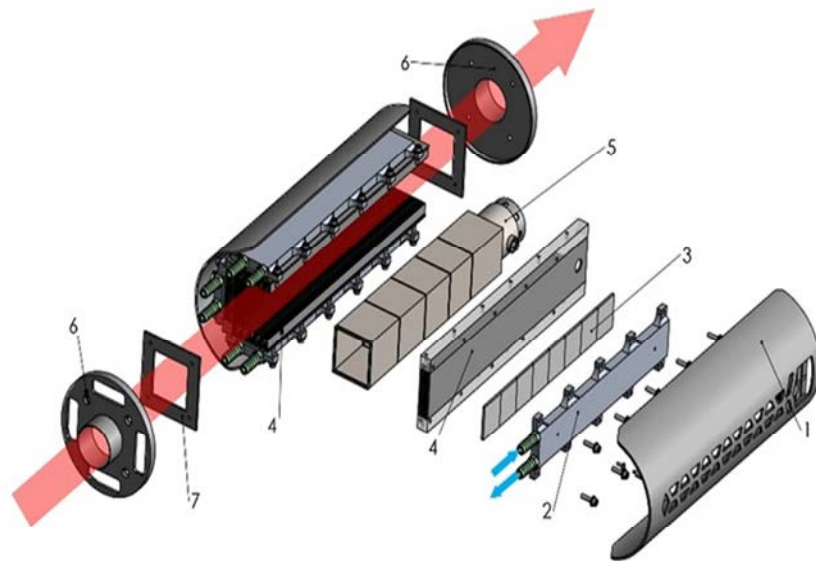


Fig. 2. Exploded view of the prototype: (1) cover, (2) cold plates, (3) thermoelectric modules, (4) heat exchanger, (5) butterfly valve, (6) inlet and outlet exhaust fumes, and (7) junction. In red, exhaust gases. In blue, cooling system water. (For interpretation of the references to colour in this figure legend, the reader is referred to the web version of this article.)

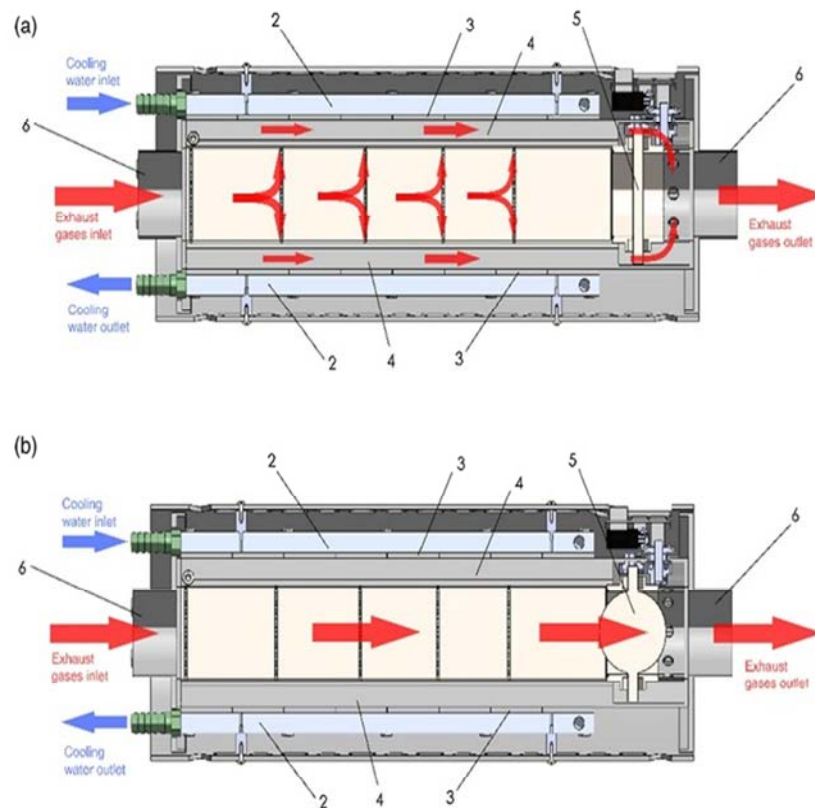


Fig. 3. Cross section of ATEG. Elements as in Fig. 2. (a) Position with butterfly valve fully closed. (B) Position with butterfly valve fully opened.



temperature. This temperature corresponds to the point located in the contact surface between the heat exchanger (4) and TEMs (3). If the hot side temperature does not exceed the maximum allowable value of 230 °C (maximum allowable temperature in order to prevent TEMs to be damaged), the butterfly valve (5) remains fully closed. In this position, the exhaust gases flow through the finned heat exchanger (4) (see Fig. 3a). If the hot side temperature exceeds the maximum temperature of 230 °C, the butterfly valve (5) opens in order to let exhaust gases exit the ATEG without flowing through the heat exchanger (4) (see Fig. 3b). This ATEG design allows a thermal protection of TEMs and guarantees a constant hot side temperature whatever the exhaust gases temperature is.

The cooling system consists of one pump and a water-to-air heat exchanger. The cooling fluid used is water with a constant volumetric flow rate of 0.12 l/s. The pump, with a mean power consumption value of 20 W, moves the water through the cold plates (element (2) in Fig. 3) connected in series.

An independent cooling circuit is used because it allows to obtain a lower temperature of the cooling fluid. The ATEG integration process into the vehicle is also easier. Although this consideration can differ from a real vehicle situation, authors strongly believe that it is worthy to install a dedicated heat exchanger for the ATEG. The system's improvement of using a dedicated 3 kW heat exchanger for the ATEG

represents about 80 W of net extra power, and the impact on the extra cost is only of about 70€, which can be regarded as non-significant taking into account the large-scale prices of the components.

All TEMs are interconnected forming an electrical array as presented in Fig. 4, where the configurations for Test 1 (ATEG + battery) and Test 2 (alternator + battery) are also shown. In Fig. 4, each TEM is represented by a voltage source  $V_{1,...,34}$  and an internal resistance  $R_{1,...,34}$  [29,30].

Although there are several ways to electrically interconnect TEMs, the way selected allows us to obtain a proper relationship between current and voltage in order to feed the DC/DC power converting unit (PCU). The PCU, model Victron Bluesolar 100/35, adapts the generated voltage by the ATEG to the adequate value for charging the battery. The PCU has been designed to charge all kind of batteries, such as the absorber glass mat (AGM) battery preinstalled on the test vehicle. It has a nominal conversion power of 500 W, a maximum rated charge current of 35 A, a maximum open circuit voltage of 150 V and an efficiency of 84%. It makes use of a maximum power point tracking (MPPT) algorithm to continuously adjust the impedance to keep the system operating at, or close to, the peak power point of the ATEG under varying conditions, like those corresponding to different engine loads and, therefore, different values of exhaust gases temperatures and flow rate. In the experiments, the initial state of charge (SOC) of the battery is

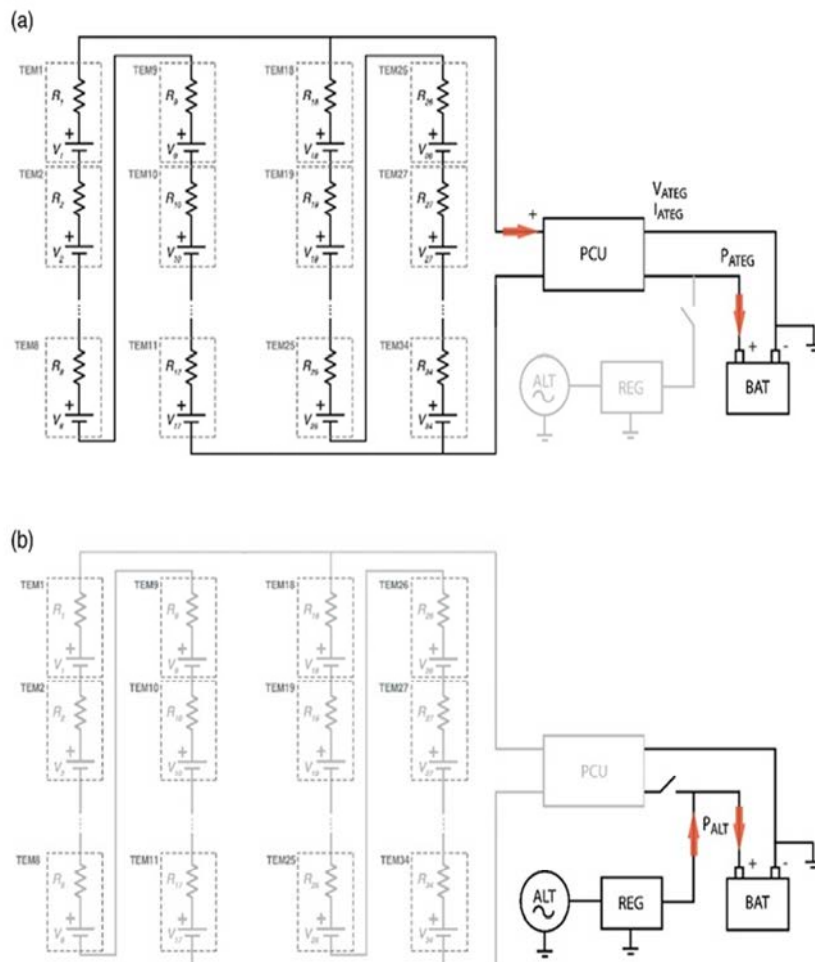


Fig. 4. Electrical schematic of the array of TEMs connected to the load. (a) Test 1: ATEG is charging the vehicle battery, and (b) Test 2: Vehicle alternator is charging the vehicle battery.

**Table 2**  
Main specifications of tested engine.

Parameter	Value
Maker	BMW
Model	X1 sDrive18i 6-speed Steptronic
Gearbox	Automatic
Max. rated power	100 kW (at 4400 rpm)
Max. rated torque	220 Nm (at 1250 rpm)
Cylinders	3
Bore (mm)	82
Stroke (mm)	94.6
Swept volume (cm <sup>3</sup> )	1499
Compression ratio	11:1
Tire diameter (m)	0.658
Axle ratio	4.103
Transmission ratio 1st	4.459:1
Transmission ratio 2nd	2.508:1
Transmission ratio 3rd	1.556:1
Transmission ratio 4th	1.142:1
Transmission ratio 5th	0.851:1
Transmission ratio 6th	0.672:1

40% in order to guarantee that all the energy produced by the ATEG will be injected to it.

In the Test 1, SOC is 40% and the alternator is electrically disconnected from the system. This assures that all the energy produced by the ATEG will be injected to the battery.

Test 2 starts with the same SOC but the alternator is normally connected to the system, forcing it to operate continuously. The ATEG runs normally but its electric power is not injected to the battery. In this test the fuel consumption is maximum.

### 3. Experiment

To assess the ATEG performance under steady-state and transient conditions, experimental tests were accomplished on a certified roller test bench of IDIADA Automotive Technology S.A. A BMW X1 sDrive18i was employed as the experimental unit. Its specifications are listed in

Table 2. In this study the ATEG was installed downstream of the catalyst, close to the engine (see Figs. 5 and 6).

As said in Section 1, the objective of this study is to test the aforementioned ATEG and to obtain experimental data at various steady-state engine conditions. Four steady-state engine modes were defined by setting constant values of engine speed and torque, which allow us to obtain constant values of the exhaust gases temperature and mass flow rate. To obtain representative steady-state conditions, the vehicle was tested at constant speeds of 50, 80, 100 and 120 km/h. These values were chosen because they are typical road speed limits. The car used is equipped with an automatic gearbox.

Overall, four steady-state points were established:

- Point 1: 50 km/h at 1509 rpm and 32.5% of pedal accelerator position.
- Point 2: 80 km/h at 1807 rpm and 47.1% of pedal accelerator position.
- Point 3: 100 km/h at 2180 rpm and 71.5% of pedal accelerator position.
- Point 4: 120 km/h at 2838 rpm and 79.0% of pedal accelerator position.

Fig. 7 shows the sensors installed on the ATEG. The acquired data are: exhaust gas inlet  $T_{EXH\_IN}$  and outlet  $T_{EXH\_OUT}$  temperatures, water cooling inlet  $T_{REF\_IN}$  and outlet  $T_{REF\_OUT}$  temperatures, TEM hot side  $T_{HOT}$  and cold side  $T_{COLD}$  temperatures at the ATEG central point. Additionally, parameters such the generated voltage  $V_{ATEG}$ , current  $I_{ATEG}$  and power  $P_{ATEG}$ , and torque  $T$ , fuel consumption  $F$ , engine power  $P$ , and thermal efficiency  $\eta$  have also been obtained.

The roller test bench used incorporates a brake system that applies a load on the vehicle. This load applied corresponds to the air resistance of the vehicle in a flat road. The vehicle's drag coefficient and drag surface are shown in Table 4.

### 4. Results and discussion

In order to analyze the impact of the ATEG on the overall fuel

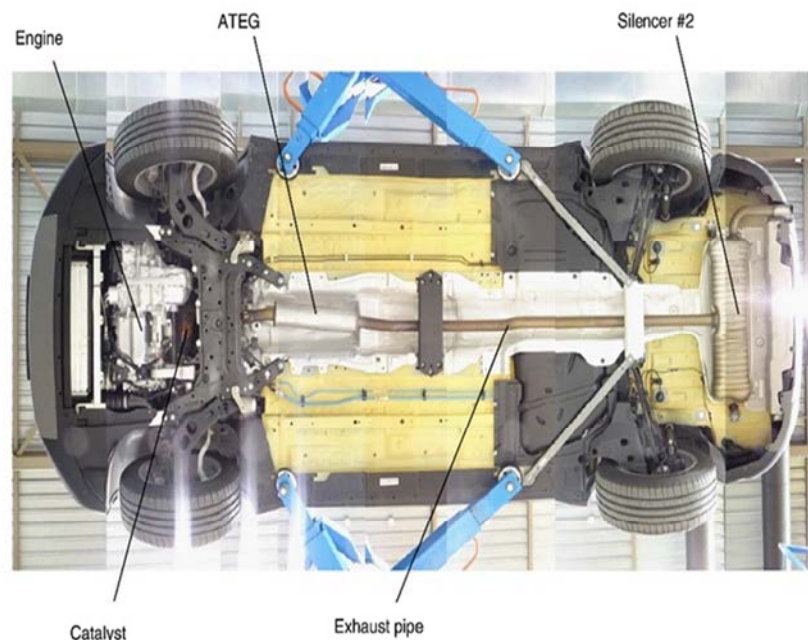


Fig. 5. Underneath view of vehicle and ATEG location.





Fig. 6. Details of the ATEG installed on the exhaust system of the engine cell.

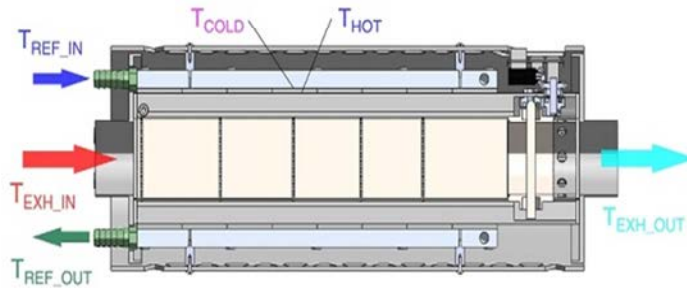


Fig. 7. Details of sensors installed on the ATEG.

economy of the vehicle, two different set up tests were defined. Test 1 was carried out by connecting the ATEG to the battery while the alternator was disconnected from the electrical system. In contrast, Test 2 was performed connecting the alternator to the electrical system while the ATEG was disconnected. In this way, it is possible to analyze the performance of each component separately and combine the data obtained to calculate the fuel savings.

4.1. Test 1: ATEG feeding the battery and alternator disconnected.

In Fig. 8, it can be observed that  $V_{ATEG}$  remains constant for all four points. This is because the DC/DC converter stabilizes and adjusts the output voltage to the adequate charging voltage of the battery. In this case, the battery was deeply discharged to 40% SOC to guarantee that all the energy produced by the ATEG was effectively injected to the

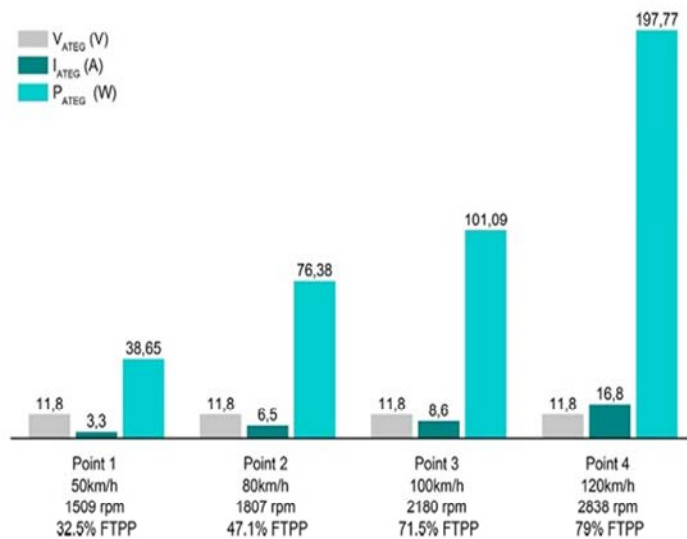


Fig. 8. ATEG electrical outputs under different steady-state conditions.

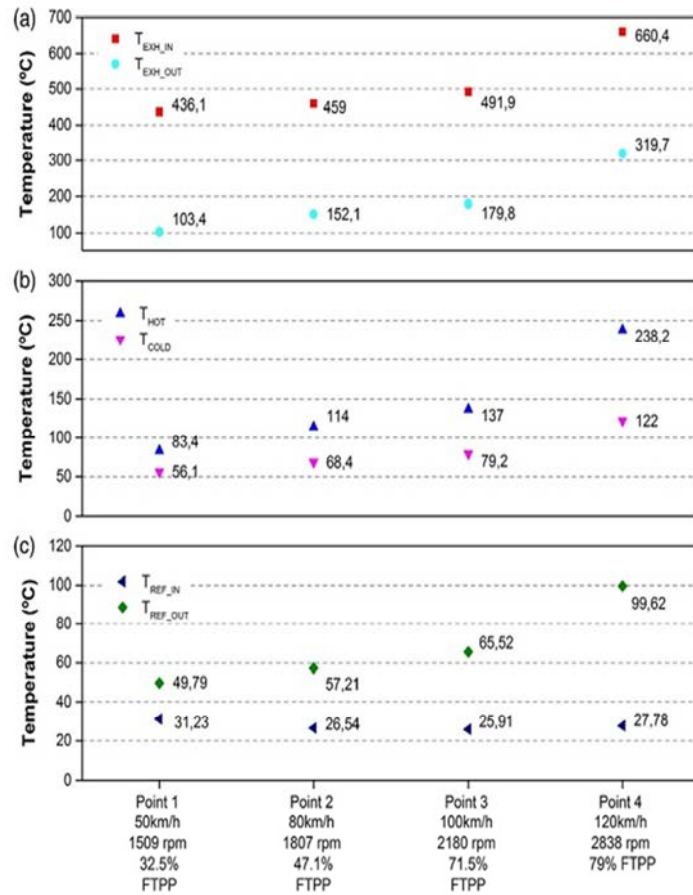


Fig. 9. (a) ATEG inlet and outlet exhaust temperatures, (b) thermoelectric hot and cold side temperatures at central ATEG point and (c) water cooling inlet and outlet temperatures.

battery. That is why  $V_{ATEG}$ , which corresponds to the battery voltage, is lower than the expected 12.8 V of an AGM battery with a 100% SOC. Other electrical parameters such as  $I_{ATEG}$  and  $P_{ATEG}$  increase with the engine load.

As it can be seen in Fig. 9a, the greater the engine load is, the higher the exhaust gas temperature and flow rate become and, consequently, the greater the power generated by the ATEG is. The exhaust temperature lost ( $T_{EXH\_IN} - T_{EXH\_OUT}$ ) through the ATEG remains almost constant throughout all the tests. In Fig. 9b it can also be observed that the temperature differences on TEMs ( $T_{HOT} - T_{COLD}$ ) are only significant for high engine regimes, like Point 4. This can be explained by the low heat extraction capacity from exhaust gases. It can be observed in Fig. 8 Point 4 that a temperature of  $T_{EXH\_IN} = 660.4$  °C is needed to reach the maximum  $T_{HOT} = 238.2$  °C.

Due to the fact that the ATEG cooling circuit was independent from the engine cooling system, the inlet cooling temperatures in Fig. 9c are lower than the operating temperature of the engine, about 80 °C. These lower cooling temperatures allow the ATEG to keep a low cold side temperature on most of the TEMs that form the ATEG, see Fig. 9c. Consequently, as it can be seen in Fig. 8, voltage, current and power generated are higher in this configuration than in the same ATEG cooled by the engine cooling system.

Considering the data obtained from the experiments, the way in which the vehicles are driven is a significant factor affecting the ATEG performance for waste heat recovery. It can be found that the higher the engine speed and load are, the better the performance of the ATEG is.

In the four experimental steady-state points the engine load corresponding to vehicle speed desired is achieved with the precise Full Throttle Pedal Position (FTTP). The increase of vehicle speed in a flat road also requires the rise in engine load. When the situation requires more engine load it is necessary burning more fuel, and consequently the air introduced, which obviously requires another FTTP, so the exhaust mass flow gases and their temperature are increased. The tested vehicle is equipped with Otto engine, in this kind of engines the exhaust gases temperature depends of the load and the engine speed, independently. In all of the four points the engine speed also increases when the vehicle speed rise.

On the other hand, most of the ATEGs developed in the literature have been designed to withstand the maximum temperature of the exhaust gases. Here, however, the ATEG was designed to withstand the maximum allowable temperature of the TEMs used, which was  $T_{HOT} = 230$  °C at  $T_{EXH\_IN} = 660$  °C. For temperatures higher than 230 °C, the butterfly valve of the ATEG gradually opens in order to bypass the exhaust fumes. This system enables the hot side temperature to be limited to a predefined set point, allowing any kind of TEM material to be used. From Fig. 9 it can be seen that the protection system was not activated in Points 1 to 3 because the threshold value of the hot side temperature was not reached. Temperature of Point 4 reaches 238 °C, exceeding the maximum allowable temperature. This happens because there is a small delay between butterfly valve activation and the hot side temperature variation due to the thermal inertial of the ATEG, leading to momentary temperature surpassings. Despite this,

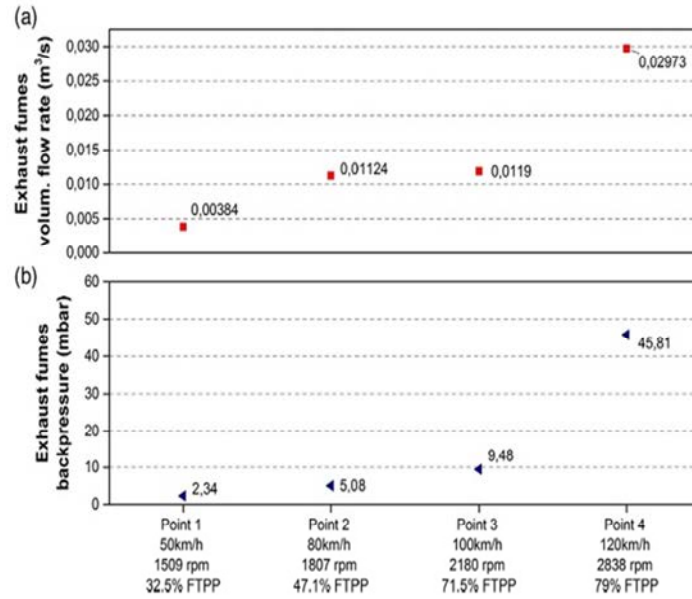


Fig. 10. (a) ATEG exhaust gases volumetric flow rate and (b) ATEG exhaust backpressure.

TEMs used work properly under a temperature up to 250 °C for short periods of time.

Values related to exhaust gases volumetric flow rate and obstruction are shown in Fig. 10.

#### 4.2. Test 2: ATEG disconnected and alternator feeding the battery

Test 2 is carried out following the same initial conditions and steady-state points as Test 1. However, now, the ATEG is electrically disconnected and the alternator is the only generator that feeds the battery. Thus, it is possible to find out the alternator influence on the vehicle's fuel consumption. In Fig. 10, ALT subscript in power  $P$ , fuel consumption  $F$  and CO<sub>2</sub> emissions  $E$ , is related to the alternator.

Fig. 11a shows a comparison between the power generated by the default BMW X1 alternator system (Test 2) and the proposed ATEG system (Test 1) for the four engine regimes analyzed. Unlike ATEG, the alternator produces almost the same amount of power independently of the engine regime. Fig. 11b and Table 3 demonstrates that the alternator is responsible of up to 11.38% of the vehicle's fuel consumption and CO<sub>2</sub> emissions (from Points 1 to 4). From Table 3 it can also be stated that the use of an ATEG can reduce the vehicle fuel consumption and CO<sub>2</sub> emissions up to 1.08%. It is a combination of low backpressure and high ATEG generation that produces a significant improve on fuel savings and CO<sub>2</sub> emissions reduction.

The most significant ATEG generation is observed on high acceleration regimes, when the exhaust gas flow rate and temperature are maximum. However, high gas flow rates increase the back pressure of the engine, due to the additional pressure loss provided by the ATEG. Engine exhaust backpressure is defined as the exhaust pressure required to overcome the hydraulic resistance of the exhaust system in order to discharge the gases into the atmosphere. An increase of the back pressure levels involves additional mechanical work of the engine and/or less energy extracted by the exhaust turbine (in turbocharged engines) that can reduce the boost pressure of the intake manifold [31].

In spite of the fuel consumption increment due to the additional backpressure, the energy recovered from the exhaust in the ATEG reverts this effect and produces a significant decrease on the vehicle fuel consumption by reducing the load on the car alternator (see Table 3 ATEG Fuel Savings).

Although Point 2 provided the highest benefits due to this combination of factors, not all four regimes achieved the same value. Point 1, e.g., produced a low backpressure effect, however the ATEG generation was too low to provide a significant benefit. Contrarily, Points 3 and 4 produced high ATEG generation but also an excessive backpressure.

#### 5. Fuel economy assessment

In [28], Massaguer et al. described a method to predict the ATEG performance in terms of fuel economy. The authors presented some mathematical equations to obtain valuable information about the influence of three key parameters on ATEG in real vehicle applications. Eq. (1) describes the fuel economy calculation in terms of these three key design parameters: the backpressure  $BP$ , the ATEG weight  $W$ , and the ATEG net power generation  $P_{G_{net}}$ .

$$F_c = \frac{s_1 P_{G_{net}} \sqrt{K} + s_2 BP \sqrt{BP} + s_3 HW \sqrt{K} \sqrt{BP}}{H \sqrt{K} \sqrt{BP} \left( \xi g W_v + \frac{1}{2} d_c \rho_{air} S_d H^2 BP \right)}, \quad (1)$$

where  $s_1$ ,  $s_2$ , and  $s_3$  are

$$s_1 = \frac{100 \eta_{PCU}}{\eta_G} \quad (2)$$

$$s_2 = -10^4 \quad (3)$$

$$s_3 = -\frac{100 \xi}{\eta_D}, \quad (4)$$

representing the slopes of the linear relationship between the fuel economy and the ATEG power generation  $s_1$ , the backpressure  $s_2$  and the ATEG weight  $s_3$ .  $\eta_{PCU}$ ,  $\eta_G$ , and  $\xi$  are the PCU efficiency, alternator efficiency, and vehicle rolling resistance coefficient, respectively. Moreover,  $K$ ,  $H$ ,  $\rho_{air}$ ,  $W$ ,  $W_v$ ,  $d_c$ , and  $S_d$  are a coefficient that represents the slope of the relationship between BP and the quadratic exhaust gases volumetric flow rate  $v_{ex}^2$ , a coefficient that represents the linear relationship between vehicle velocity  $v$  and the square root of BP, the air density, the ATEG weight, the vehicle's weight, the drag coefficient and the drag surface of the vehicle, respectively.

The  $K$  coefficient can be calculated using Eq. (5).



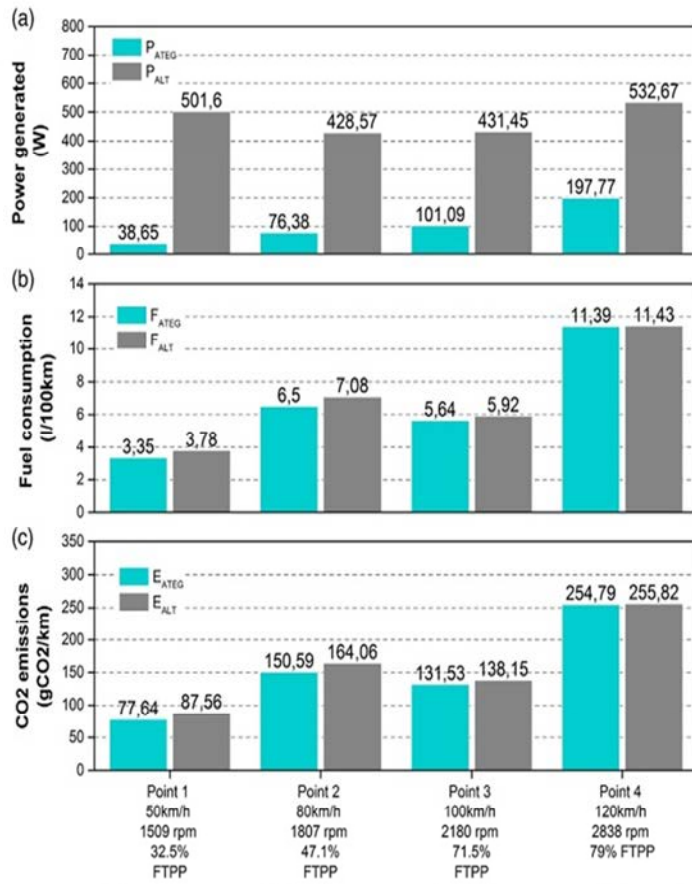


Fig. 11. ATEG and alternator comparison: (a) electrical power generated, (b) fuel consumption and (c) CO<sub>2</sub> emissions.

$$BP = K v_{ex}^2 \quad (5)$$

Then, Fig. 12 shows the relationship between BP and  $v_{ex}^2$ . Pressure sensor used was a 6 bar transducer IMPRESS/IMP-G60000-7A4.

As seen in Fig. 12, the relationship between both parameters shows good agreement with a linear correlation. Consequently, the value of

coefficient is  $K = 52, 018$ .

The  $H$  coefficient can be calculated as follows:

$$v = \frac{\phi_T \pi}{60 AXTR SV \eta_v FTTP P_{in}} \frac{\sqrt{BP}}{\sqrt{K}} = H \sqrt{BP}. \quad (6)$$

This coefficient depends on the vehicle driving conditions.

Table 3  
Power production comparison.

	Point 1 50 km/h 1509 rpm 32.5% FTTP	Point 2 80 km/h 1807 rpm 47.1% FTTP	Point 3 100 km/h 2180 rpm 71.5% FTTP	Point 4 120 km/h 2838 rpm 79.0% FTTP
$P_{ATEG}$ (W)	38.65	76.38	101.09	197.77
$P_{ALT}$ (W)	501.5	428.57	431.45	532.67
$F_{ATEG}$ (l/100 km)	3.35	6.5	5.64	11.39
$F_{ALT}$ (l/100 km)	3.78	7.08	5.92	11.43
$E_{ATEG}$ (gCO <sub>2</sub> /km)	77.64	150.59	131.53	254.79
$E_{ALT}$ (gCO <sub>2</sub> /km)	87.56	164.06	138.15	255.82
Cooling pump power consumption (W)	20	20	20	20
$P_p$				
Alternator fuel consumption (%)	11.38%	8.19%	4.73%	0.35%
$(F_{ALT} - F_{ATEG})/F_{ALT}$				
Power generation ratio (%)	3.72%	13.16%	18.79%	33.37%
$P_{RATIO}((P_{ATEG} - P_p)/P_{ALT}) \cdot 100$				
ATEG fuel savings (l/100 km)	0.0160 (0.42%)	0.0763 (1.08%)	0.0526 (0.89%)	0.0133 (0.12%)
$(F_{ALT} - F_{ATEG}) \cdot P_{RATIO}$				
ATEG CO <sub>2</sub> emissions reduction (gCO <sub>2</sub> /km)	0.3689 (0.42%)	1.7720 (1.08%)	1.2442 (0.90%)	0.3437 (0.13%)
$E_{RATIO} = (E_{ALT} - E_{ATEG}) \cdot P_{RATIO}$				

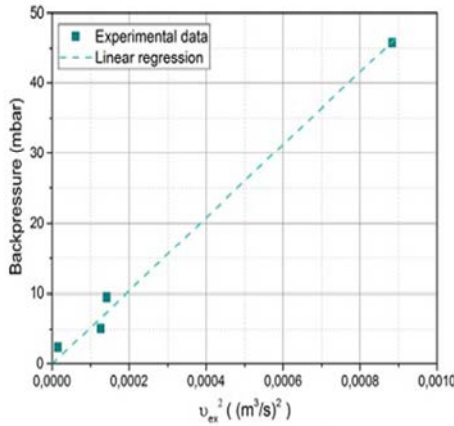


Fig. 12. Relationship between BP and  $v_{ex}^2$  of ATEG.

**Table 4**  
Parameters used for the ATEG performance predictions.

Parameter	Value
$a$	-0.138
$b$	10,217
$c$	-19.91
$\eta_{rcv}$ (%)	0.84
$\eta_c$ (%)	0.5
$\xi$	0.01
$\eta_D$ (%)	0.9
$K \left( \frac{\text{mbar}^2}{\text{m}^6} \right)$	52,018
$\frac{f_{in}}{f_{out}}$	1.5
$d_c$	0.29
$S_d$ (m <sup>2</sup> )	2.46
$\varphi_t$ (m)	0.658
$AX$	4.103
$\eta_p$ (%)	0.85
$P_p$ (W)	20

On the other hand, the net power generation  $P_{Gnet}$  can be calculated using Eq. (7),

$$P_{Gnet} = P_G - P_p = aBP^2 + bBP + c - P_p \quad (7)$$

where  $P_G$  is the ATEG power generation and  $P_p$  is the cooling pump power.  $P_G$  can be found extracting the quadratic correlation between ATEG power generation and BP.  $a$ ,  $b$ , and  $c$  values are shown in Table 4.

In addition, Eq. (8) describes the minimum ATEG power generation to obtain a positive fuel economy.

$$P_{Cr} = -\frac{s_2 BP \sqrt{BP}}{s_1 \sqrt{K}} - \frac{s_3 HW \sqrt{BP}}{s_1} \quad (8)$$

Finally, the variation of  $P_{Gnet}$ ,  $P_{Cr}$  and  $F_e$  as a function of the backpressure values are plotted in Fig. 13.

Results show that the ATEG presented in this study achieves a maximum fuel economy value of 1.06%. The positive fuel economy values are obtained in the range of 0.67–54.49 mbar, with a minimum ATEG power generation of 6 W. Higher backpressure values stand for an excessive obstruction of exhaust gases leading to a reduction of engine efficiency. Basically, the BP increases the pumping losses in the exhaust system. The piston, in the exhaust stroke, works against the fluid resistance caused by the exhaust line, also including the ATEG. Higher BP makes the engine less efficient because it can't supply the same power in the crankshaft. But the BP does not only affect the exhaust stroke. The cylinder's pressure, at the beginning of the intake

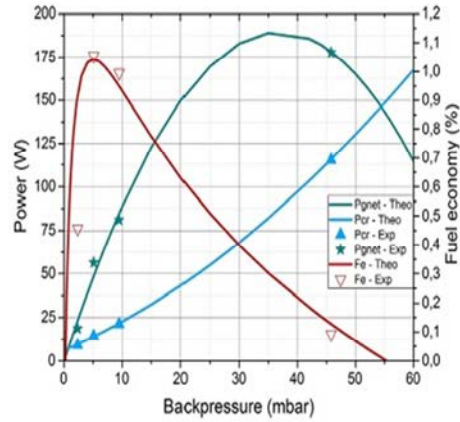


Fig. 13. Net power generation ( $P_{gnet}$ ), critical power ( $P_{cr}$ ) and fuel economy ( $F_e$ ) of the ATEG.

stroke, is higher than in normal conditions, e.g. without the ATEG, so this reduce the volumetric efficiency during the intake stroke and consequently the same quantity of fuel cannot be ignited. Finally, if the BP is too high, certain quantity of residual gases don't leave the cylinder and they are mixed with the fresh air during the intake stroke. These residual gases reduce the volumetric efficiency and warm the fresh air, causing possible knocking problems. In a similar case, engine and vehicle manufacturers have had important problems related with the emissions control system, like catalyst, FAP systems or shoot burners, all due to the mentioned losses.

Then, backpressure values exceeding 54.49 mbar lead to an engine efficiency reduction. This reduction is much critical than the positive effect of the ATEG power generation.

Finally, by using these equations, it is possible to calculate the theoretical expected fuel economy achieved by the ATEG presented. The following Table 5 summarizes the results.

## 6. Conclusions

Because of the increasing importance of environmental protection, thermoelectric energy harvesters applied to automotive sector are being extensively studied. The electricity recovered and generated from exhaust gases might serve to decrease the fuel consumption.

In this study, an automotive thermoelectric generator has been developed. The ATEG system behavior is investigated for constant driving conditions. It is found that the vehicle speed and load are significant factors affecting the ATEG performance for waste heat recovery. In steady-state conditions, the maximum power output is 197.77 W at 2838 rpm and 79.0% FTTP, corresponding to a vehicle velocity of 120 km/h on a flat road and aerodynamic resistance. Experiments show that fuel economy values strongly depend on the power generation and backpressure. The maximum  $F_e$  value obtained was 1.08% at 1807 rpm and 47.1% FTTP, corresponding to a vehicle velocity of 80 km/h.

The results show that the model is useful for predicting the ATEG

**Table 5**  
Comparison of the ATEG performance between test and theory.

Velocity (km/h)	FTTP (%)	II	Pcr (W)	Fe theoretical (%)	Fe experimental (%)	Error (%)
50	0.325	10.26	9.08	0.456	0.42	8.57%
80	0.471	9.69	14.32	1.055	1.08	-2.31%
100	0.715	8.55	21.28	0.994	0.89	11.69%
120	0.790	9.80	115.34	0.093	0.12	-22.5%

performance, with an average error of 11.27%. The potential reason for this discrepancy comes from the simplifications considered in the model and the experimental variabilities. Constant values of volumetric efficiency, and inlet and outlet air densities, are considered.

In addition, experiments show a maximum  $F_{\dot{E}}$  point found at low backpressure values. This behavior collides with the idea of higher power generation may contribute better on  $F_{\dot{E}}$ . The higher the vehicle speed and load are, the higher the temperature of the exhaust gases, which is favorable for the ATEG. However, backpressure caused to the engine also increases, leading to a worse engine performance and lower  $F_{\dot{E}}$  values.

#### Acknowledgments

This work has been partially funded by the University of Girona under Grant MPCUdG 2016-4.

#### References

- [1] S. Kim, S. Park, S. Kim, S.H. Rhi, A thermoelectric generator using engine coolant for light-duty internal combustion engine-powered vehicles, *J. Electron. Mater.* 40 (2011) 812–816, <https://doi.org/10.1007/s11664-011-1580-6>.
- [2] A. Shabashevich, N. Richards, J. Hwang, P.A. Erickson, Analysis of powertrain design on effective waste heat recovery from conventional and hybrid electric vehicles, *Appl. Energy*. 157 (2015) 754–761, <https://doi.org/10.1016/j.apenergy.2015.02.067>.
- [3] R. Saidur, M. Rezaei, W.K. Muzammil, M.H. Hassan, S. Paria, M. Hasanuzzaman, Technologies to recover exhaust heat from internal combustion engines, *Renew. Sustain. Energy Rev.* 16 (2012) 5649–5659, <https://doi.org/10.1016/j.rser.2012.05.018>.
- [4] M. Karvonen, R. Kapoor, A. Uusitalo, V. Ojanen, Technology competition in the internal combustion engine waste heat recovery: a patent landscape analysis, *J. Clean. Prod.* 112 (2016) 3735–3743, <https://doi.org/10.1016/j.jclepro.2015.06.031>.
- [5] Z. Peng, T. Wang, Y. He, X. Yang, L. Lu, Analysis of environmental and economic benefits of integrated exhaust energy recovery (EER) for vehicles, *Appl. Energy* 105 (2013) 238–243, <https://doi.org/10.1016/j.apenergy.2013.01.004>.
- [6] A.F. Agudelo, R. Garcia-Contreras, J.R. Agudelo, O. Armas, Potential for exhaust gas energy recovery in a diesel passenger car under European driving cycle, *Appl. Energy* 174 (2016) 201–212, <https://doi.org/10.1016/j.apenergy.2016.04.092>.
- [7] N.D. Love, J.P. Szybist, C.S. Sluder, Effect of heat exchanger material and fouling on thermoelectric exhaust heat recovery, *Appl. Energy* 89 (2012) 322–328, <https://doi.org/10.1016/j.apenergy.2011.07.042>.
- [8] A. Rahman, F. Razzak, R. Afroz, M. AKM, M. Hawlader, Power generation from waste of IC engines, *Renew. Sustain. Energy Rev.* 51 (2015) 382–395, <https://doi.org/10.1016/j.rser.2015.05.077>.
- [9] E. Avaritsioti, Environmental and economic benefits of car exhaust heat recovery, *Transp. Res. Procedia*. 14 (2016) 1003–1012, <https://doi.org/10.1016/j.trpro.2016.05.080>.
- [10] D. Di Battista, M. Mauriello, R. Cipollone, Waste heat recovery of an ORC-based power unit in a turbocharged diesel engine propelling a light duty vehicle, *Appl. Energy* 152 (2015) 109–120, <https://doi.org/10.1016/j.apenergy.2015.04.088>.
- [11] A.A. Boretti, Transient operation of internal combustion engines with Rankine waste heat recovery systems, *Appl. Therm. Eng.* 48 (2012) 18–23, <https://doi.org/10.1016/j.applthermaleng.2012.04.043>.
- [12] V. Grelet, T. Reiche, V. Lemort, M. Nadri, P. Dufour, Transient performance evaluation of waste heat recovery rankine cycle based system for heavy duty trucks, *Appl. Energy* 165 (2016) 878–892, <https://doi.org/10.1016/j.apenergy.2015.11.004>.
- [13] J.C. Bass, N.B. Elsner, F.A. Leavitt, Performance of the 1 kW thermoelectric generator for diesel engines, *AIP Conf. Proc.* 316 (1994) 295–298, <https://doi.org/10.1063/1.46818>.
- [14] K. Matsubara, Development of a high efficient thermoelectric stack for a waste exhaust heat recovery of vehicles, in: Twenty-First Int. Conf. Thermoelectr. Proc. ICT '02, IEEE, 2002, pp. 418–423. 10.1109/ICT.2002.1190350.
- [15] A. Massaguer, E. Massaguer, M. Comamala, T. Pujol, L. Montoro, M.D. Cardenas, D. Carbonell, A.J. Bueno, Transient behavior under a normalized driving cycle of an automotive thermoelectric generator, *Appl. Energy* 206 (2017) 1282–1296, <https://doi.org/10.1016/j.apenergy.2017.10.015>.
- [16] J.G. Haidar, J.I. Ghojel, Waste heat recovery from the exhaust of low-power diesel engine using thermoelectric generators, in: Proc. ICT2001. 20 Int. Conf. Thermoelectr. (Cat. No.01TH8589), IEEE, 2001, pp. 413–418. 10.1109/ICT.2001.979919.
- [17] D.T. Crane, J. Lagrandeur, Thermoelectric waste heat recovery program for passenger vehicles. 2012 Vehicle Technologies Program Annual Merit Review, Present. Slide. (n.d.), pp. 1–23.
- [18] K. Ikoma, M. Munekiyo, K. Furuya, M. Kobayashi, T. Izumi, K. Shinohara, Thermoelectric module and generator for gasoline engine vehicles, in: Seventeenth Int. Conf. Thermoelectr. Proc. ICT98 (Cat. No.98TH8365), 1998, pp. 464–467. 10.1109/ICT.1998.740419.
- [19] E.F. Thacher, B.T. Helenbrook, M.A. Karri, C.J. Richter, Testing of an automobile exhaust thermoelectric generator in a light truck, 221, Proc. Inst. Mech. Eng. Part D J. Automob. Eng. (2007) 95–107, <https://doi.org/10.1243/09544070JAUT051>.
- [20] S. Kumar, S.D. Heister, X. Xu, J.R. Salvador, G.P. Meisner, Thermoelectric generators for automotive waste heat recovery systems part II: parametric evaluation and topological studies, *J. Electron. Mater.* 42 (2013) 944–955, <https://doi.org/10.1007/s11664-013-2472-8>.
- [21] S. Kim, B. Won, S. Rhi, S. Kim, J. Yoo, J. Jang, Thermoelectric power generation system for future hybrid vehicles using hot exhaust gas, *J. Electron. Mater.* 40 (2011) 778–783, <https://doi.org/10.1007/s11664-011-1569-1>.
- [22] L. Aixala, RENOTER project introduction - volvo group, Thermoelectr. Appl. Work. (2011).
- [23] D. Magnetto, M. Brignone, A. Ziggioni, HeatRecar Thermoelectric Waste Heat Recovery in Light Duty Trucks optimal use of energy Consortium and main objectives, Present. Slide, 2010.
- [24] P. He, Y. Li, L. Zhao, Study on exhaust system parameters for fuel economy improvement of small gasoline, (n.d.), 2009.
- [25] N.A. Khripach, B.A. Papkin, V.S. Korotkov, A.S. Nekrasov, Effect of a thermoelectric generator on the fuel economy of a vehicle operating in a real-world environment, *Biosci. Biotechnol. Res. Asia* 12 (2015) 375–386.
- [26] R. Vijayagopal, N. Shidore, M. Reynolds, C. Folkerts, A. Rousseau, Fuel displacement potential of a thermoelectric generator in a conventional vehicle, *World Electr. Veh. J.* 6 (2013) 663–668, <https://doi.org/10.1109/EVS.2013.6914719>.
- [27] M. Comamala, I.R. C  zar, A. Massaguer, E. Massaguer, T. Pujol, Effects of design parameters on fuel economy and output power in an automotive thermoelectric generator, *Energies* 11 (2018) 3274, <https://doi.org/10.3390/en11123274>.
- [28] A. Massaguer, E. Massaguer, M. Comamala, T. Pujol, J.R. Gonz  lez, M.D. Cardenas, D. Carbonell, A.J. Bueno, A method to assess the fuel economy of automotive thermoelectric generators, *Appl. Energy* 222 (2018) 42–58, <https://doi.org/10.1016/j.apenergy.2018.03.169>.
- [29] E. Massaguer, A. Massaguer, T. Pujol, J.R. Gonzalez, L. Montoro, Modelling and analysis of longitudinal thermoelectric energy harvesters considering series-parallel interconnection effect, *Energy* 129 (2017) 59–69, <https://doi.org/10.1016/j.energy.2017.04.061>.
- [30] E. Massaguer, A. Massaguer, L. Montoro, J.R. Gonzalez, Development and validation of a new TRNSYS type for the simulation of thermoelectric generators, *Appl. Energy* 134 (2014) 65–74, <https://doi.org/10.1016/j.apenergy.2014.08.010>.
- [31] J. Heywood, Internal Combustion Engine Fundamentals 2E, McGraw-Hill Education, 2018 <https://books.google.es/books?id=OmJUDwAAQBAJ>.



# Chapter 5

## Results and discussion

---



In Chapter 2 of this thesis, the first objective was to achieve a simulated model with the software GT SUITE of the ATEG prototype in essay on the XUD7/K diesel engine. The experimental results compared to the results of the simulation show that the thermal behavior of the model conforms very well to the conditions observed in the laboratory, with little significant differences with regard to the temperature of the cooling water output and which in any case, they exceed 5%. The output temperature of the combustion gases of the ATEG shows a remarkable match with differences also always less than 5% compared to the experimental data. This indicates that the model used correctly simulates heat transfers in this ATEG prototype and therefore the results of the geometric changes and changes in fluid conditions can be reproduced with great reliability. In this regard, our main objective has been to investigate the benefits of the ATEG prototype in terms of generation of electric energy and fuel economy by changing different design parameters in hot and cold face heat exchangers. For a fixed distribution of the TEMs the diameter of the holes has been modified in the HSHE while maintaining the same length. In the CSHE the changes have been carried out in the volumetric volume of cooling water and in the transverse section of the water channels.

The results of the simulation show that in the CSHE it is necessary to maximize the speed of the cooling water to obtain the maximum heat transfer, but this causes a greater hydraulic work to the pump that will have to be deduced from the electrical power generated. However, it is observed that despite the increase in product  $hA$ , it no longer has an influence on the maximum generation of electrical energy. In the opposite direction, a value of  $hA$  below  $2.70\text{WK}^{-1}$  implies a significant decrease in the transfer of heat and seeds to a low production of electrical energy.

If we put the focus on the HSHE, the results show a behavior very similar to that seen in the CSHE but here is added the component of the back pressure offered by the cylindrical holes of the exchanger. The calculated magnitudes vary between 955 mbar for a  $D = 8$  mm and 17 mbar for a hole diameter  $D = 20$  mm. In the same way that the CSHE has proceeded with its  $hA$  product clearly

indicates the same behavior. Thanks to the semi-empirical equations deduced in previous works and improved in the present, the expected fuel savings can be calculated with relative ease when carrying out all the modifications proposed in chapter 2. None of the configurations studied in chapter 2 show a reduction of consumption. The combination of the best configuration to obtain the maximum electrical power and the one that provides the lower counter pressure does not manage to diminish the consumption with respect to the original configuration without the installation of an ATEG. The best consumption obtained is 0.19% higher than the original configuration.

However, the use of specialized software is confirmed as a very useful tool to establish an ATEG design as efficiently as possible. Despite the integration of the thermoelectric recovery in the vehicle as a whole, including all the peripheral systems of the same, as well as its dynamic behavior it consumes a very important amount of time. If a conventional computer is used as in our case, the simulation time of a parametric optimization study of only 3 variables (diameter of the holes in the HSHE, engine load and coolant flow in the CSHE) would occupy approximately 300 days.

A new recovery design and its experimental tests are shown in chapter 3. It is expected to obtain a saving of consumption using a design in the hot gas heat recovery that minimizes backpressure as much as possible, at the same time thanks to the tests experiments carried out in Chapter 2, use TEMs that work at a lower temperature in their hot face so that it is located in the zone of maximum thermoelectric conversion. Another advantage is that the TEM can be free of Pb since this material is the one that allows the use to high temperature, which can contribute remarkably to the efficient recycling of future generators installed in series.

The simulations of this radial ATEG have been carried out with ANSYS CFX that allows studying the 3D geometry of all the components. The results of the simulation also show a very large match with the experimental results.

One of the variations made in the radial ATEG was the total surface of the heat exchange flaps in the hot gas area.

With the aim of maximizing the heat transfer of gases to the TEM, the surface of the fins is also increased. One of the direct consequences of this modification is that the backpressure also increases, and so in the 1.6At case for high regimes and high loads, consumption worsens. Only in intermediate regimes and medium loads can an improvement in overall consumption be observed.

The results show that the ZTe values below 0.21 are not feasible, especially as already mentioned, when the flow of gases and their temperature are important, a situation that occurs in high rotation regimes and high loads .

However, thanks to the simulations, it can be seen that if a material with a value of ZTe was obtained above 0.63 then consumption savings are produced in all the studied cases.

Once again it is demonstrated for an ATEG that the condition of maximum electrical power generated is not synonymous with lower fuel consumption because the parameter of the backpressure is very important. This point of view must be a very important parameter for future design of thermoelectric heat recovery systems.

Finally, our research carried out at our Thermal Engines Laboratory is tested in a real vehicle at the IDIADA APPLUS research center located in L'Albornar (Tarragona). The comparison of the real fuel savings thanks to the installation of a latest generation ATEG jointly designed between NABLA THERMOELECTRICS and our GREFEMA research team in a BMW X1 vehicle is carried out.

In chapter 4 it is exposed that the exhaust gas temperature is higher as the engine load is increased and when more energy generated by the ATEG is produced.

The thermal behavior of this ATEG shows an almost constant temperature difference between the inlet and outlet of exhaust gases regardless of the load to which the engine is subjected. The maximum temperature reached on a hot face is 238.2°C, for a combustion gas temperature at the inlet of 660.4°C. This great difference can be explained by the low capacity of extraction of heat of the exhaust gases.

Regarding the electronic management of battery charging and operation of the alternator, it is observed that in the test vehicle the alternator develops an almost constant power (400 to 500W) while it is in operation. The loading strategy must be taken into account when it comes to including an ATEG in the vehicle's electric system. Chapter 4 of this thesis describes the method used to integrate the ATEG electrically into the electric charge system of the vehicle.

All 4 stationary points studied in Chapter 4 show a reduction in consumption. This fuel economy is not as optimistic as we expected at the beginning and its range is between 1.08% at best and 0.12% at worst.

The most significant electrical power generation is observed in high load regimes, when the flow and the exhaust gas temperature are maximum. However, the increase in gas flow increases the backpressure, due to the additional loss of pressure provided by the ATEG. As discussed above, the engine backpressure is defined as the exhaust pressure necessary to overcome the hydraulic resistance of the exhaust system in order to discharge the gases into the atmosphere. An increase in backpressure levels is an additional mechanical work of the engine and / or less energy extracted for the exhaust turbine (in supercharged engines) that can reduce the intake pressure to the engine.

Despite the increase in fuel consumption due to the additional backpressure, the energy recovered from the exhaust at the ATEG reverses this effect and produces a significant reduction in fuel consumption of the vehicle, reducing the load to the alternator.

Although trial point 2 provided the greatest benefits due to this combination of factors, not all four regimens achieved the same value. Point 1, for example, produced a low counter-effect, but the generation of ATEG was too low to provide a significant benefit. In contrast, points 3 and 4 generated a large generation of ATEG, but also an excessive counterpoint.

The positive values of fuel saving are obtained in the range of 0.67 to 54.49 mbar, with a generation of minimum power of 6 W of ATEG. The higher backpressure values represent an excessive exhaust gas barrier leading to a reduction in engine efficiency.

The high back pressure makes the engine less efficient because it cannot supply the same power to the crankshaft. The backpressure does not only affect the exhaust stroke; the cylinder pressure, at the beginning of the admission stroke, is above to normal conditions, for example, without the ATEG. This reduces the volumetric efficiency during intake and, therefore, the same amount of fuel cannot be introduced. Finally, if the backpressure is too high, a certain amount of residual gases do not come out of the cylinder and mixed with fresh air during the suction phase. These residual gases reduce the volumetric efficiency and warm the fresh air, causing possible knocking problems. In a similar case, the manufacturers of engines and vehicles have had important problems related to the system of control of emissions, like the catalyst, the FAP systems, all because of the exhaust backpressure.

Backpressure values greater than 54.49 mbar lead to a reduction in engine efficiency. This reduction is more damaging than the positive effect of ATEG energy generation.

In stationary conditions, the maximum electrical power generated by ATEG is 197.77 W at 2838 rpm and 79.0% accelerator position, corresponding to a vehicle speed of 120 km / h on a flat road and including aerodynamic resistance. The experiments show that the values of the fuel economy depend a lot on the generation of energy and the counter pressure. The value of maximum consumption savings obtained was 1.08% at 1807 rpm and 47.1% throttle position, corresponding to a vehicle speed of 80 km / h.

The results show that semi-empirical equations are useful for predicting ATEG performance, with a maximum observed error of 11.27%. In addition, the experiments show a maximum fuel economy found in low backpressure values. This behavior combines with the idea of a greater generation of energy that can contribute better to save fuel. The higher the speed and the load of the vehicle, the greater the temperature of the exhaust gases, which is favorable for the ATEG. However, the backpressure caused to the engine also increases, resulting in a lower engine performance and a lower saving of consumption.

Thanks to the use of these equations you can see where the area that produces fuel economy is found by incorporating the ATEG. The maximum saving point,

which corresponds to 1.08%, would be achieved with an electrical production in the ATEG of only 15W but with a very low backpressure value, only 5mbar.





## Chapter 6

### Conclusions

---

This thesis proposes and analyzes one technical solution that allows the recovery of residual heat in vehicles. The work focuses on the use of thermoelectric materials in order to recover the residual heat that is thrown by the exhaust pipe of combustion engines, in order to reduce their fuel consumption.

The thesis is based on developments prior to this work, which have been cited in the bibliography, which have allowed them to achieve a significant level of learning in the field of thermoelectric recovery. This learning has allowed identifying points of improvement, which have been studied and analyzed in this work. Below are the main conclusions obtained:

- The state of the art in thermoelectrically recovery has a clear direction towards the search for new materials with high temperature ZT (500°C-700°C). These materials allow withstanding the high temperatures of exhaust gases. However, they are made up of rare earths that are very expensive for commercial solutions and hence impede their application in the real world.
- The exhaust temperatures are very variable. The most common temperatures are between 250°C and 350°C; while intermittently 700°C peaks can be reached. It has been shown that the use of high temperature materials ensures that the heat recovery system is not damaged during temperature peaks. Taking into account that the thermoelectric generation is proportional to  $\Delta T^2$ , it can easily be observed that the ATEG will work at its optimal operating point (maximum electrical output or maximum efficiency) in a timely manner, only during the temperature points. Therefore, for most of the time, the ATEG generates a very small part of the total power installed.
- To maximize the electrical generation, it is necessary to allow the TEGs to work at all times near their maximum operating point, where the electrical generation and its performance are high. It is also important to point out that using materials with elevated ZT at low temperatures, such as the BiTe that achieves an efficiency of 5% at 200°C, is better than using them to use other preparations for high temperature > 500°C. This is explained by the fact that the most common exhaust temperatures are close to the optimal BiTe temperature.

In order to be able to carry out effectively what has been mentioned in the previous points, it is necessary to deal with the temperature points and ensure that the material does not degrade by overheating. It is for this reason that, in the latest design, a mechanism has been designed to regulate the temperature of the hot face of the TEGs. By adjusting the amount of smoke that passes through the exchanger and what is derived by the butterfly valve, it can be guaranteed that not only the TEGs can never exceed the optimum working temperature, but also that they operate at their optimum operating point the greater possible time

Keep in mind that heat recovery depends exclusively on the flow rates and exhaust temperatures, and hence the type of vehicle and driving.

The fuel economy depends on:

- The extra backpressure that the ATEG adds to the exhaust.
- The electrical generation of the ATEG.
- The added weight of ATEG.

Of the three previous parameters, the backpressure is those that have a greater impact on the saving of fuel. An ATEG with a loss of excessive load can cause increases in fuel consumption despite generating large amounts of electricity.

The shape of the combustion gas exchanger has an important impact on the overall efficiency of ATEG. The convection coefficient must be as high as possible so that the maximum energy of the smoke can be captured. However, without compromising the backpressure mentioned in the previous point.

It is important to point out that the maximum point of electric generation of the ATEG does not correspond to the point of maximum fuel economy. This will be studied in more detail in future projects.

The use of simulation software such as ANSYS or GT-SUITE has been decisive in the study of the impact of certain geometrical characteristics on the behavior of the ATEG's, such as the provision of TEG modules in parallel series, radial configuration or Axial in respect to the residual heat flow or the relation of the backpressure with the coefficient of convection in the exchange smoke-TEG. On the other hand, this study has made it possible to optimize its operation.

The validity of the 1D GT-SUITE software for studies of ATEG generators of non-complex geometries is confirmed as proposed in Chapter 2 of the thesis and also when they want to make ATEG integration simulations in a vehicle, while that for ATEG's of complex geometry like the one proposed in chapter 3, the use of CFD programs capable of simulating 3D like ANSYS-CFX is considered more appropriate.

The dimensionless expression  $P_{n,ATEG}/(\dot{V}_g \Delta p_{bp})$  is proposed to determine the viability of an ATEG. Only cases in which  $P_{n,ATEG}/(\dot{V}_g \Delta p_{bp}) > 1$  are of interest in terms of fuel economy.

For a given ATEG there is a threshold value of the effective value of the merit figure  $ZTe$ , from which there are positive fuel savings. In the presented designs, values of  $ZTe = 0.63$  produce fuel consumption reductions of 1.3% with conversion efficiency of 6%.